University of Crete

Chemistry Department

General Postgraduate Program

Applied Spectroscopy Laboratory

Master's Thesis

Biomolecular Residue Analysis in Archaeological Potsherds by means of UV-vis Absorption and Fluorescence Spectroscopy

ANTONIA INTZE

Master Thesis Supervisor: Professor Demetrios Anglos

Heraklion 2020

Πανεπιστήμιο Κρήτης

Τμήμα Χημείας

Γενικό Μεταπτυχιακό Πρόγραμμα

Εργαστήριο Εφαρμοσμένης Φασματοσκοπίας

Μεταπτυχιακό Δίπλωμα Ειδίκευσης

Μελέτη Βιομοριακών Δεικτών με Φασματοσκοπία Απορρόφησης Υπεριώδους-Ορατού και Φθορισμού για τον Χαρακτηρισμό Οργανικών Καταλοίπων σε Αρχαιολογικά Κεραμικά

ΑΝΤΩΝΙΑ ΙΝΤΖΕ

Επιβλέπων Καθηγητής: Δημήτριος Άγγλος

Ηράκλειο 2020

“I hope you accept Nature as She is – absurd”

RICHARD FEYNMAN

Thesis Committee

Demetrios Anglos (Supervisor)

Professor of Physical Chemistry

Apostolos Spyros

Associate Professor of Analytical Chemistry

Ioannis Pavlidis

Assistant Professor of Biological Chemist

Acknowledgements

I would like to thank my supervisor, Prof. Demetrios Anglos, for his insightful comments and suggestions throughout my Master's journey. I am also especially grateful to Dr Aggelos Philippidis for his encouragement, insights on the project, and review of the draft chapters. Many colleagues gave their advice and support until the completion of the project too. I therefore wish to express my appreciation and thanks to the following individuals:

Dr Olga Kokkinaki	Giorgos Stavrakakis
Dr Panagiotis Siozos	Irene Malegiannaki
Dr Paraskevi Pouli	Katerina Stamataki
Dr Sophia Sotiropoulou	Kristalia Melessanaki
Dr George Tserevelakis	Lampros Papoutsakis
Angelina Mamali	Lampros Spanos
Dimitrios Hatzigiannis	Manos Orfanakis
Evangelia Dimitroulaki	Marilena Konstantinou
Evangelia Kapourani	Nikos Fragkoulis
Evangelia Sarafi	Renate Kontzedaki

I should also thank the Foundation for Research and Technology-Hellas (FORTH) for its financial support of this Master's project.

Last but not least, I express my gratitude to Ioannis, Anastasia, Konstantinos, and Antonia Intze for their unreserved and wholehearted support through all the past years of my life.

Curriculum Vitae

Personal

Name: Antonia Intze

Date of birth: 5th July 1996

Nationality: Greek

Home address: Dexitheas 16, 71305, Heraklion, Crete

Mobile: 0030 698 57 81 209

Email address: antoniaintze1@hotmail.com

Education

Oct 2018 – Dec 2020	**MSc** at Department of Chemistry, University of Crete, Greece
Oct 2014 – Oct 2018	**BSc** at Department of Chemistry, University of Crete, Greece Grade Point Average: 8.21 (out of 10.00)

Research experience

Nov 2018 – Nov 2020	**Master Thesis**: '*Biomolecular residue analysis in archaeological potsherds by means of UV-vis absorption and fluorescence spectroscopy'* Foundation for Research and Technology Hellas, Institute of Electronic Structure and Laser, Crete, Greece Supervisor: Prof. Demetrios Anglos
Mar 1 – Jun 30, 2020	**Erasmus+ fellowship** mobility program: *'Analysis of collagen in samples from archaeological bone using analytical pyrolysis'* Università di Pisa, Dipartimento di Chimica e Chimica Industriale, Pisa, Italy Supervisors: Prof. Ilaria Bonaduce and Prof. Erika Ribechini
Oct 2017 – Jun 2018	**Bachelor Thesis**: *'Atmospheric processes, climatic change and air quality: UV and infrared absorption cross sections determination for critical volatile organic compounds and heterogeneous interaction of gaseous SO2 with dust surfaces'* Laboratory of Photochemistry and Chemical Kinetics, University of Crete, Department of Chemistry, Crete, Greece Supervisor: Dr. Vassileios C. Papadimitriou

Jul 1 – Sep 30, 2017	**Erasmus+ fellowship** mobility program: '*Investigation of temperature dependence of UV-vis cross-sections for several ketones'* Institut de Combustion Aérothermique Réactivité Environnement, ICARE, CNRS, Orléans, France Supervisor: Dr. Abdelwahid Mellouki

Laboratory experience

- Very low pressure reactor coupled with quadruple mass spectrometry detection technique

- Knudsen reactor technique

- Fourier transformed infrared spectroscopy

- Raman spectroscopy

- Absorption spectroscopy

- Fluorescence spectroscopy

Computational experience

- Microsoft office suite programs (*Word, Excel, Power Point, Access*)

- Igor suite

- OriginLab suite

Additional experience

Feb – Apr 2019	Assistant in undergraduate General Chemistry laboratories
Oct – Dec 2018	Assistant in undergraduate Physical Chemistry laboratory
Apr – Nov 2016	Conducted experiments as a member of a team in order to explain the findings of chemistry in primary school students
Jan – May 2016	Undergraduate assistant in General Chemistry laboratories

Research interests

- Fundamental and applied research in the area of experimental Physical Chemistry

- Determination of UV-vis and IR absorption cross-sections of crucial organic compounds

- Study of potsherds using UV-vis absorption and fluorescence spectroscopy to unveil information about commercial development, diet, and burial practices of Minoan civilization

- Examination of human bone collagen by pyrolysis-GC/MS

Participation in summer schools

Jul, 3 – Jul, 7 2017 *'The Voltaire Atmospheric Chemistry Summer School: Fundamentals for Atmospheric Chemistry'*
CNRS, Orléans, France

Languages

- Greek (mother tongue)

- English (fluent, Certificate of Proficiency in English – University of Michigan)

- German (Goethe-Zertifikat B2)

- French

- Italian

Activities and interests

- 1st Dan holder in Shito Ryu Karate Do and member of Sheinshinkai Karate Union

- Music knowledge

- Member of youth choir in Heraklion

- Keen on hiking, theater, and literature

Βιογραφικό Σημείωμα

Προσωπικές πληροφορίες

Ονοματεπώνυμο: Αντωνία Ιντζέ

Ημερομηνία γέννησης: 5η Ιουλίου 1996

Ιθαγένεια: Ελληνική

Διεύθυνση κατοικίας: Δεξιθέας 16, 71305, Ηράκλειο, Κρήτη

Κινητό τηλέφωνο: 0030 698 57 81 209

Διεύθυνση email: antoniaintze1@hotmail.com

Εκπαίδευση

Οκτ 2018 – Δεκ 2020	**Μεταπτυχιακό** στο Τμήμα Χημείας, Πανεπιστήμιο Κρήτης,
Οκτ 2014 – Οκτ 2018	**Πτυχίο** Χημείας στο Τμήμα Χημείας, Πανεπιστήμιο Κρήτης, Βαθμός: 8.21 (στα 10.00)

Ερευνητική εμπειρία

Νοε 2018 – Νοε 2020	**Μεταπτυχιακή εργασία**: '*Μελέτη βιομοριακών δεικτών με φασματοσκοπία απορρόφησης υπεριώδους-ορατού και φθορισμού για τον χαρακτηρισμό οργανικών καταλοίπων σε αρχαιολογικά κεραμικά'* Ίδρυμα Τεχνολογίας και Έρευνας, Ινστιτούτο Ηλεκτρονικής Δομής και Λέιζερ, Ηράκλειο, Κρήτη, Ελλάδα Υπεύθυνος καθηγητής: Δημήτριος Άγγλος
Μαρ 1 – Ιουν 30, 2020	**Erasmus+ υποτροφία** προγράμματος κινητικότητας: *'Ανάλυση κολλαγόνου σε αρχαιολογικά οστά με πυρόλυση-GC/MS'* Universit*à* di Pisa, Dipartimento di Chimica e Chimica Industriale, Πίζα, Ιταλία Υπεύθυνες καθηγήτριες: Ilaria Bonaduce και Erika Ribechini
Οκτ 2017 – Ιουν 2018	**Πτυχιακή εργασία**: *'Ατμοσφαιρικές διεργασίες, κλιματική αλλαγή και ποιότητα ατμόσφαιρας: Προσδιορισμός τιμών ενεργούς διατομής απορρόφησης υπερύθρου και υπεριώδους κρίσιμων πτητικών οργανικών ενώσεων και ετερογενής αλληλεπίδραση SO_2 με σωματίδια σκόνης'* Εργαστήριο Φωτοχημείας και Χημικής Κινητικής, Πανεπιστήμιο Κρήτης, Τμήμα Χημείας, Κρήτη, Ελλάδα Υπεύθυνος: Δρ. Βασίλειος Χ. Παπαδημητρίου
Ιουλ 1 – Σεπ 30, 2017	**Erasmus+ υποτροφία** προγράμματος κινητικότητας: '*Προσδιορισμός θερμοκρασιακής εξάρτησης των τιμών*

ενεργούς διατομής απορρόφησης υπεριώδους-ορατού για διάφορες κετόνες'
Institut de Combustion Aérothermique Réactivité Environnement, ICARE, CNRS, Ορλεάνη, Γαλλία
Υπεύθυνος: Δρ. Abdelwahid Mellouki

Εργαστηριακή εμπειρία

- Αντιδραστήρας πολύ-χαμηλής πίεσης συζευγμένος με φασματομετρία μάζας

- Τεχνική αντιδραστήρα Knudsen

- Φασματοσκοπία υπερύθρου

- Φασματοσκοπία Raman

- Φασματοσκοπία απορρόφησης

- Φασματοσκοπία φθορισμού

Υπολογιστική εμπειρία

- Πακέτο προγραμμάτων Microsoft office (*Word, Excel, Power Point, Access*)

- Πρόγραμμα Igor

- Πρόγραμμα OriginLab

Επιπρόσθετη εμπειρία

Φεβ – Απρ 2019	Βοηθός στα προπτυχιακά εργαστήρια Γενικής Χημείας
Οκτ – Δεκ 2018	Βοηθός στο προπτυχιακό εργαστήριο Φυσικοχημείας
Απρ – Νοε 2016	Μέλος πανεπιστημιακής ομάδας με στόχο την εξοικείωση μαθητών δημοτικού με την επιστήμη της Χημείας
Ιαν – Μαϊ 2016	Βοηθός στα προπτυχιακά εργαστήρια Γενικής Χημείας

Ερευνητικά ενδιαφέροντα

- Θεμελιώδης και εφαρμοσμένη έρευνα στο πεδίο πειραματικής Φυσικοχημείας

- Προσδιορισμός των UV-vis και IR ενεργών διατομών απορρόφησης κρίσιμων οργανικών ενώσεων

- Μελέτη αρχαιολογικών κεραμικών με φασματοσκοπία απορρόφησης φθορισμού για την αποκάλυψη πληροφοριών σχετικών με την εμπορική ανάπτυξη, τη διατροφή και τις ταφικές πρακτικές στον Μινωικό πολιτισμό

- Μελέτη κολλαγόνου σε ανθρώπινα οστά με πυρόλυση-GC/MS

Συμμετοχή σε θερινά σχολεία

Ιουλ, 3 – Ιουλ, 7 2017	'*The Voltaire Atmospheric Chemistry Summer School: Fundamentals for Atmospheric Chemistry'* CNRS, Ορλεάνη, Γαλλία

Γλώσσες

- Αγγλικά (ευφραδής, Certificate of Proficiency in English – University of Michigan)
- Γερμανικά (Goethe-Zertifikat B2)
- Γαλλικά
- Ιταλικά

Δραστηριότητες και ενδιαφέροντα

- Κάτοχος 1st Dan στο Shito Ryu Karate Do και μέλος της ένωσης Sheinshinkai Karate
- Μουσικές γνώσεις
- Μέλος της νεανικής χορωδίας Ηρακλείου
- Λάτρης πεζοπορiών, θεάτρου και λογοτεχνίας

Abstract

Bio-organic residue analysis of archaeological artefacts sheds light on human activities and surviving practices during historic and prehistoric times using powerful analytical methodologies based mainly on chromatographic techniques coupled with mass spectrometry. In the context of archaeo-residue analysis, spectroscopic methods are advantageous since they enable fast-screening of samples via prompt detection of biomarkers and, thus, expedite the further study of promising samples by high-end analytical tools.

The present master's thesis focuses on the study of archaeological potsherds originating from the Minoan civilization by means of UV-vis absorption and fluorescence spectroscopy with the aim of developing efficient detection and characterization methodologies of biomarker compounds. Analyses of samples are conducted in solutions deriving from solvent treatment of the sherds. The analytical methodology relies at first on recording UV-vis absorption spectra and then on recording emission and excitation fluorescence spectra in extracted solutions originating from three parts of the potsherds: inner, outer, and inner soil crust. Detailed examination of fluorescent data allows the construction of three-dimensional fluorescence excitation-emission maps for each sample and subsequently the comparison of the fluorescent profiles of unknown samples with those of standard solutions.

Standard aqueous solutions of phenolic acids (ferulic acid, gallic acid, caffeic acid, syringic acid, and vanillin) were prepared and studied as they comprise an important class of intrinsic fluorophores in wine that is known to preserve over archaeological timescales. Phenolic compounds were proposed to serve as wine markers, while secondary oxidation products of unsaturated lipids were suggested to compose oil markers. Based on the identification of such molecular indicators it is proposed that a Minoan amphora has been used to stored oil and wine, while two Minoan cylinder vessels were utilised as oil containers. Fluorophores in archaeological samples were also quantified, assuming that they were represented by phenolic acid compounds. To this end, a comparative study to reference compounds was conducted and it was concluded that the concentration of fluorescent molecules is about 400 μg/g of potsherd.

At the same time, a methodology for organic residue recovery from modern potsherds was designed on the basis of intact olive oil as model sample and isooctane as extracting solvent. The extraction efficiency of developed protocol was evaluated monitoring the intensity of chlorophyll's *a* emission band. Afterwards, two potsherds were spiked with phenolic standard mixture and with olive oil and were transferred to a custom-built chamber for artificial aging upon UV-irradiation. The absorption and fluorescence study of aged samples showed that non-conjugated double and triple bonds in lipid structures present in olive oils convert into conjugated bonds in di- and tri-enes carrying carbonyl functional groups (secondary oxidation products) and that phenolic acids photo-decompose via cleavage of acrylic acid group.

Keywords: archaeometry, UV-vis absorption spectroscopy, fluorescence spectroscopy, potsherd, organic residue, fluorescent biomarker, phenolic acid, artificial aging

Περίληψη

Το πεδίο της ανάλυσης αρχαιολογικών βιο-οργανικών καταλοίπων συνεισφέρει στη συγκέντρωση πληροφοριών σχετικών με την ανθρώπινη δραστηριότητα και τις πρακτικές διαβίωσης στους ιστορικούς και προϊστορικούς χρόνους, χρησιμοποιώντας προηγμένες αναλυτικές μεθόδους. Παρόλο που οι κλασικές χρωματογραφικές τεχνικές συζευγμένες με φασματομετρία μάζας προσφέρουν ακριβείς και ποσοτικές πληροφορίες σχετικά με τα αναλυόμενα δείγματα, είναι εντούτοις χρονοβόρες και δαπανηρές. Γι' αυτόν το λόγο, στο πλαίσιο της μελέτης αρχαιο-οργανικών καταλοίπων αναπτύχθηκαν εναλλακτικές, απλές και γρήγορες φασματοσκοπικές μέθοδοι που συνδράμουν στην ταχεία ανάλυση και διαλογή των δειγμάτων μέσω της ανίχνευσης βιομοριακών δεικτών, μέρος των οποίων μελετάται εν συνεχεία διεξοδικά με τις κλασικές τεχνικές υψηλής ανάλυσης.

Η παρούσα μεταπτυχιακή ερευνητική εργασία εστιάζεται στη μελέτη αρχαιολογικών κεραμικών οστράκων μινωικής προέλευσης, με σκοπό την ανάπτυξη μεθοδολογίας ανίχνευσης και χαρακτηρισμού οργανικών καταλοίπων, με βάση τη χρήση των φασματοσκοπικών τεχνικών απορρόφησης στην περιοχή υπεριώδους-ορατού και φθορισμού. Η ανάλυση πραγματοποιείται σε διαλύματα που προκύπτουν από κατάλληλη εκχυλιστική επεξεργασία των κεραμικών. Η μεθοδολογία ανάλυσης περιλαμβάνει αρχικά την καταγραφή φασμάτων απορρόφησης υπεριώδους-ορατού και στη συνέχεια φασμάτων εκπομπής και διέγερσης φθορισμού σε διαλύματα εκχυλισμάτων προερχόμενων από τρία τμήματα των κεραμικών οστράκων: εσωτερικό, εξωτερικό και επιφανειακή κρούστα χώματος στο εσωτερικό. Λεπτομερής μελέτη των χαρακτηριστικών φθορισμού οδηγεί σε δεδομένα με τη μορφή χαρτών εκπομπής-διέγερσης φθορισμού, που επιτρέπουν την τρισδιάστατη αναπαράσταση του φασματοσκοπικού προφίλ κάθε αναλυόμενου διαλύματος και σύγκριση αυτού με δείγματα αναφοράς.

Πρότυπα υδατικά διαλύματα φαινολικών ενώσεων (φερουλικό οξύ, γαλλικό οξύ, καφεϊκό οξύ, συριγγικό οξύ και βανιλίνη) παρασκευάστηκαν και μελετήθηκαν, καθώς απαρτίζουν μία σημαντική οικογένεια φθοριζόντων ενώσεων που περιέχεται στο κρασί και είναι γνωστό ότι διατηρείται για μεγάλο χρονικό διάστημα. Οι μοριακοί δείκτες φαινολικών οξέων συσχετίστηκαν με την ύπαρξη κρασιού, ενώ τα δευτερογενή προϊόντα οξείδωσης των ακόρεστων λιπαρών οξέων αποδόθηκαν στην ύπαρξη λαδιού. Η ανίχνευση των παραπάνω βιοδεικτών στα αρχαιολογικά δείγματα συνιστά τη φύλαξη ελαιολάδου και κρασιού σε έναν μινωικό κεραμικό αμφορέα, ενώ την αποθήκευση ελαιολάδου σε δύο μινωικά κυλινδρικά αγγεία. Ακολούθησε εκτίμηση της ποσότητας των φθορίζοντων ενώσεων που περιέχονται στα εν λόγω αρχαιολογικά δείγματα, υποθέτοντας ότι εκπροσωπούνται από μέλη της οικογένειας φαινολικών οξέων. Για τον λόγο αυτό, πραγματοποιήθηκε συγκριτική μελέτη ως προς το φθορισμό μορίων αναφοράς, η οποία οδήγησε στο συμπέρασμα ότι η συγκέντρωση των αρχαιολογικών φθορίζοντων ενώσεων είναι περίπου 400 μg/g κεραμικού.

Παράλληλα, αναπτύχθηκε πρωτόκολλο ανάκτησης οργανικών καταλοίπων από σύγχρονα κεραμικά θραύσματα κάνοντας χρήση δείγματος ελαιολάδου και εκχυλιστικού μέσου ισοοκτανίου. Η αποτελεσματικότητα της εκχυλιστικής μεθοδολογίας αξιολογήθηκε μέσω της

κορυφής φθορισμού που αντιστοιχεί στη χλωροφύλλη a. Στη συνέχεια, δύο κεραμικά θραύσματα εμποτίστηκαν στο πρότυπο διάλυμα φαινολικών ενώσεων και σε ελαιόλαδο και μεταφέρθηκαν σε θάλαμο τεχνητής γήρανσης μέσω υπεριώδης ακτινοβολίας. Η μελέτη των φασμάτων απορρόφησης και φθορισμού των γηρασμένων δειγμάτων έδειξε ότι τα μη-συζυγή ακόρεστα λιπαρά οξέα που περιέχονται στο ελαιόλαδο φωτοαποδομούνται σε συζυγή διένια και τριένια που περιέχουν καρβονυλικές ομάδες στη δομή τους (δευτερογενή προϊόντα οξείδωσης) και ότι τα φαινολικά οξέα υπόκεινται σε θραύση της ακρυλικής λειτουργικής ομάδας.

Λέξεις κλειδιά: αρχαιομετρία, φασματοσκοπία απορρόφησης υπεριώδους-ορατού, φασματοσκοπία φθορισμού, κεραμικό υπόστρωμα, οργανικό κατάλοιπο, φθορίζων βιοδείκτης, φαινολικό οξύ, τεχνητή γήρανσ

Table of Contents

CHAPTER 1: Bio-organic Residues in Archaeological Science 1
1.1 Classes of Bio-organic Archaeological Residues 1
1.2 Effect of Cooking and Natural Aging in Protein Residue Preservation-likelihood 5
1.3 Fluorescent Biomarkers 6
1.3.1 Intrinsic 7
1.3.2 Extrinsic 9
CHAPTER 2: Spectroscopic Techniques for Archaeological Residue Analysis 12
2.1 Analytical Techniques in Archaeometry 12
2.2 Absorption Spectroscopy 14
2.3 Fluorescence Spectroscopy 16
CHAPTER 3: Spectrometers and Methodology 23
3.1 Absorption and Fluorescence Spectrometers 23
3.2 Absorption and Fluorescence Measurements Procedure 25
3.3 Correction of Fluorescence Spectra 26
3.4 Purity Classification of Solvents 27
3.5 Solution Preparation 28
3.6 Hydrophilic and Lipophilic Compounds Extraction from Archaeological Potsherds 31
CHAPTER 4: Comparison of Residues from Archaeological Potsherds with Phenolic Standard Solution 32
4.1 Storage of Goods, Types of Containers, and Processing of Foodstuffs in Minoan Civilization 32
4.2 Organic Residues in Wine: Fluorophores Preservation over Time 34
4.3 ^{1}H NMR Study 36
4.4 Results 37
4.4.1 Absorption and Fluorescence Study of Biomarkers found in Archaeological Potsherds from Minoan Palace in Archanes 37
4.4.2 Absorption and Fluorescence Study of Phenolic Standard Solution 44
4.4.3 Archaeological Biomarkers Quantification using Reference Standards 47
4.5 Discussion 49
CHAPTER 5: Organic Residue Extraction from Modern and Artificially Aged Potsherds 52
5.1 Analytical Protocol for Olive Oil Extraction from Potsherds 52

5.2 Evaluating the Success Rate of Extraction Protocol 53
5.3 UV Artificial Aging Process 55
5.4 Results 57
5.4.1 Absorption and Fluorescence Study of Artificially Aged Samples 57
5.5 Discussion 59
Conclusion.....62
Future Perspectives 63
References 64

List of Schemes

Scheme 1. Encrusted residues adhered to potsherds. Adapted from Historic England (2017a). 1

Scheme 2. Main input, loss, and transformation processes of organic residues occurring during usage, interment, and post-excavation handling of ceramic vessels. Reproduced from Roffet-Salque et al. (2017). 3

Scheme 3. Structures of the most common post-excavation lipid contaminants due to handling: (a) cholesterol and (b) squalene. 4

Scheme 4. Maillard reaction between D-glucose (a) and L-lysine (b) to form N-glucosylamine (c) (Schiff base) and ultimately aminodeoxyketose (d) via Amadori rearrangement. Adapted from Bailey et al. (1998). 6

Scheme 5. Structures of: (a) riboflavin, (b) lumiflavin, (c) lumichrome. 7

Scheme 6. Structures of: (a) dihydroxyhenylalanine (a phenylalanine photooxidation product), (b) dityrosine (a UV polymerisation product of tyrosine), (c) *N*-formylkynurenine (a tryptophan photooxidation product), (d) pentosidine (a glycation endproduct). 9

Scheme 7. Jablonski diagram for a hypothetical molecule. S_0 is the electronic ground state, S_1 and S_2 are the excited single states, T_1 is the excited triplet state, A is the absorption, F is the fluorescence, P is the phosphorescence, VR is the vibrational relaxation, IC is the internal conversion, ISC is the inter-system crossing, and EC is the external conversion. 16

Scheme 11. Structures of: (a) anthracene, (b) quinine bisulfate dihydrate, and (c) *N*-acetyl-DL-tryptophan. 29

Scheme 12. Structures of phenolic compounds studied in this Master Thesis.....30

Scheme 13. (a) Ground plan of the excavated Royal Minoan Palace at Archanes, Heraklion, Crete. The red arrows indicate the storage rooms of pithoi and vessels. (b) Unearthed vessels layout at one of the storage rooms. 34

Scheme 15. Structures of wine biomarkers (a) acetoin, (b) 2,3-butanediol and oil biomarkers (c) oleic acid, (d) linoleic acid detected by NMR spectroscopy. 36

Scheme 16. The sampling and extraction protocol established for this project. 56

Scheme 17. Potsherds spiked with neat olive oil and phenolic standard solution and transferred in a custom-built UV-aging chamber. 56

Scheme 18. Structures of major phenolic compounds present in olive oil: (a) oleuropein; (b) vanillic acid; (c) tyrosol (R=H), hydroxytyrosol (R=OH). 60

Scheme 19. Structures of: (a) an unsaturated lipid; (b) and (c) conjugated dienes of a lipid hydroxyperoxide (primary oxidation products); conjugated diene of a lipid (d) ketone, (e) alcohol and (f) aldehyde (secondary oxidation products). 61

List of Figures

Figure 1. Effect of absorbance units on their relative error percentage. 15

Figure 2. Fluorescence excitation and emission spectra of Ac-(DL)Trp-OH in water, $6x10^{-5}$ M. 17

Figure 3. Spectra of Ac-(DL)Trp-OH in water with concentration ($x10^{-5}$ M) 0.2, 1, 1.4, 2, 4, 6, 8, 10, 12, 14, 16: (a) absorption spectra, (b) fluorescence excitation spectra at emission wavelength 360 nm and fluorescence emission spectra at excitation wavelength 280 nm. 18

Figure 4. Effect of: (a) concentration of Ac-(DL)Trp-OH in water on the absorbance unit at 280.5 nm, (b) absorbance of Ac-(DL)Trp-OH in water at 280.5 nm on the fluorescence emission intensity at 360 nm.....19

Figure 5. Spectra of anthracene in ethanol with concentration ($x10^{-5}$ M) 0.3 (1), 3 (2), 30 (3), 300 (4): (a) absorption spectra, (b) fluorescence emission spectra at excitation wavelength 340 nm, (c) fluorescence excitation spectra at emission wavelength 420 nm. 20

Figure 6. Raman scattering obtained from water/methanol (4:1) v/v at excitation wavelength (nm): 325 (1), 350 (2), 375 (3), 400 (4), 425 (5), 450 (6).....22

Figure 7. Anthracene in ethanol 3×10^{-5} M at excitation wavelength 340 nm: (a) Fluorescence emission spectra, incident beam bandpass 1 nm, and fluorescent beam bandpass (nm): 1, 2, 3, 5, 10; (b) effect of fluorescent beam bandpass on fluorescence emission intensity at 400 nm. 25

Figure 8. Fluorescence emission spectra at excitation wavelength 350 nm of H_2O/CH_3OH (4:1) v/v (1), archaeological sample in H_2O/CH_3OH (4:1) v/v (2), after solvent subtraction (3). 26

Figure 9. Spectra of ethanol contaminated by anthracene remains in an optical cell: (a) absorption spectrum, (b) fluorescence emission spectrum at excitation wavelength 300 nm. 27

Figure 10. Spectra of methanol Sigma-Aldrich HPLC grade >99.9% (1) and methanol Fischer Scientific HPLC gradient grade >99.9% (2): (a) absorption spectra, (b) fluorescence emission spectra at excitation wavelength 250 nm, (c) fluorescence emission spectra at excitation wavelength 300 nm. 28

Figure 11. Spectra of sample MP1I in water/methanol (4:1) v/v: (a) absorption spectrum; (b) fluorescence emission spectra at excitation wavelength 250 nm (1), 275 nm (2), 300 nm (3), 325 nm (4), 350 nm (5); (c) fluorescence excitation spectrum at emission wavelength 420 nm; (d) 2D fluorescence emission-excitation spectral map. 38

Figure 12. Spectra of sample MP1O in water/methanol (4:1) v/v: (a) absorption spectrum; (b) fluorescence emission spectra at excitation wavelength 250 nm (1), 275 nm (2), 300 nm (3), 325 nm (4), 350 nm (5); (c) fluorescence excitation spectrum at emission wavelength 420 nm; (d) 2D fluorescence emission-excitation spectral map. 39

Figure 13. Spectra of sample MP1S in water/methanol (4:1) v/v: (a) absorption spectrum; (b) fluorescence emission spectra at excitation wavelength 250 nm (1), 275 nm (2), 300 nm (3), 325 nm (4), 350 nm (5); (c) fluorescence excitation spectrum at emission wavelength 420 nm; (d) 2D fluorescence emission-excitation spectral map. 40

Figure 14. Spectra of sample MP1I in chloroform: (a) absorption spectrum; (b) fluorescence emission spectra at excitation wavelength 275 nm (1), 300 nm (2), 350 nm (3); (c) fluorescence excitation spectrum at emission wavelength 360 nm (1) and 435 nm (2); (d) 2D fluorescence emission-excitation spectral map. 41

Figure 15. Spectra of sample MP1S in chloroform: (a) absorption spectrum; (b) fluorescence emission spectra at excitation wavelength 300 nm (1), 325 nm (2), 350 nm (3); (c) fluorescence excitation spectrum at emission wavelength 410 nm; (d) 2D fluorescence emission-excitation spectral map. 42

Figure 16. Spectra of sample MP2S in water/methanol (4:1) v/v: (a) absorption spectrum; (b) fluorescence emission spectra at excitation wavelength 275 nm (1), 300 nm (2), 325 nm (3), 350 nm (4); (c) fluorescence excitation spectrum at emission wavelength 450 nm; (d) 2D fluorescence emission-excitation spectral map. 43

Figure 17. Spectra of sample MP3S in chloroform: (a) absorption spectrum; (b) fluorescence emission spectra at excitation wavelength 325 nm (1), 350 nm (2), 375 nm (3); (c) fluorescence excitation spectrum at emission wavelength 450 nm; (d) 2D fluorescence emission-excitation spectral map. 44

Figure 18. Absorption spectra of phenolic standard solutions in water: (a) gallic acid (1), ferulic acid (2), vanillin (3); (b) syringic acid (1), caffeic acid (2), phenolic standard solution (3). The concentrations of pure phenolic acid solutions are $2x10^{-5}$ M; in mixture each fluorophore is $4x10^{-6}$ M. 45

Figure 19. Fluorescence emission spectra of phenolic standard solutions in water: (a) excitation wavelength 275 nm syringic acid (1), gallic acid (2), phenolic standard solution (3); (b) excitation wavelength 275 nm ferulic acid (1), phenolic standard solution (2), caffeic acid (3), vanillin (4); (c) excitation wavelength 325 nm ferulic acid (1), caffeic acid (2), phenolic standard solution (3), vanillin (4).....45

Figure 20. Fluorescence excitation spectra of phenolic standard solutions in water: (a) syringic acid Em 360 nm (1), gallic acid Em 350 nm (2), phenolic standard solution Em 350 nm (3); (b)

ferulic acid Em 410 nm (1), caffeic acid Em 420 nm (2), phenolic standard solution Em 415 nm (3), vanillin Em 420 nm (4). 46

Figure 21. 2D fluorescence emission-excitation spectral map of phenolic standard solution in water.....47

Figure 22. Spectra of sample MP1I in water/methanol (4:1) v/v (1); quinine sulfate dihydrate in 0.5 M sulfuric acid, $2.5x10^{-7}$ M (2); ferulic acid in water, $2x10^{-6}$ M (3); anthracene in ethanol, $6x10^{-6}$ M (4): (a) absorption spectra, (b) fluorescence emission spectra at excitation wavelength 325 nm. 48

Figure 23. Spectra of extra virgin olive oil in isooctane with concentration 0.92 (1), 1.10 (2), 1.37 (3), 1.83 (4), 3.03 (5), 9.17 (6) μg/mL: (a) absorption spectra; (b) fluorescence emission spectra at excitation wavelength 400 nm; (c) fluorescence excitation spectra at emission wavelength 670 nm; (d) calibration curve showing the effect of concentration of extra virgin olive oil in isooctane on the emission intensity of chlorophyll *a* at 670 nm. 54

Figure 24. Fluorescence emission spectrum of chlorophyll *a* extracted from 500 mg ceramic using isooctane at excitation wavelength 400 nm.....55

Figure 25. Spectra of artificially aged phenolic standard solution in water: (a) absorption spectrum; (b) fluorescence emission spectra at excitation wavelength 275 nm (1), 300 nm (2), 325 nm (3); (c) fluorescence excitation spectrum at emission wavelength 360 nm; (d) 2D fluorescence emission-excitation spectral map.....58

Figure 26. Spectra of artificially aged extra virgin olive oil in isooctane: (a) absorption spectrum; (b) fluorescence emission spectra at excitation wavelength 275 nm (1), 300 nm (2), 400 nm (3); (c) fluorescence excitation spectra at emission wavelength 350 nm (1), 420 nm (2); (d) 2D fluorescence emission-excitation spectral map. 59

List of Tables

Table 1. Overview of fluorescent organic residues present in intact food, wax, and bone materials, reproduced from Christensen et al. (2006). 6

Table 2. Overview of inherent fluorophores present in food systems and artworks and their fluorescence properties. 8

Table 3. List of fluorescent stains for organic residue tagging. 10

Table 4. Transmittance units calculated from given absorbance units. 15

Table 5. Optimal linear and exponential regression curve of the data points in Figure..... 19

Table 6. Excitation wavelength, Raman scattering wavelength and difference between them. Data retrieved from Fig. 13. 22

Table 7. Scan parameters for acquisition of 2D spectral maps, absorption, emission, and excitation spectra. 26

Table 8. Molecular formulae, molecular weights, excitation and fluorescence properties of anthracene, quinine sulfate, and tryptophan (Dixon et al., 2005). Underlined numbers indicate excitation or emission maxima. 29

Table 9. Molecular formulae, molecular weights, excitation and emission maxima of fluorescence spectra of several phenolic compounds in water (Rodriguez-Delgado et al., 2001). 30

Table 10. Archaeological samples collected from ancient Minoan potsherds. 31

Table 11. Biomarkers from ancient Minoan potsherds detected by NMR spectroscopy..... 36

Table 12. Fluorescence quantum yields of quinine sulfate, anthracene, and ferulic acid. 47

Table 13. Absorbance at 325 nm and fluorescence emission intensity of sample MP1I in H_2O/MeOH (4:1) v/v and reference standards quinine sulfate dihydrate in 0.5 M H_2SO_4, anthracene in ethanol, and ferulic acid in water. 48

Table 14. Concentration of fluorophores in sample MP1I in H_2O/MeOH (4:1) v/v using quinine sulfate, anthracene, and ferulic acid as reference fluorophores. 49

Table 15. Analytical protocol for cleaning, spiking and recover organic residues from ceramic fragments..... 53

Abbreviations

cw	continuous wave
FT-IR	Fourier-transform infrared
GC	gas chromatography
LC	liquid chromatography
LIF	laser induced fluorescence
MALDI	matrix-assisted laser desorption/ionization
MS	mass spectrometry
NAD	nicotinamide adenine dinucleotide
NIR	near-infrared
NMR	nuclear magnetic resonance
PMF	peptide mass fingerprint
PMT	photomultiplier tube
Q	quadrupole
SERS	surface-enhanced Raman scattering
TOF	time of flight
UV	ultraviolet
Vis	visible
λ_{emi}	emission wavelength
λ_{exc}	excitation wavelength

CHAPTER 1: Bio-organic Residues in Archaeological Science

1.1 Classes of Bio-organic Archaeological Residues

Archaeometry is a burgeoning research domain that combines analytical methods to obtain the most information possible concerning materials from fragile artefacts. Archaeological residue analysis is a field of archaeometry that develops since the beginning of the 20th century (Gill, 1906) while organized research started in the early 1980s. Organic residue analysis provides a holistic understanding of everyday utilitarian artefacts such as textile, cosmetic, houseware, artwork, and hunting weapon.

Bio-organic archaeological residue is an umbrella term that refers to a set of amorphous organic materials present in artefacts. Organic residues could be remnants of the original content of a vessel or parts of the vessel itself (e.g. surface sealant, decorating material, adhesive) and are commonly absorbed within the walls or adhered to the surface of a ceramic vessel or a stone tool (Scheme 1). Organic residues can be also found within bone, wood, and textile. Resin, bitumen (natural asphalt), and tar vastly survive as visible surface deposits and their study usually involves microscopic analysis. This research approach is proved to be ambiguous, considering the objective interpretation of residues based solely on their morphological patterns (Monnier et al., 2012).

Scheme 1. Encrusted residues adhered to potsherds. Adapted from Historic England (2017a).

Archaeological biomarkers are compounds that indicate the content or the past usage of an artefact. In order to gain this information, the preserved biomarkers should link to natural products, for example resin and bitumen originate from plant, honeybee and milk from animal, dairy product and wine associate with human activity (Craig et al., 2000; Roffet-Salque et al., 2015). Organic archaeological biomarkers may belong in a wide variety of chemical substances

such as nucleic acid, protein, lipid, sugar, and carbohydrate. Among these biomarkers, lipids endure the most during degradation processes over long timescales due to their hydrophobic nature. Triacylglycerols account for about 95% of lipids in human diet, including meat, fish, and dairy products. Resin, bitumen, and tar comprise the main lipid forms in non-dietary products such as cosmetic, medicine, and sealant.

An example of marine fat biomarker is ω-(*o*-alkylphenyl)alkanoic acid that is formed when polyunsaturated fatty acids are heated at 270°C within a clay matrix. ω-(*o*-Alkylphenyl)alkanoic acids of C_{18} and C_{20} are produced during thermally-induced reactions when heating triunsaturated fatty acids, that are found in marine tissues. Thus, ω-(*o*-alkylphenyl)alkanoic acids provide evidence and act as biomarkers for the processing of marine animal fats (Evershed et al., 2008; Hansel et al., 2004). Another example is terpane polycyclic alkanes that comprise the most common class of bitumen biomarkers (Connan, 1999).

The detection and characterization of organic archaeological residues sheds light on the dietary habits, the storage and processing of foodstuffs depending on vessel type, the trade activity, the ancient rituals, and the domestication of animals and plants among ancient people. It is essential to consider information about archeozoological and archaeobotanical context of the region and period from which archaeological samples originate, thereby deducing meaningful interpretations by applying organic residue analyses. A statement claims that 'absence of evidence is not evidence of absence' and this alludes to the cautious interpretation of the archaeological findings. In the context of organic residue analysis, one should ascertain that the results remain unbiased from sensitivity of analytical methods before concluding the lack of organic remains.

Among the principal analytical methods to identify and characterize lipids from archaeological record, chromatographic techniques gas chromatography (GC) coupled with mass spectrometry (MS). When evidence is based solely on GC-MS profiles, the classification of lipids is constrained to animal, plant, or marine origin (Stacey, 2009). Identified sterols in artefacts are possible to reveal the origin of the substances from: animal (zoosterols such as cholesterol), plant (phytosterols such as stigmasterol), and fungi (mycosterols such as ergosterol) (Rosial et al., 2020).

Current radiocarbon dating shows that the invention of ceramic fabric initiated around 18000 BCE (Late Pleistocene) in East Asia (Wu et al., 2012). It is rather possible that pottery vessels were originally used to store subsistence foodstuffs or to conduct ancient rituals; the use of vessels for culinary purposes developed afterwards (Craig et al., 2013). Ceramics are silicate-containing materials that consist of crystalline and amorphous phases. Organic residues can survive over archaeological time inside the voids (pores) of ceramics or on the surface of clay particles in soils (Scheme 2). The burial conditions seem more decisive in enabling biomarker survival compared to the burial time span. There is evidence that small ceramic pores inhibit the entry of microorganisms and hydrolytic enzymes, protecting thus partially the organic residues from degradation and dissolution (Mayer, 1994). Also, arid and anoxic burial sites

have been shown to favor the preservation of organic residues (Regert et al., 1998). An arid site inhibits hydrolysis processes whilst an anaerobic environment prevents organic residues from microbial attacks.

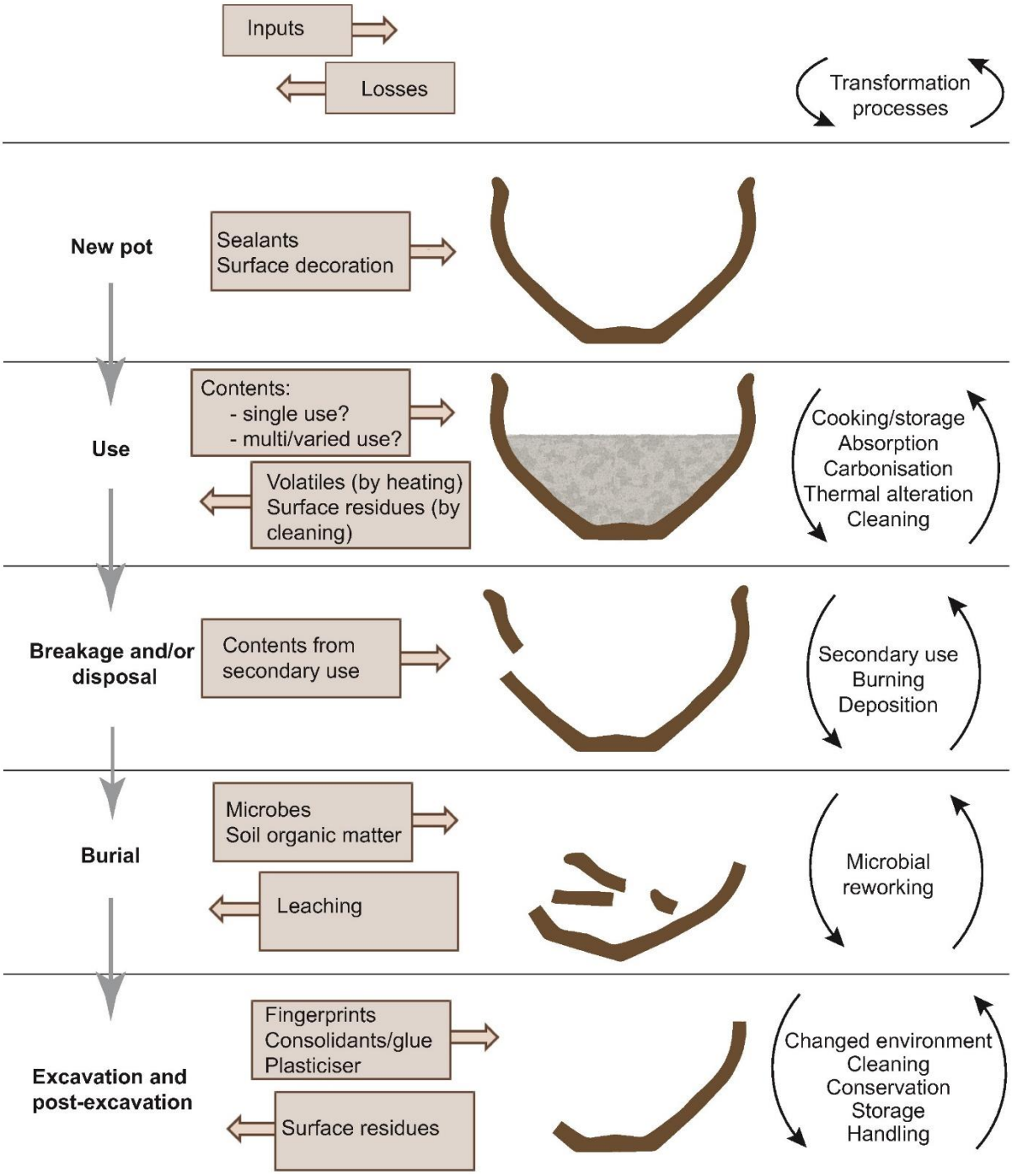

Scheme 2. Main input, loss, and transformation processes of organic residues occurring during usage, interment, and post-excavation handling of ceramic vessels. Reproduced from Roffet-Salque et al. (2017).

The planning process of an archaeological project could start by addressing the questions that organic residue analysis intends to reply. Then researchers could propose possible scenarios

and examine their accuracy by carefully designed experiments. The selection of analytical methods that would study the organic residues relies on the research questions to be tackled. It is crucial to follow a proper sampling protocol that minimizes the risk of sample contamination. Also, cautious sample handling, which involves experimental measurements and storage, could give the opportunity for future analyses (Historic England, 2017a; Historic England, 2017b).

Challenges arise from the reliable recognition of archaeological organic residues when they are present in trace amounts and need to be separated from similar-structured contaminants of modern origin such as compounds from sun screens and pesticides. Squalene and cholesterol have been recognized as surface lipids on human skin (Scheme 3). Squalene is probably unlikely to survive over time, considering its susceptibility to degrade owing to the large number of double bonds it contains. Thus, when both squalene and cholesterol are identified in archaeological materials, they should possibly be ascribed to post-excavational contamination due to handling rather than to preserved residues (Evershed, 1993). One common way to assess contamination is to examine the soil from the burial site and the exterior surface of the studying potsherds. If organic residues are present neither in the soil nor in the exterior part of the sherd, the identified residues in the interior surface can be reported of archaeological origin.

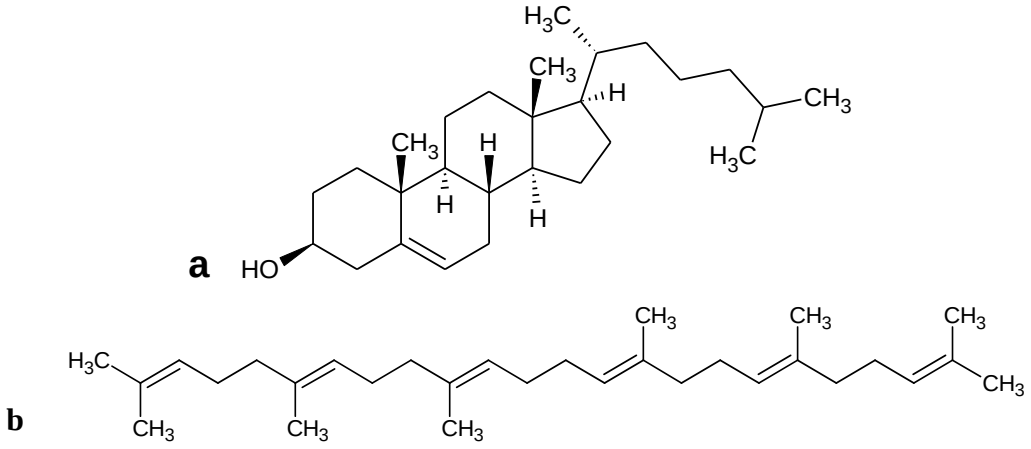

Scheme 3. Structures of the most common post-excavation lipid contaminants due to handling: (a) cholesterol and (b) squalene.

It is recommended that surface layers suspicious for contamination should be removed from archaeological artefacts (Heron et al., 1991). As a rule of a thumb, the washing or soaking of sherds should be avoided during post-excavation treatment, since it is likely to remove organic residues.

Crucial questions still remain regarding the nature of organic residues. For example, do residues from ceramic potsherds indicate the first, the last, or the overall use of an artefact? How exactly does the extent of pot exposure to fire and the presence of metal ions (cooper, iron) within the clay affect the preservation of organic materials? Also, what are the optimal conditions in terms of local climate, pH, water content, and chemical composition of soil at the burial site that enhance the preservation of organic residues? Future research should illuminate

these issues in order to enrich our understanding of ancient lifestyles (Steele, 2013).

1.2 Effect of Cooking and Natural Aging in Protein Residue Preservation-likelihood

Organic residue loss and distortion processes initiate when the holding vessels are utilized in the quotidian (cooking, cleaning) and maximize during burial. Protein residues in particular are subjected to degradation pathways that can be divided into three main types: (1) biological deterioration, that is microbial attack, (2) chemical deterioration, and (3) Maillard reaction between amino acids and sugars during cooking. All these alterations affect proteinaceous material survival and identification within archaeological contexts. Protein residues from potsherds were for long debatable whether they can persist over archaeological timescales due to their hydrolysable nature (Evershed and Tuross, 1996).

Proteinaceous materials are susceptible to microbiological digestion that results in loss of protein residues (Barnard et al., 2007). Briefly, microbiological enzymes from the soil fragment the polypeptide chains and thus impede their preservation in the context within archaeological periods. Protein residues may undergo different chemical degradation processes: (1) deamidation: a non-enzymatic reaction that occurs in asparagine (Asn) and glutamine (Gln) residues and results in dissociation or displacement of the amide functional group. Leo *et al.* (2011) reported that deamidation of Asn is up to 10 times more expeditious than that of Gln and suggested that the extent of Gln deamidation can be exploited to determine the age of a historical object; (2) decarboxylation: eliminates a carboxyl group from an amino acid and releases carbon dioxide. Decarboxylation of all amino acids is slower in the absence of oxygen, for example during interment (Bada, 1991); (3) racemization: a post-mortem transformation of L-amino acids into their D-enantiomers. Racemization of aspartic acid residue in proteins increases with time and can be thus utilized for estimation of the age of a sample (Bailey et al., 1998); (4) hydrolysis: destructs the peptide bonds, producing small peptide fragments and free amino acids that can leach out from the holding matrices; (5) cross-linking: a non-enzymatic reaction that includes covalent or ionic bonds between polypeptide chains, often catalysed by transition metals (Boatman et al., 2019); (6) aggregation: encompasses hydrogen bonds and hydrophobic interactions among proteins.

Maillard reaction (also known as non-enzymatic browning) commonly describes the condensation of a sugar with the free amino moiety of a protein's side chain that occurs during food processing, chiefly heating (glycation reaction). Scheme 4 shows that the amino-carbonyl reaction forms a Schiff base and ultimately yields dark-colored polymers known as melanoidins after a series of rearrangement reactions (Ames, 1992). Although by-products of Maillard reaction toughens the identification of paeleo-proteins, they also favor the preservation of protein residues by hindering hydrolysis of peptide bonds and microbial digestion (Baker et al., 2012).

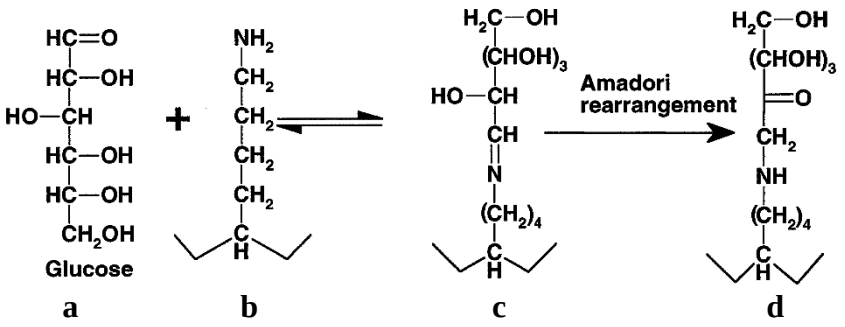

Scheme 4. Maillard reaction between D-glucose (a) and L-lysine (b) to form N-glucosylamine (c) (Schiff base) and ultimately aminodeoxyketose (d) via Amadori rearrangement. Adapted from Bailey et al. (1998).

1.3 Fluorescent Biomarkers

In the context of bio-organic residue analysis, fluorescence spectroscopy provides fast-screening of samples via rapid detection of fluorescent biomarkers that are present in food systems, colorants, cosmetics, and textiles. Fluorescence studies of intact food have been extensively reported in literature for quality control of foodstuffs. As an introduction to autofluorescence, i.e. intrinsic fluorescence, of food constituents, Table 1 lists several fluorophores inherent in intact food samples. In particular, fluorescence studies of both meat and fish are dominated by the autofluorescence of NADH and different types of collagen present in adipose and connective tissues (Christensen et al., 2006). The intrinsic fluorescence of dairy products and milk is assigned to NADH, proteins albumin and casein and, vitamins A (retinol) and B_2 (riboflavin) (Becker et al., 2003; Dufour and Riaublanc, 1997). Edible oils are broadly categorised into olive, pomace, linseed, corn, and sunflower oils. In general, neat edible oils display fluorescence landscapes due to the presence of riboflavin, α-tocopherol, polyphenols, and chlorophylls *a* and *b* (Guimet et al., 2004).

Table 1. Overview of fluorescent organic residues present in intact food, wax, and bone materials, reproduced from Christensen et al. (2006).

Biomaterial	Fluorescent organic residue
Animal glue	Protein (collagen)
Beeswax	Flavonoid / Resin
Bone	Protein (collagen / keratin / osteocalcin)
Dairy products / Milk	NADH / Protein (casein / albumin) / Vitamin (A / B_2)
Edible oil	Vitamin (B_2 / E) / Polyphenol / Chlorophyll
Fish	NADH / Protein (collagen)
Meat	NADH / Protein (collagen)

Fluorescence studies are also conducted in bone and wax samples. In the case of bone analysis, the fluorescence is exhibited due to the presence of proteins collagen, keratin, and osteocalcin (Fratzl and Weinkamer, 2007). In the latter case of wax, emission is mainly due to flavonoids and resins (Connan, 1999).

Fluorophores are broadly categorized into intrinsic and extrinsic. Intrinsic are called the natural-occurring fluorophores such as aromatic amino acids, flavonoids, vitamins, carotenes, and chlorophylls. Whereas, extrinsic fluorescent probes are used to label non-fluorescent molecules of interest or to enhance the signal of poorly fluorescent fluorophores. Among exogenous fluorophores, dansyl chloride, fluoresceins, and rhodamines are the most favored.

1.3.1 Intrinsic

Intrinsic fluorophores are those that occur inherently in nature and embrace a diverse range of biomolecules such as nicotinamide adenine dinucleotide in its reduced form (NADH), proteins, and vitamins. Table 2 gives an overview of the fluorescence properties of intrinsic fluorophores preset in natural systems. Proteins exhibit intrinsic fluorescence due to the three aromatic amino acids: tryptophan, tyrosine, and phenylalanine. Aromatic amino acids contribute unequally to protein fluorescence: Tryptophan residues have the highest quantum yield (0.20) compared with tyrosine (0.14) and phenylalanine (0.04) (Nevin et al., 2008a). Furthermore, emission of tyrosine and phenylalanine is often quenched by the local environment. For these reasons, tryptophan emission often dominates the overall fluorescence of proteins. Other intrinsic biomolecules include vitamins such as retinol, riboflavin, and α-tocopherol. In UV light, riboflavin degrades into lumichrome and lumiflavin (Scheme 5). Another class of fluorophores consists of phenolic acids, resins, and pigments.

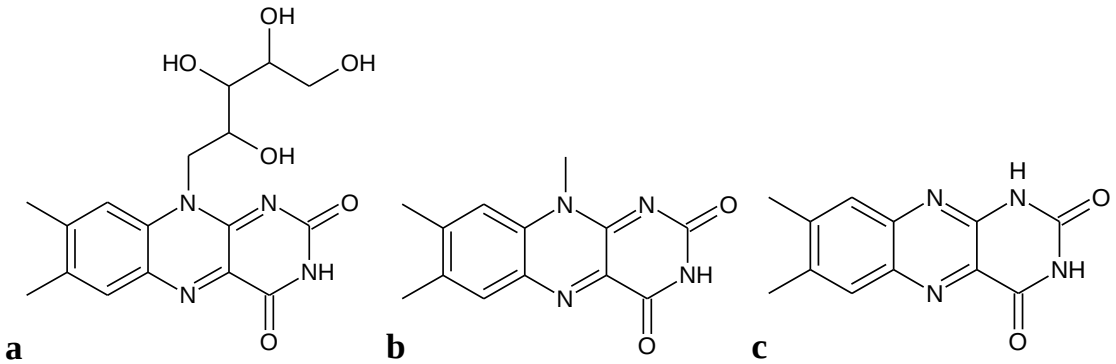

Scheme 5. Structures of: (a) riboflavin, (b) lumiflavin, (c) lumichrome.

Archaeological samples pose additional difficulties when one tries to interpret their fluorescence spectra compared to intact samples. Apart from naturally occurring fluorophores that indicate the original content, secondary fluorescent biomarkers that originate from degradation of intact fluorophores may contribute to the final fluorescence fingerprint. A large

Table 2. Overview of inherent fluorophores present in food systems and artworks and their fluorescence properties.

Organic residue	Fluorescent compound	λ_{exc} (nm)	λ_{emi} (nm)
Biomolecule	NADH[a]	340	455
Phenolic acid	Caffeic acid[b]	262	426
	Syringic acid[b]	278	360
Pigment	Chlorophyll *b*[c]	427/455/643	670
	Purpurin[d]	250/510	570
Protein	L-Phenylalanine[c]	247/252/258/263	280
	L-Tryptophan[c]	272/280/287	355
	L-Tyrosine[c]	275/280	303
Protein oxidation product	Dihydroxyphenylalanine[e]	355	480
	N-formylkynurenine[e]	355	440
	Dityrosine[e]	355	415
	Pentosidine[f]	248	385
	Maillard-reaction products[f]	360	440
Resin	Dammar[g]	UV region	455
	Pistacia[h]	UV region	550
Vitamin	Vitamin A (retinol)[d]	360	430
	Vitamin B_2 (riboflavin)[a]	263/345/450	530
	Vitamin E (α-tocopherol)[a]	205/293	325
Vitamin B_2 oxidation product	Lumichrome[a]	380	480
	Lumiflavin[a]	380	530

Data from (a) Sadecka et al., 2007, (b) Rodriguez-Delgado et al., 2001, (c) PhotochemCAD Database at www.photochemcad.com, (d) Ahmadi et al., 2014, (e) Nevin et al., 2006, (f) Nevin et al., 2008b, (g) Rene de la Rie, 1982, (h) Stern et al., 2008.

range of fluorescent degradation products of amino acids have been identified as a consequence of polymerisation and oxidative reactions. Among these products, dihydroxyphenylalanine, dityrosine, and *N*-formylkynurenine, as seen in Scheme 6, exemplify the fluorescent photooxidation products of phenylalanine, tyrosine, and tryptophan, respectively. (Nevin et al., 2006). In addition, glycation products, which are formed by Maillard reaction, attest the presence of proteins and sugars within an examining context. An example of such a fluorescent

product is pentosidine that is formed upon condensation of a free sugar (ribose) with free amino acids (arginine and lysine) (Dallongeville et al., 2016).

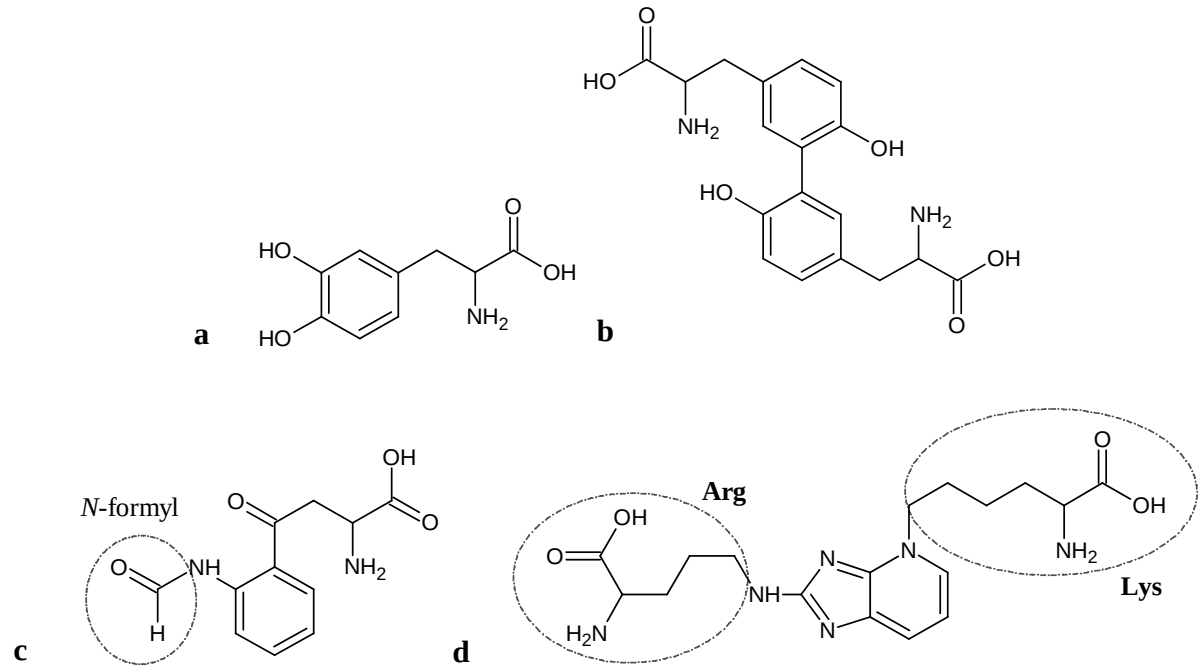

Scheme 6. Structures of: (a) dihydroxyhenylalanine (a phenylalanine photooxidation product), (b) dityrosine (a UV polymerisation product of tyrosine), (c) *N*-formylkynurenine (a tryptophan photooxidation product), (d) pentosidine (a glycation endproduct).

1.3.2 Extrinsic

Extrinsic probes selectively bind to organic residues enabling the detection of non-fluorescent molecules –lipids, polysaccharides, etc.– and the emission signal amplification of poorly fluorescent compounds. To accomplish these expectations, immunofluorescence microscopy employs fluorophore-labeled antibodies to identify specific proteins. For instance, the Sypro Ruby probe has been used to detect ovalbumin and phosphitin that are the most abundant proteins in egg white and egg yolk, respectively, facilitating the localization of proteinaceous binders used in tempera paintings (Sandu et al., 2012a). Another example is dansyl chloride that has been used to label bovine serum albumin (BSA) by forming a covalent bond with lysine residues (Levi and Flecha, 2003).

Among lipophilic dyes cited in the literature, Nile Blue, Oil Red O, and Sudan Black B have been shown to stain lipids present in oil paints. In particular, Nile Blue offers the ability to differentiate neutral lipids (acylglycerols, steroids), which stain pink, from acid lipids (fatty acids, phospholipids), which stain blue (Sandu et al., 2012b).

Several stains have been used in archaeological residue studies for detecting non-fluorescent remnants. For example, the Congo Red dye has been used to stain cellulose and starch residues

in cooked starch grains found on stone artefacts from Aboriginal communities in Australia (Lamb and Loy, 2005). In alkaline conditions, Congo Red stains amyloid fibrils (protein), whereas at a neutral pH it binds to cellulose and starch (carbohydrate) that are not inherently fluorescent (Yakupova et al., 2019). Another example of extrinsic probe is Picro Sirius Red that has been employed to selectively stain Types I, II, and III collagen from archaeological samples (Stephenson, 2015). Table 3 lists several extrinsic probes that have been used to stain organic residues.

Table 3. List of fluorescent stains for organic residue tagging.

Organic residue	Fluorescent probe	Molecular structure
Lipid	Nile Blue[a]	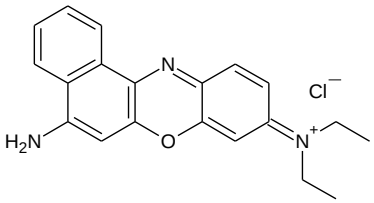
	Oil Red O[a]	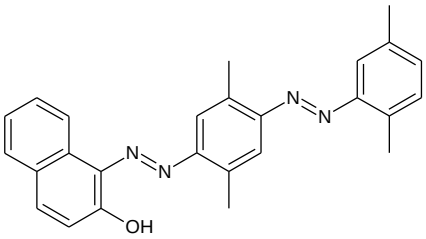
	Sudan Black B[a]	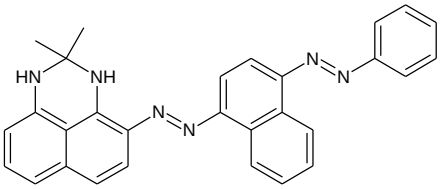
Polysaccharide (starch/cellulose)	Congo Red[b, c]	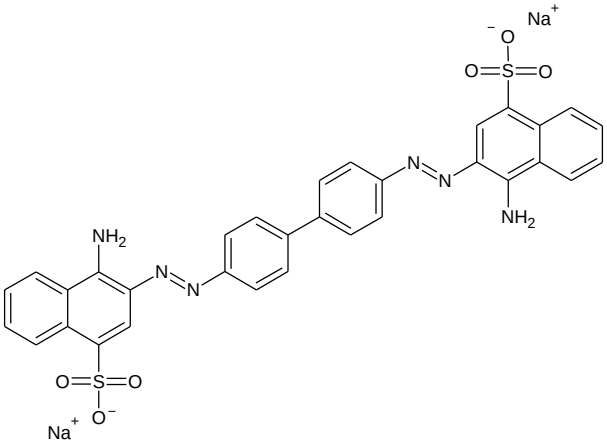

Protein	Collagen	Picro-Sirius Red (PSR)[d]	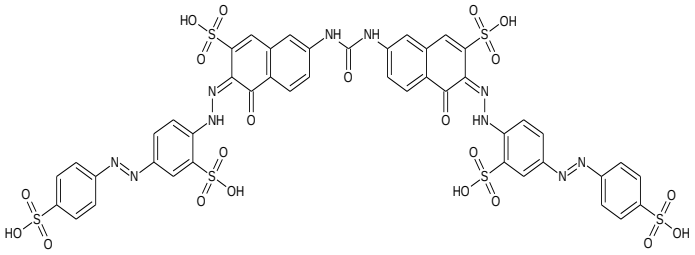
	Bovine serum albumin	Dansyl chloride[e]	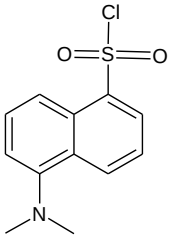
	Ovalbumin Phosphitin	Sypro Ruby[f]	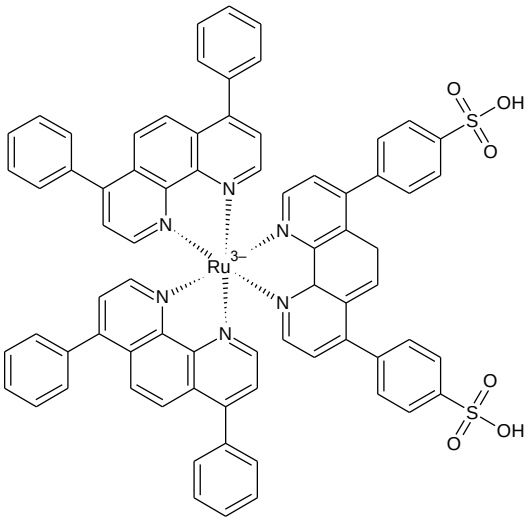

Data from (a) Sandu et al., 2012b, (b) Lamb and Loy, 2005, (c) Yakupova et al., 2019, (d) Stephenson, 2015, (e) Levi and Flecha, 2003, (f) Sandu et al., 2012a

CHAPTER 2: Spectroscopic Techniques for Archaeological Residue Analysis

2.1 Analytical Techniques in Archaeometry

The molecular study of bio-organic archaeological residues provides evidence to reconstruct agricultural, culinary, textile fabric, ritual, artistic, and trading practices of the past populations. The past three decades, organic residue analyses have chiefly employed liquid chromatography-mass spectrometry (LC-MS), gas chromatography-mass spectrometry (GC-MS), and pyrolysis-GC-MS to study the artefacts of interest. These analytical methods allow detection of organic materials down to nanogram levels and are thus considered as high sensitivity techniques (Roffet-Salque et al., 2017). They also empower separation of components in complex mixtures from more than one sources and chemical characterization of organic materials. Although, chromatography-based methods accomplish quantitative identification of proteins, lipids, and carbohydrates, they still demand expensive equipment, require elaborate sample preparation, and consume sample during analysis (Degano et al., 2018). As a consequent limitation, the use of these analytical methods limits the number of the investigating samples in a given timetable.

GC-MS permits separation and identification of organic materials –lipids resins, waxes, etc.– within ancient samples. Important studies were conducted, for example, on determination of natural substances processed in pottery vessels, including plant and animal fats. The identification of terpenoids points to plant resins that used in antiquity as sealants or ritual balms (Colombini et al., 2005), whilst the concomitant detection of palmitic acid ($C_{16:0}$), stearic acid ($C_{18:0}$), and odd-numbered carbon fatty acids may indicate degraded animal fats (Van de Velde et al., 2019). The distinction between ruminant (e.g. from goat, sheep, or cattle) and non-ruminant (e.g. from pig) fats is also feasible by stable carbon isotopic analysis with GC-combustion-isotope ratio mass spectrometry (GC-C-IRMS) (Matlova et al., 2017).

Pyrolysis coupled to GC-MS (Py-GC-MS) enables the identification of high molecular weight organic materials such as wax, resin, proteinaceous material, organic pigment, and dye (Heron and Stacey, 2000). The pyrolysed sample consists of a complex mixture of molecules, called pyrolysis products, which can be separated by GC and further detected by MS. Py-GC-MS has been applied in the field of cultural heritage to identify proteins and other materials in samples of unknown composition such as the study of mural paintings (Bonaduce and Colombini, 2003). Py-GC-MS has been also applied in the context of archaeological wood studies. For instance, it has been used to assess the quality of wood preservation in two Iberian shipwrecks originating from 16th to 18th century CE (Traore et al., 2017). The degree of wood preservation was evaluated by studying the pyrolysis products of polysaccharides (cellulose, hemicellulose)

and lignin (guaiacyl, syringyl lignin).

In the context of archaeo-residue analysis, fluorescence, Fourier transform infrared (FT-IR), nuclear magnetic resonance (NMR), and Raman spectroscopies are among the spectrochemical tools that require minimal sample preparation and offer fast-screening of samples investigated, enabling thus the analyst to classify the artefacts with detectable biomarkers. By applying these techniques first, one can promptly select artefacts that are most likely to yield promising results for the archaeological record and meticulously study them by high-end analytical techniques. Among these spectroscopic methods, for instance, fluorescence spectroscopy in conjunction with SERS has been used for the identification of proteins in egg yolk, egg white, and milk due to the intrinsic fluorescence properties of aromatic amino acids tyrosine, tryptophan, and phenylalanine (Philippidis et al., 2016). In particular, LIF has been used as a fast-screening method to study aged protein samples that are known to exhibit fluorescence owing to degradation products such as di-tyrosine, *N*-formylkynurenine (a tryptophan oxidation product), dihydroxyphenylalanine, and pentosidine (a glycation product) (Nevin et al., 2006). Although LIF is a rapid and non-invasive technique, it yet lacks specificity and thus provides a limited diagnostic potential for similar structured proteins.

Raman spectroscopy has been applied to investigate art and archaeological objects. The principal advantages of Raman spectroscopic technique are the non-destructive character due to low laser power and the opportunity for in situ investigation because of portable equipment. Within the archaeological context, Raman spectroscopy has been used to study pigments on rock and wall paintings, organic dyes on faience and pottery fragments, skin of mummified bodies, and human teeth (Vandenabeele et al., 2006). Moreover, ^{13}C NMR has been deployed alongside FT-IR spectroscopy to detect resinous materials (*Pistacia* resin and mastic) coming from the interior of a 1500-year-old Roman sarcophagus (Bruni and Guglielmi, 2014).

Pivotal research topics also include the detection, identification, and characterization of proteins in objects of cultural heritage using immunological and proteomics approaches. Immunological techniques are based on the use of labelled antibodies to detect the proteins of interest. Although these methods are sensitive and protein specific, they show a big drawback: the foresight of the peptides structure in question and the unpredictable effect of degradation phenomena, leading to false negatives (Barnard et al., 2007). For example, Nerlich et al. (1993) showed through immunohistochemical analysis that the mummification process preserves the genetic material as well as proteins over time by slowing down considerably their hydrolysis.

Proteomics methods, which are based on the use of advanced mass spectrometric tools, rely on the identification of ancient proteins by software-assisted comparison of experimental mass spectrometric data to theoretical mass spectra, calculated on the basis of the protein primary structure (Cappellini et al., 2018). The main limitation of this technique comes from the insolubility of ancient and degraded proteins, as well as on the still limited knowledge of degradation pathways at the level of the polypeptide chain (Hendy et al., 2018). Given the continuous implementation of instrumental features and bioinformatics tools, proteomics are gaining increasing success to the field of archaeological and paleontological research. An

example of an application is represented by a study based on microcapillary LC/MS/MS, that achieved to sequence collagen proteins derived from fossilized bones of a 68-million-year-old *Tyrannosaurus rex* dinosaur and a 0.16- to 0.60-million-year-old *Mammut americanum* mastodon via peptide fragmentation patterns (Asara et al., 2007). Liquid chromatography quadrupole time of flight mass spectrometry (LC-Q-TOF-MS) analysis was also used to study the protein modifications in the rib bone of a 13th century CE mummy unearthed in Verona, Italy (Miksik et al., 2016).

Peptide mass fingerprinting (PMF) is another mass spectrometric tool, belonging to the wider field of proteomics, for the analysis of proteins in historic artefacts and phylogenetic studies in the context of palaeontology. PMF uses digestive enzymes (e.g. trypsin) to cleave the proteins of interest in smaller peptides and then employs matrix-assisted laser desorption/ionization time of flight mass spectrometry (MALDI-TOF-MS) to record the so-called "peptide mass fingerprint". Materials identification is based on the comparison between the recorded spectra of the unknown compounds and cited spectra in libraries of reference materials (Kirby et al., 2013).

2.2 Absorption Spectroscopy

Measurement of light absorption is essential to gain insight into the optical density of molecules in a solution. In the context of molecular spectroscopy, spectral bands in absorption spectra stem from transitions within electronic, vibrational, and rotational energy levels. At a given frequency, the ratio of the intensity of transmitted beam, I, to the intensity of incident beam, I_0, is called transmittance, T, of the sample:

$$T = \frac{I}{I_0} \tag{2.1}$$

Beer-Lambert equation shows the dependence of molar extinction coefficient, ε (in $cm^2\ mol^{-1}$), optical pathlength, b (in cm), and molar concentration of absorbing molecules, C (in mol cm^{-3}), on transmitted intensity:

$$I = I_0 \times 10^{-\varepsilon bC} \tag{2.2}$$

Rearrangement and integration of equations 2.1 and 2.2 as well as introduction of absorbance term, A, yields an alternative form of Beer-Lambert law:

$$A = -\log T = \varepsilon bC \tag{2.3}$$

Table 4 shows the application of Beer-Lambert equation in terms of absorbance and transmittance units.

Table 4. Transmittance units calculated from given absorbance units.

Absorbance	% Transmittance
0.10	79%
0.20	63%
0.49	32%
1	10%
2	1%

The following expression describes the Beer-Lambert law when the base of the logarithm is converted to constant e:

$$A = -\log(T) = -\log(2.72)\ln(T) = -0.43\ln(T) \tag{2.4}$$

Relative error in absorption, which is also called photometric error, can be calculated by differentiating the equation 2.4:

$$dA = -0.43\frac{dT}{T} \tag{2.5}$$

Dividing both sides of the equation 2.5 by absorbance term results in:

$$\frac{dA}{A} = -0.43\frac{dT}{AT} = 0.43\frac{dT}{\log(T)T} \tag{2.6}$$

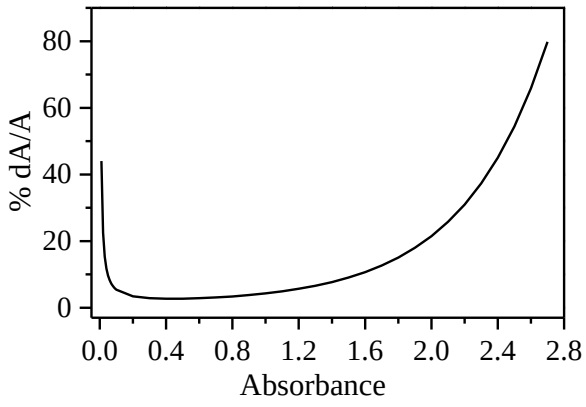

Figure 1. Effect of absorbance units on their relative error percentage.

If it is assumed that the transmittance absolute error is constant and equal to 0.01, then the photometric error percentage is given by the following equation:

$$\frac{\mathrm{dA}}{\mathrm{A}} \times 100 = \frac{0.43}{\log(\mathrm{T})\mathrm{T}} \times 0.01 \times 100 \tag{2.7}$$

Figure 1. shows that photometric error minimizes at 0.4 absorbance unit (2.7%) and is less than 5%, between 0.15 and 1.10 absorbance units.

2.3 Fluorescence Spectroscopy

A Jablonski diagram illustrates the molecular processes within electronic states that lead to luminescence (fluorescence and phosphorescence) and its deactivation (Scheme 7). The terms S and T refer to the singlet and the triplet electronic states, while the subscripts 0, 1, and 2 denote ground, first excited, and second excited states, respectively. According to the Frank-Condon principle, absorption of a photon occurs in 0.1–1 fs (Barnett and Francis, 2005) and results in promotion of a fluorophore to an excited vibrational level of S_1 or S_2. Then, the molecule rapidly relaxes until the lowest vibrational level of S_2 via a process called vibrational relaxation (VR). Due to overlapping of S_2 and S_1 vibrational levels, the excited fluorophore transits to vibrational levels of S_1 through a process denoted as internal conversion (IC). With a few rare exceptions, fluorescence emission is generated by the lowest energy vibrational state of S_1 causing the shape of emission spectra to be independent of excitation wavelength. This is known as Kasha's rule.

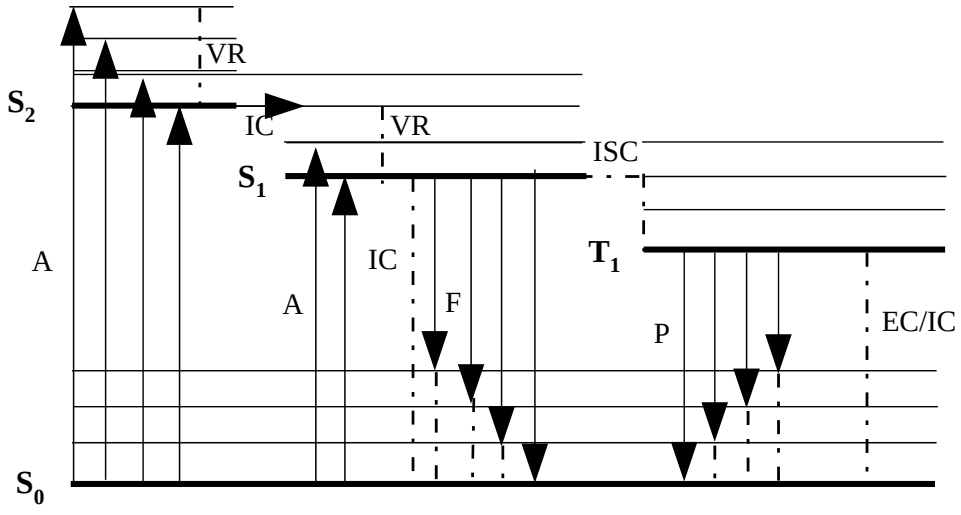

Scheme 7. Jablonski diagram for a hypothetical molecule. S_0 is the electronic ground state, S_1 and S_2 are the excited single states, T_1 is the excited triplet state, A is the absorption, F is the fluorescence, P is the phosphorescence, VR is the vibrational relaxation, IC is the internal conversion, ISC is the inter-system crossing, and EC is the external conversion.

Since fluorescence lifetime is considered as long (typically around 10^{-8} s), a molecule in the zeroth vibrational level of S_1 may undergo nonradiative deexcitation (internal conversion) to S_0 or inter-system crossing (ISC) to the first triplet state. Emission from lowest vibrational level

of T_1 is termed phosphorescence. Although inter-system crossing rate competes against fluorescence lifetime (both range from 10^{-10} to 10^{-7} s), a singlet-triplet transition is forbidden and thus 10^6 times less likely to occur compared to fluorescence emission (Lakowicz, 2006). Small energy difference between S_1 and T_1 and the presence of heavy atoms in a molecule (increases spin-orbit coupling) enhance the likelihood of inter-system crossing. Nevertheless, the long phosphorescence lifetime, which ranges from 10^{-4} to 10^2 s, facilitates the phosphorescence emission dissipation via collisional deactivation.

Steady-state fluorescence measurements rely on constant illumination of the sample and detection of the exhibiting fluorescence. Typically, molecules that contain highly conjugated π-electron systems exhibit detectable fluorescence properties. Molecules that contain fused aromatic rings, show increased capability to fluoresce as a result of the extended resonance. The presence of heteroatoms, however, leads to $n \rightarrow \pi^*$ transitions that result in inter-system crossing (singlet-triplet transitions) and decrease of fluorescence emission signal.

Fluorescence is prone to interactions between fluorophores and other species owing to long fluorescence lifetime and can thus be used to monitor molecular dynamics. Emission spectra depend on the chemical structure of the fluorophore, the solvent, the pH, and the temperature of the solution. The major advantage of fluorometric methods is their low limit of detection, typically down to 1 pM.

Stokes shift: The energy difference between maxima of fluorescence excitation, $(\tilde{\nu}_{exc})_{max}$, and emission, $(\tilde{\nu}_F)_{max}$, bands is termed Stokes shift (Eqn 2.8). It expresses the energy loss due to vibrational relaxation of a fluorophore from an excited vibrational level of S_2 or S_1 to the zeroth vibrational level of S_1. As a result of Stokes shift, absorption occurs at lower wavelengths than fluorescence emission.

$$\text{Stokes shift} = (\tilde{\nu}_{exc})_{max} - (\tilde{\nu}_F)_{max} \tag{2.8}$$

Figure 2 shows both excitation and emission spectra of *N*-acetyl-DL-tryptophan in water. In this case, Stokes shift is 75 nm.

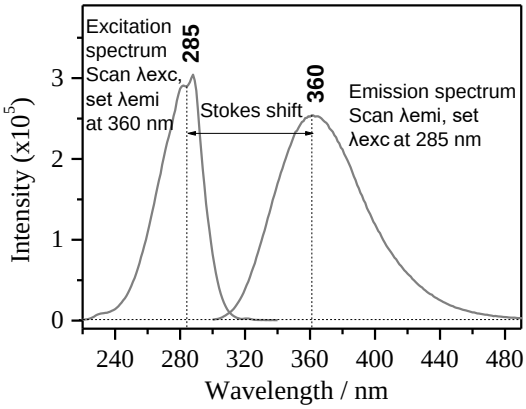

Figure 2. Fluorescence excitation and emission spectra of Ac-(DL)Trp-OH in water, 6×10^{-5} M.

Inner-filter effect: The intensity of fluorescence emitted light, I_F, is proportional to the intensity of incident beam, I_0, the quantum yield, Φ_F, the molar extinction coefficient, ε (in cm^2 mol^{-1}), the optical pathlength, b (in cm), and the concentration of fluorophores (in mol cm^{-3}):

$$I_F = 2.303\ \Phi_F I_0 \varepsilon b C \qquad (2.9)$$

Equation 2.9 indicates the linear relationship between concentration of fluorophores and intensity of exhibiting fluorescence. This linearity validates for diluted solutions, in which absorbance is less than 0.05 ($\varepsilon bC < 0.05$). In solutions with higher concentrations, the intensity of incident beam attenuates at the point of observation resulting in decrease of fluorescence intensity. This process is called primary absorption. If the absorption and emission spectra of a fluorophore overlap, part of fluorescence emission is absorbed by the analyte causing emission signal decrease and apparent shift of emission bands. This is known as secondary absorption or self-absorption. Both primary and secondary absorption are denoted as inner-filter effect.

Figure 3 shows the absorption and fluorescence spectra of tryptophan in water with different concentrations. The indole group of tryptophan residue is responsible for exhibiting fluorescence showing maximum absorption and emission at 280 and 360 nm, respectively. From saturation of fluorescence intensity, it is apparent that primary absorption becomes more important as concentration increases.

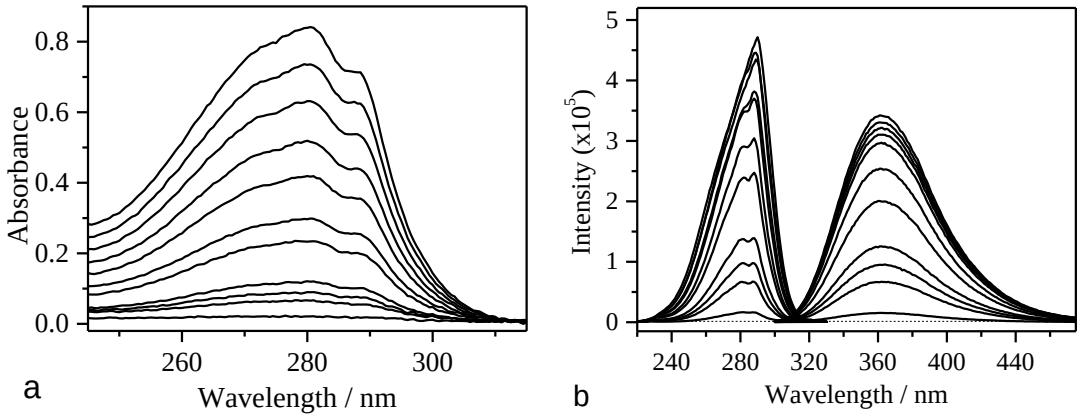

Figure 3. Spectra of Ac-(DL)Trp-OH in water with concentration ($x10^{-5}$ M) 0.2, 1, 1.4, 2, 4, 6, 8, 10, 12, 14, 16: (a) absorption spectra, (b) fluorescence excitation spectra at emission wavelength 360 nm and fluorescence emission spectra at excitation wavelength 280 nm.

Linear profile of Figure 4a validates the Beer-Lambert law for diluted solutions. Exponential profile of Figure 4b is due to the increasing importance of primary absorption. Plateau is reached because fewer molecules are being excited at the point of observation, i.e. centre of the cuvette, as absorbance increases.

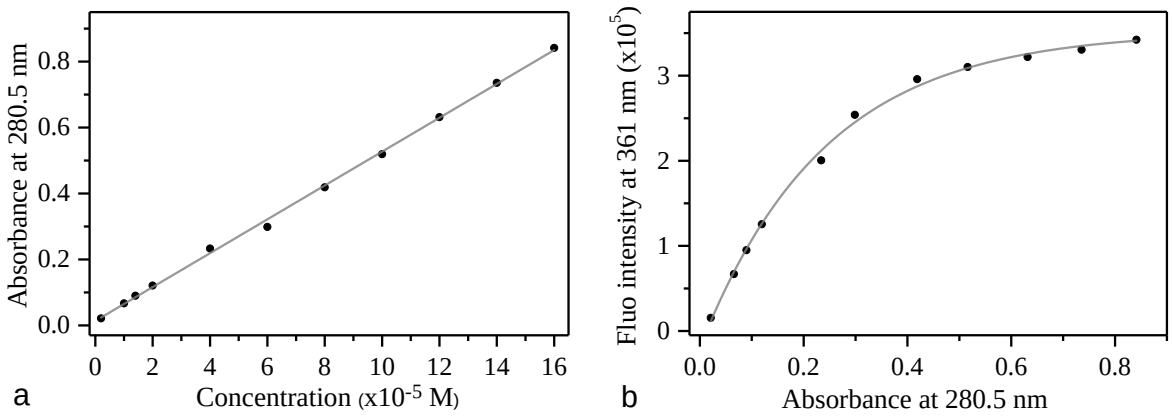

Figure 4. Effect of: (a) concentration of Ac-(DL)Trp-OH in water on the absorbance unit at 280.5 nm, (b) absorbance of Ac-(DL)Trp-OH in water at 280.5 nm on the fluorescence emission intensity at 360 nm.

Table 5. Optimal linear and exponential regression curve of the data points in Figure.

y = A·x + B		**y = C·e^(-x/D) + F**	
A	0.00513 ± 0.00006	C	–372218.3 ± 6443.3
B	0.013 ± 0.005	D	0.24 ± 0.01
		F	352241.9 ± 5893.7

Figure 5 shows the absorption, emission, and excitation profiles of anthracene in ethanol. The distinct bands are due to transitions within vibrational levels. As seen, anthracene has a peak at 376 nm which coincides in both absorption and emission spectra. This fluorescence peak shifts about 5 nm in solution $30x10^{-5}$ M, i.e. at 381 nm, while is missing in solution $300x10^{-5}$ M (Fig. 5b) as a result of secondary absorption effect. Note that absorption and fluorescence excitation spectra of anthracene solutions with concentration $30x10^{-5}$ M and $300x10^{-5}$ M are not displayed because they exceed absorbance unity and Beer-Lambert law is inapplicable.

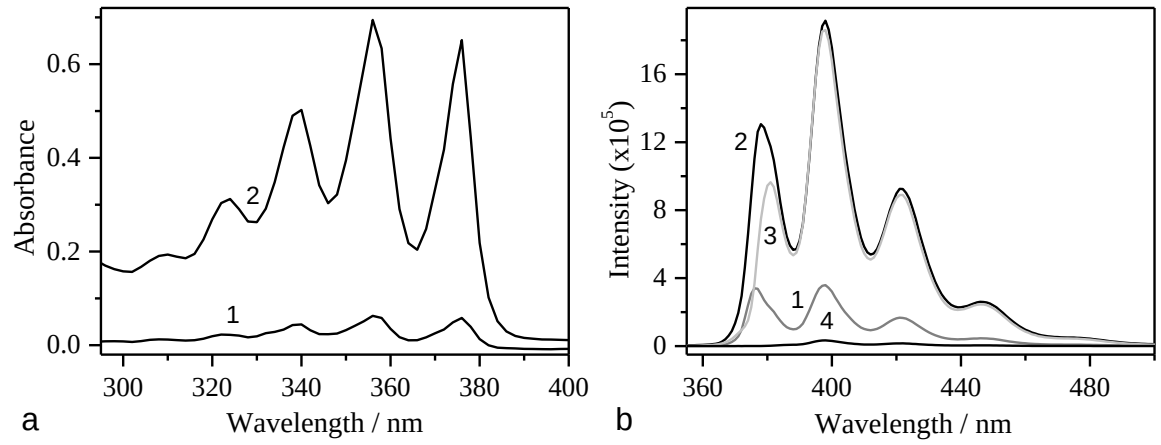

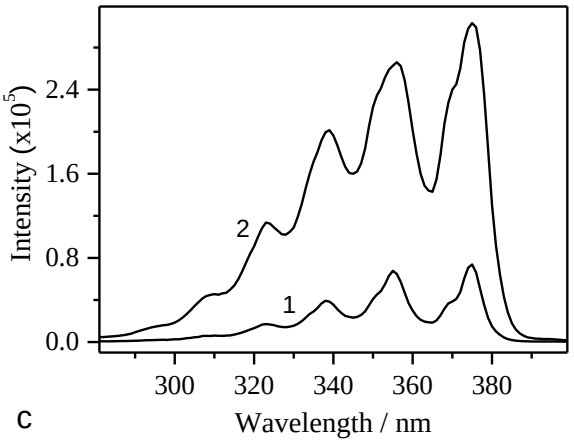

Figure 5. Spectra of anthracene in ethanol with concentration (x10^{-5} M) 0.3 (1), 3 (2), 30 (3), 300 (4): (a) absorption spectra, (b) fluorescence emission spectra at excitation wavelength 340 nm, (c) fluorescence excitation spectra at emission wavelength 420 nm.

Fluorescence quenching: So far it is explained how primary and secondary absorption decrease the fluorescence signal. Besides inner-filter effect, quencher molecules may inhibit the emission of fluorescence. The process of quenching requires interaction between the fluorophore and the quencher. Typically, fluorescence quenching refers to two types: dynamic and static. In dynamic quenching (collisional quenching), an excited fluorophore transfers its excess energy to other species. The energy-transfer demands a collision between the fluorophore and the quencher and leads to nonradiative processes. As dynamic quenchers may act electron-deficient groups, e.g. –COOH, $–NH_3^+$ and small molecules, e.g. oxygen, amines, etc. In static quenching, a fluorophore and a quencher molecule form a complex in the ground state. This binding prevents fluorophores from absorbing photons and solely unbound fluorophores emit radiation. An example of a static quenching process is the decrease of ethidium bromide's fluorescence signal by caffeine.

Fluorescence lifetime and quantum yield: Fluorescence lifetime, τ, and quantum yield, Φ_F, (quantum efficiency) are typical features of a fluorophore. The quantum yield is defined as the number of emitted photons to the number of absorbed photons (Eqn 2.10). The upper bound of quantum yield is the unity.

$$\Phi_F = \frac{\#\ \text{of emitted photons}}{\#\ \text{of absorbed photons}} \tag{2.10}$$

Fluorescence lifetime (Eqn 2.11) refers to the average time that a fluorophore lies in the excited electronic state before returning to the ground state. Both the emissive rate of the fluorophore and the rate of non-radiative decay depopulate the excited state and are abbreviated as Γ and k_{nr}, respectively:

$$\tau = \frac{1}{\Gamma + k_{nr}} \tag{2.11}$$

Effect of solvent Raman scattering in fluorescence spectra: A molecule can interact with light in three different ways: absorb, emit, or scatter a photon. In the case of scattered light, a molecule may scatter photons either elastically or in-elastically. In elastic scattering (also known as Rayleigh scattering), the scattered photons have the same frequency as the incident light. In-elastic scattering (or Raman scattering) involves scattering of a photon in lower energy (Stokes scattering) or higher energy (anti-Stokes scattering) compared to the incident photon frequency. Both Stokes and anti-Stokes lines are affected by the population of vibrational states involved in the transition. Since anti-Stokes scattering requires population of excited vibrational states, anti-Stokes lines are weaker compared with Stokes lines and are less likely to be detected in a fluorescence spectrum. Scheme 8 summarises the main interaction processes between light and molecules in a solution.

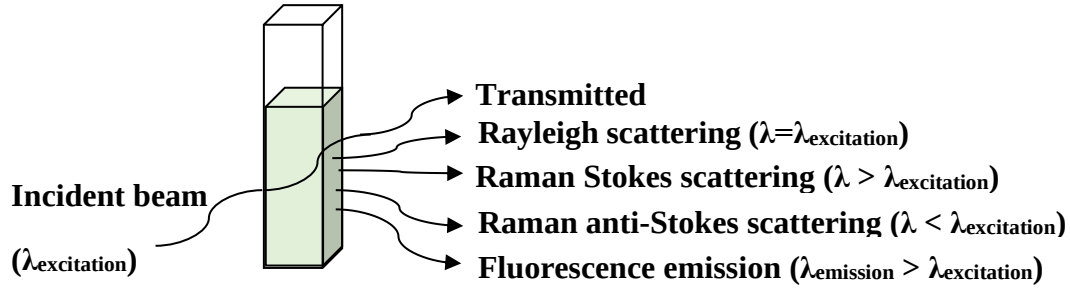

Scheme 8. Visual representation of fluorescence, elastic and inelastic scattering processes.

A Raman peak depends on incident frequency and thus shifts at different excitation wavelengths. Unlike Raman scattering, fluorescence emission is independent of incident frequency as a result of Kasha's rule. Hence, Raman artefacts can be identified by varying the excitation wavelength. An additional way to discriminate between Raman and fluorescence peaks is the fact that a Raman band is narrower compared to a fluorescence one. The frequency of a vibrational mode is termed absolute Raman frequency. Equation 2.12 shows how Raman shift, $\tilde{\nu}$, results from excitation, λ_{exc}, and Raman scattering, λ_{Raman}, wavelength:

$$\tilde{\nu} = \frac{1}{\lambda_{exc}} - \frac{1}{\lambda_{Raman}} \tag{2.12}$$

Differentiating the equation 2.12 yields:

$$d\tilde{\nu} = \frac{-1}{\lambda_{exc}^2} d\lambda \tag{2.13}$$

Equation 2.13 shows that the wavelength difference between scattered and incident photons is proportional to the second power of excitation wavelength. The intensity of Raman scattering, I_{Raman}, is proportional to the intensity of incident beam, I_0, and inversely proportional to the fourth power of excitation wavelength, λ_{exc} as shown in equation 2.12 (Demtroeder, 2008):

$$I_{Raman} \propto \frac{I_0}{\lambda_{exc}{}^4} \quad (2.14)$$

Figure 6 and Table 6 illustrate that scattered intensity is inversely proportional to the excitation wavelength and that the wavelength difference between scattered and incident light becomes bigger as excitation wavelength increases.

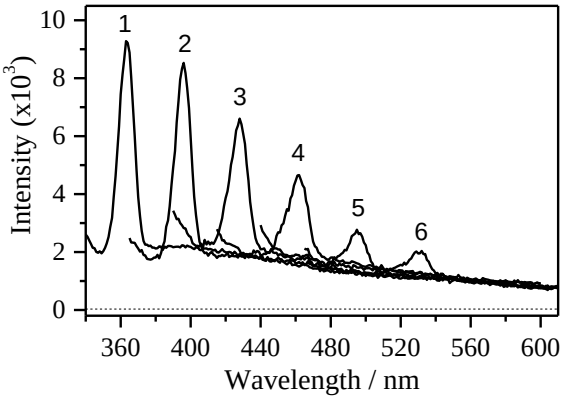

Figure 6. Raman scattering obtained from water/methanol (4:1) v/v at excitation wavelength (nm): 325 (1), 350 (2), 375 (3), 400 (4), 425 (5), 450 (6).

In Figure 6, the Raman peak generated by excitation at 350 nm corresponds to 3255 cm^{-1} Raman shift and is due to both water and methanol vibrational stretching in the O–H region. This is in agreement with the literature as the Raman peak of methanol at 3210 cm^{-1} has been assigned to O–H symmetric stretching (Iwaki and Dlott, 2000), whereas the Raman peak of water at 3375 cm^{-1} has been ascribed to O–H symmetric stretching (Auer and Skinner, 2008).

In case of unknown samples, Raman peaks may contribute to fluorescence spectra misinterpretation. An efficient method to eliminate Raman scattering interference is to record emission of pure solvent and then subtract it from the emission of fluorophore solution.

Table 6. Excitation wavelength, Raman scattering wavelength and difference between them. Data retrieved from Fig. 13.

λ_{exc} (nm)	λ_{Raman} (nm)	$\Delta\lambda$ (nm)
325	363	38
350	396	46
375	428	53
400	462	62
425	495	70
450	531	81

CHAPTER 3: Spectrometers and Methodology

3.1 Absorption and Fluorescence Spectrometers

The absorption study was carried out using a UV-1900 spectrophotometer (Shimadzu Corp., Japan) equipped with a deuterium and a 20 W tungsten-halogen arc lamp, single monochromator, and a photomultiplier tube. The optical setup of the spectrophotometer utilized is shown in Scheme 9.

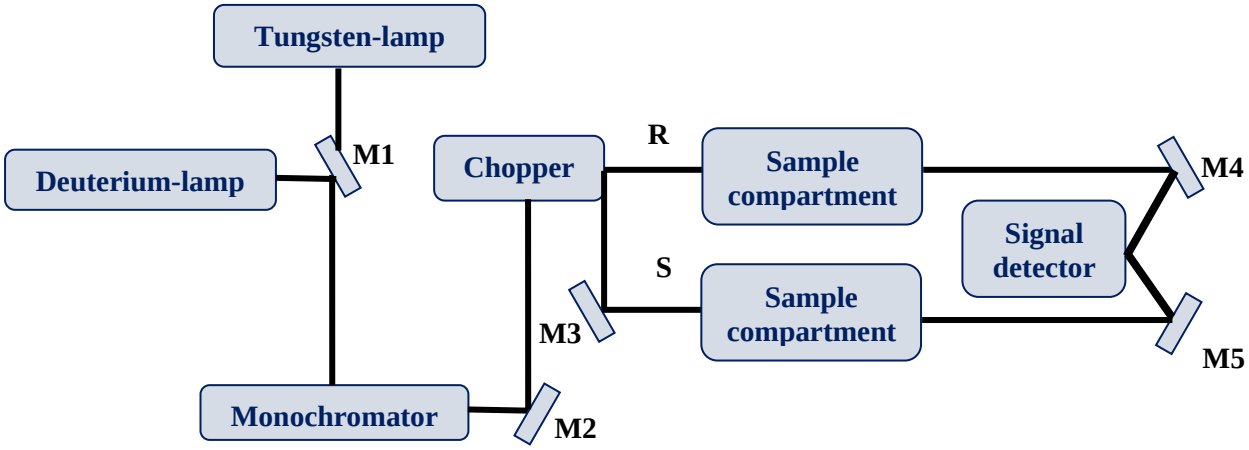

Scheme 9. Block diagram of a UV-1900 spectrophotometer optical setup (Shimadzu Corp., Japan). M: mirror, R: reference, S: sample.

Briefly, the main compartments of the spectrophotometer are: (1) illuminators: cw deuterium and tungsten-halogen arc lamps for ultraviolet and visible part of the spectrum. Both sources cover a wavelength range of 190–1100 nm. Mirror *M1* reflects radiation from one source at a time; (2) monochromator: Lo-Ray-Ligh, i.e. low stray light diffraction grating, that has the Czerny-Turner design with a grating containing 1200 grooves mm^{-1}, achieving a resolution of 1 nm; (3) chopper: splits the incident beam in two that enter the two sample compartments; (4) sample compartment: dimensions are 50 cm x 45 cm x 24 cm; (5) signal detector: a silicon photodiode. All optical components are coated with silica for increased durability. Spectrometer scans from higher to lower wavelengths to prevent samples from photo-degradation phenomena.

The fluorescence study was carried out on the basis of a FluoroMax®-P spectrofluorometer (JobinYvon Inc., USA), equipped with a 150 W xenon arc lamp, excitation and emission monochromator, and a photomultiplier tube (PMT) as a signal detector. The optical setup of the fluorescence spectrometer used for the purpose of this thesis is shown in Scheme 10.

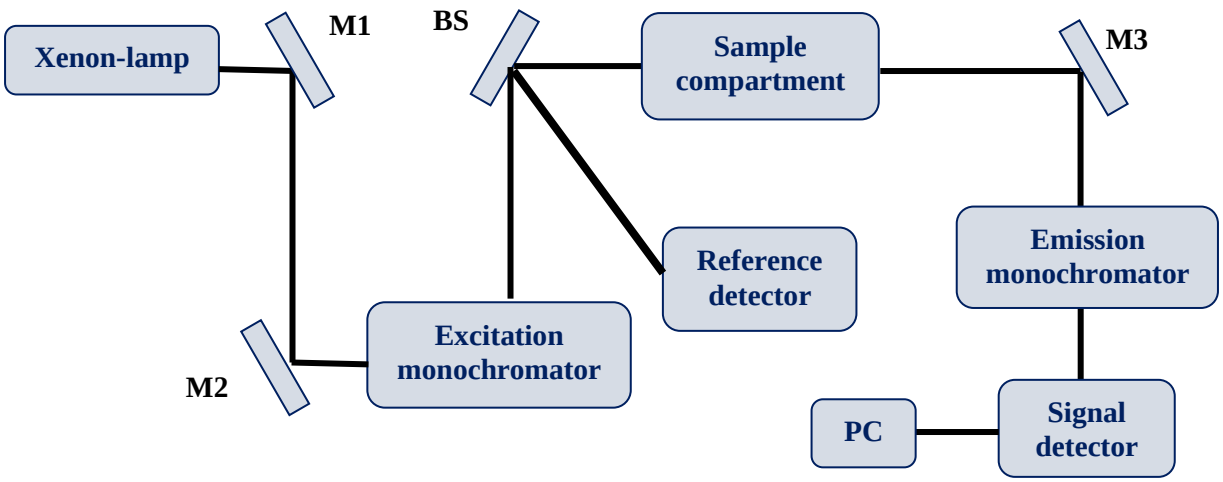

Scheme 10. Block diagram of a FluoroMax®-P spectrofluorimeter optical setup (JobinYvon Inc., USA). BS: beam splitter, M: mirror.

The basic compartments of the spectrofluorometer are: (1) illuminator: a continuous wave (cw) xenon arc lamp; (2) excitation and emission monochromators: have the Czerny-Turner design. Gratings contain 1200 grooves mm^{-1} and are coated with MgF_2 to prevent oxidation. Excitation and emission monochromator work effectively in the range of 220–600 nm and 290–850 nm, respectively. For both monochromators, slit widths of the entrance and exit ports can be adjusted by DataMax software; (3) reference detector: a photodiode that responds between 190 and 980 nm and corrects wavelength- and time-dependent output of the Xenon arc lamp. A beam splitter transfers 8% of excitation light to reference detector; (4) sample compartment: hosts detachable accessories for solid- and liquid-sample holders; (5) signal detector: a R928P photomultiplier tube that responses in the wavelength range 180–850 nm with linear response up to 4×10^6 counts per second (cps) (Horiba group, 2001).

Stray light is the radiation that reaches the detector when no sample is placed in the sample compartment. It is probably due to imperfect insulation of the spectrometer from the ambient light or scattering of excitation photons by particles in the gas-phase present in the sample compartment. In the spectrofluorometer setup used for the purpose of this thesis, stray light, i.e. background signal, was measured to have an intensity of 500 counts independent of excitation and emission wavelengths.

Bandpass slit determines the wavelength range that passes through a monochromator. For example, if one records a fluorescence emission spectrum at excitation wavelength 350 nm and sets bandpass slit for excitation monochromator at 4 nm, then only photons of wavelength range 348–352 nm will pass through the excitation monochromator and reach the sample. Equation 3.1 shows the relationship between bandpass, slit width and dispersion of excitation light.

$$\text{Bandpass slit (in nm)} = \text{Slit width (in mm)} \times \text{Dispersion (in nm mm}^{-1}\text{)} \qquad (3.1)$$

where dispersion is 4.25 nm mm^{-1} for gratings with 1200 grooves mm^{-1}.

The increase of slit width of emission monochromator rises the intensity of fluorescence signal at a cost to spectral resolution. Fig. 7a shows that spectral resolution of emission signal declines, that is broadening of fluorescence peaks, as the bandpass of emission monochromator increases. Fig. 7b illustrates the linear correlation between the intensity of fluorescence signal and the bandpass of emission monochromator.

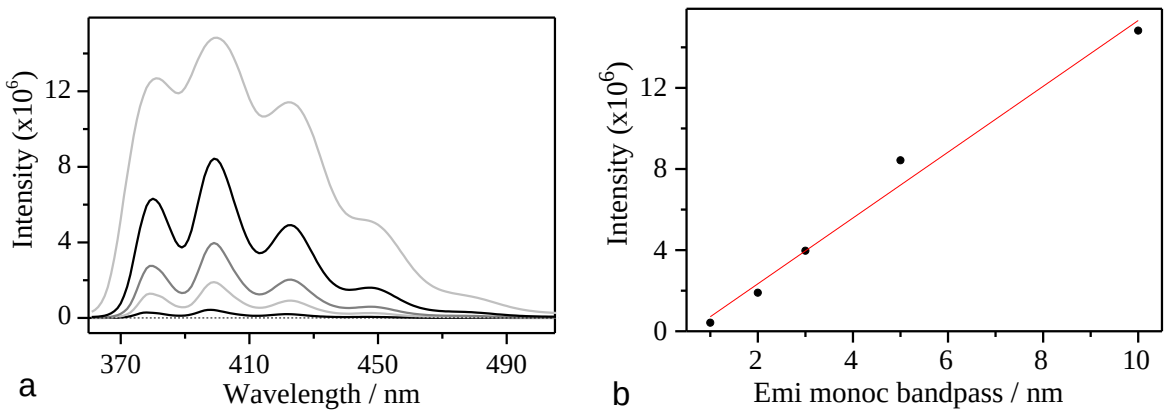

Figure 7. Anthracene in ethanol 3×10^{-5} M at excitation wavelength 340 nm: (a) Fluorescence emission spectra, incident beam bandpass 1 nm, and fluorescent beam bandpass (nm): 1, 2, 3, 5, 10; (b) effect of fluorescent beam bandpass on fluorescence emission intensity at 400 nm.

FluoroMax®-P enables to construct a 2D spectral map through the Matrix scan mode. To this end, the spectrometer runs a number of emission scans within a defined wavelength range that corresponds to a series of different excitation wavelengths. The software DataMax allows the automatic correction of 1st and 2nd order Rayleigh scatter of incident light.

3.2 Absorption and Fluorescence Measurements Procedure

Absorption and fluorescence studies of solutions were conducted using a quartz cuvette, since quartz materials are transmittable to UV radiation. The solutions were placed in a four-window quartz optical cell with 10 mm pathlength and 3.5 mL working volume.

Absorption spectra were recorded prior to fluorescence spectra for each solution in order to reveal the appropriate spectral regions in which the samples can be excited and fluoresce. Fluorescence measurements were performed at a right-angle geometry, that is angle of 90° formed by the incident beam direction with the axis of fluorescence emission detection. This arrangement is suitable for diluted solutions (absorbance < 1) as it prevents scattered and transmitted excitation light from entering the detection system (Diaz-Garcia and Badia-Laino, 2005). In order to avoid 1st and 2nd order Rayleigh scattering of incident light, the start and end positions of a spectrum should be at least set 15 nm from the excitation wavelength and two times the excitation wavelength, respectively. The spectral scan parameters, as shown in Table 7, were set using the software DataMax and UVProbe for fluorescence and absorption

measurements, respectively.

Table 7. Scan parameters for acquisition of 2D spectral maps, absorption, emission, and excitation spectra.

	Absorption spectra	Emission spectra	Excitation spectra	2D spectral maps
Increment (nm)	1	1	1	1 (emission) Variable (excitation)
Integration time (s)*	0.2	Variable	Variable	Variable
$Bandpass_{exc}$ (nm)	–	5	1	5
$Bandpass_{em}$ (nm)	–	1	5	1

* integration time affects only signal-to-noise ratio and has no effect on fluorescence intensity.

2D spectral maps enable the record of spectral features of materials present in a complex mixture, permitting their separation through the unique fluorescence fingerprint they display. There are two ways to construct a 2D spectral map: recording spectra in excitation-emission mode (matrix scan) or manually joining 1D emission spectra. Both methods were deployed in order to construct the 2D contour maps cited in the present thesis.

3.3 Correction of Fluorescence Spectra

The approach to the analysis of data was to subtract, point by point, the absorption/fluorescence of neat solvent from the solution of fluorophore in corresponding solvent, as shown in equation 3.2.

I(corrected) = I(fluorophore+solvent at x wavelength) – I(solvent at x wavelength) (3.2)

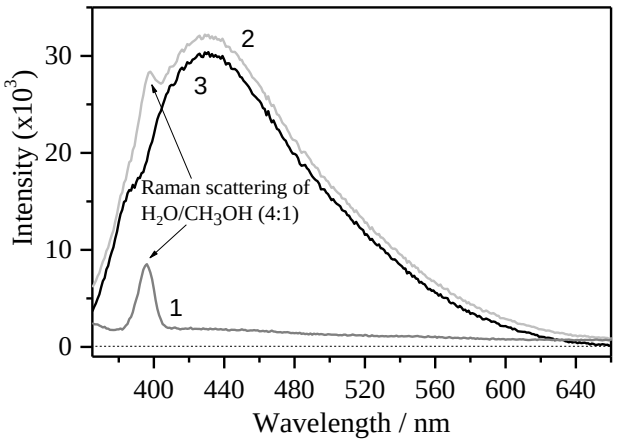

Figure 8. Fluorescence emission spectra at excitation wavelength 350 nm of H_2O/CH_3OH (4:1) v/v (1), archaeological sample in H_2O/CH_3OH (4:1) v/v (2), after solvent subtraction (3).

Figure 8 shows the corrected emission spectrum of an archaeological sample determined by the subtraction procedure. As can be seen, the fluorescence spectrum of solvent mixture (1) presents only a narrow peak at 395 nm which corresponds to Raman scattering and is superimposed atop the fluorescence emission of archaeological sample (2). If not corrected, it can lead to misinterpretation of the emission spectrum.

3.4 Purity Classification of Solvents

Fluorescence spectroscopy is at least three orders of magnitude more sensitive than absorption spectroscopy. For that reason, fluorescence spectroscopy is more favoured in terms of assessing the purity of optical cells and candidate solvents. Firstly, the cuvette should be meticulously cleaned on the basis of hydrophilic (e.g. methanol) and lipophilic (e.g. chloroform) solvents and then wiped with a lens paper. Following, the optical cell is filled with a pure solvent (e.g. nanopure water, ethanol) and the emission spectra are recorded at several excitation wavelengths in order to examine the absence of any contamination. In the case of a purified cuvette, only the Raman peaks corresponding to pure solvent are expected to be displayed. While, if the optical cell is improperly cleaned, the exhibiting fluorescence of undesirable fluorophores trapped in the cuvette walls will be recorded. Fig. 9b illustrates that anthracene remains are present within the optical cell and leads to the conclusion that the cuvette was improperly cleaned prior to solvent addition. Fig. 9a shows that absorption spectroscopy fails to demonstrate the spectral features of anthracene impurities.

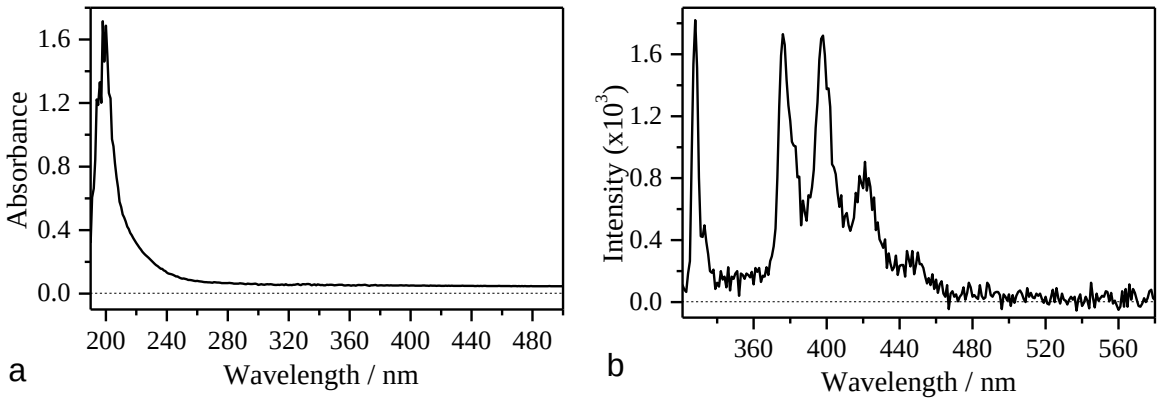

Figure 9. Spectra of ethanol contaminated by anthracene remains in an optical cell: (a) absorption spectrum, (b) fluorescence emission spectrum at excitation wavelength 300 nm.

Purity of solvents can be examined by conducting both absorption and fluorescence studies. Fig. 10a shows that absorption spectra of methanol solvents by two different suppliers –Sigma-Aldrich and Fischer Scientific– lack of distinct spectral features. Unlike absorption, emission spectra reveal the presence of fluorescent contaminants in both methanol solvents. Fig. 10b demonstrates that Sigma-Aldrich methanol may contain two different classes of impurities (λ_{emi}^{max} = 300 and 360 nm), one of which perhaps is also contained in Fischer Scientific

methanol (λ_{emi}^{max} = 300 nm). Fig. 19c shows that upon excitation at 300 nm, part of fluorescence of impurities present in Sigma-Aldrich methanol is recorded. As a result, Fischer Scientific methanol was selected to dilute several samples studied for the purpose of this thesis.

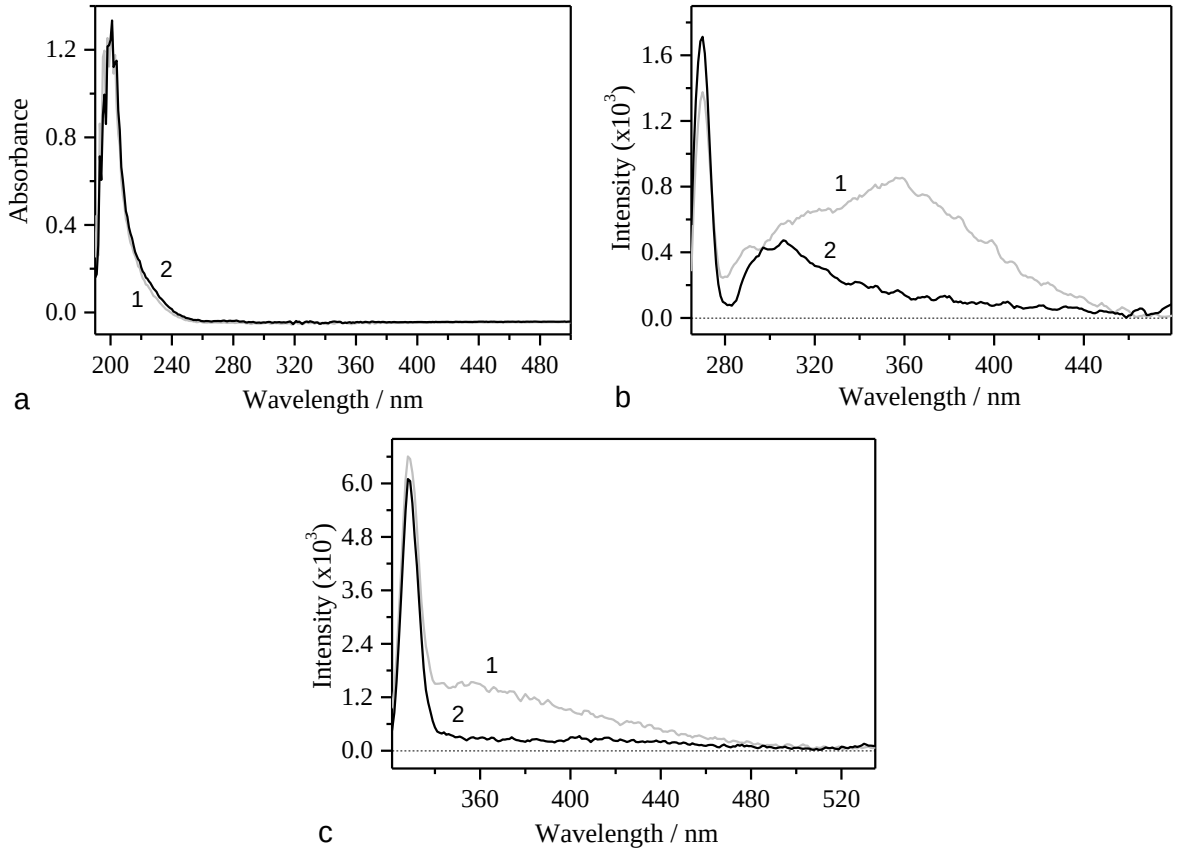

Figure 10. Spectra of methanol Sigma-Aldrich HPLC grade >99.9% (1) and methanol Fischer Scientific HPLC gradient grade >99.9% (2): (a) absorption spectra, (b) fluorescence emission spectra at excitation wavelength 250 nm, (c) fluorescence emission spectra at excitation wavelength 300 nm.

3.5 Solution Preparation

Aqueous solutions of *N*-acetyl-DL-tryptophan were used to demonstrate two fluorescence phenomena within the present thesis: Stokes shift and primary absorption (see Section 2.2). Anthracene in ethanol solutions were deployed for three main purposes: show the secondary absorption effect (see Section 2.2), study the effect of bandpass slit on fluorescence intensity and spectral resolution (see Section 3.1), and quantify the biomarkers found in archaeological samples (see Section 4.4.3). Quinine bisulfate dihydrate was used as a reference compound to quantify the biomarkers found in archaeological potsherds (see Section 4.4.3).

N-acetyl-DL-tryptophan (98% purity), anthracene (97% purity), and quinine bisulfate dihydrate were purchased from Calbiochem, Sigma-Aldrich, and Janssen Chimica, respectively. Chloroform and methanol HPLC gradient grade >99.9% were obtained from Fisher Scientific, whereas isooctane from Merck. Aqueous solutions were prepared using nano-

pure water.

Scheme 11 illustrates the molecular structures of anthracene, quinine bisulfate dihydrate, and *N*-acetyl-DL-tryptophan, while Table 8 cites their chemical and fluorescence properties.

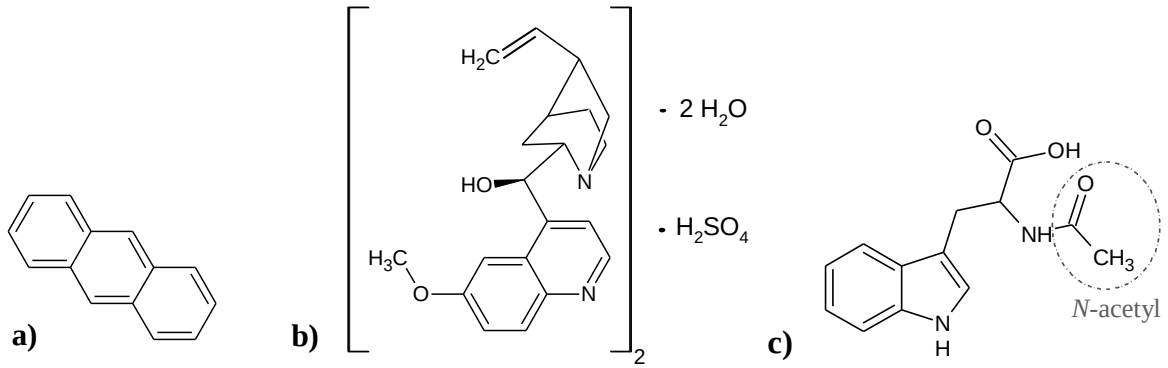

Scheme 11. Structures of: (a) anthracene, (b) quinine bisulfate dihydrate, and (c) *N*-acetyl-DL-tryptophan.

Table 8. Molecular formulae, molecular weights, excitation and fluorescence properties of anthracene, quinine sulfate, and tryptophan (Dixon et al., 2005). Underlined numbers indicate excitation or emission maxima.

Compound	Molecular formula	Molecular weight (g/mol)	Solvent	λexcitation (nm)	λemission (nm)
Anthracene	$C_{14}H_{10}$	178.23	Ethanol	309/323/340/<u>356</u>/376	376/<u>396</u>/421/446/475
Quinine sulfate	$C_{20}H_{26}N_2O_6S$	422.48	Sulfuric acid 0.5 M	318/<u>348</u>	450
Tryptophan	$C_{11}H_{12}N_2O_2$	204.23	Water	<u>278</u>/287	356

Phenolic compounds that are known to act as agro-food biomarkers were studied in the present thesis. Phenolic standard solutions were prepared in order to compare their absorption and fluorescence properties with spectral features of biomarkers found in archaeological samples. 4-Hydroxy-3-methoxybenzaldehyde (99% purity; vanillin), 3,4,5-trihydroxybenzoic acid (97%; gallic acid), trans-3,4-dihydroxycinnamic acid (97%; caffeic acid), trans-4-hydroxy-3-methoxycinnamic acid (99%; ferulic acid), and 3,5-dimethoxy-4-hydroxybenzoic acid (98%; syringic acid) were supplied by Sigma-Aldrich. For each phenolic compound, a stock solution (about 180 μg/mL) was prepared in nanopure water. Diluted aqueous solutions of vanillin, gallic acid, caffeic acid, ferulic acid, and syringic acid were prepared (at a concentration of 3.0 μg/mL, 3.4 μg/mL, 3.6 μg/mL, 3.9 μg/mL, and 4.0 μg/mL, respectively) from the stock solutions. Diluted aqueous solutions of phenolic compounds were then studied in absorption and fluorescence spectroscopy. Scheme 12 illustrates the molecular structures of phenolic

compounds while Table 9 cites their chemical and fluorescence properties.

Cinnamic-acid derivatives

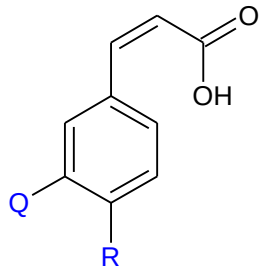

Caffeic acid : Q = R = OH
Ferulic acid : Q = OMe, R = OH

Benzoic-acid derivatives

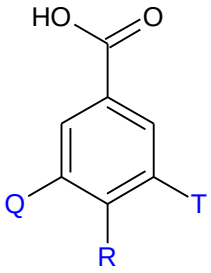

Gallic acid : Q = R = T = OH
Syringic acid : Q = T = OMe, R = OH

Vanillin

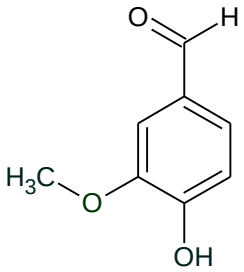

Scheme 12. Structures of phenolic compounds studied in this Master Thesis.

Table 9. Molecular formulae, molecular weights, excitation and emission maxima of fluorescence spectra of several phenolic compounds in water (Rodriguez-Delgado et al., 2001).

	Compound	Molecular formula	Molecular weight (g/mol)	λ_{exc} (nm)	λ_{emi} (nm)
Cinnamic-like	Caffeic acid	$C_9H_8O_4$	180.16	262	426
	Ferulic acid	$C_{10}H_{10}O_4$	194.18	260	422
Benzoic-like	Syringic acid	$C_9H_{10}O_5$	198.17	278	360
	Gallic acid	$C_7H_6O_5$	170.12	278	366
Benzaldehyde-like	Vanillin	$C_8H_8O_3$	152.15	260	425

Except for five individual aqueous solutions of phenolic compounds, it was also prepared a mixture of them in order to reliably simulate complex organic remains found in archaeological artefacts. The phenolic standard solution was prepared by adding equal amounts of the five diluted aqueous solutions of vanillin, gallic acid, caffeic acid, ferulic acid, and syringic acid (at a final concentration of 0.60 μg/mL, 0.68 μg/mL, 0.72 μg/mL, 0.78 μg/mL, 0.80 μg/mL,

respectively).

3.6 Hydrophilic and Lipophilic Compounds Extraction from Archaeological Potsherds

The present protocol was developed to effectively extract residues from Minoan ceramic vessels (Romanus et al., 2009) and is based on the experimental procedure followed by Tsana (2018). To this end, potsherd surfaces were cleaned using a brush and dust deposited on the surface was removed on the basis of a scalpel. Then, surface soil crust was removed from the inner part of sherds in order to be studied separately. A drill was used for sampling from a surface area of 1 cm length x 1 cm width x 2 mm depth from inner and outer parts of potsherds. Samples from the inside, outside, and soil on the inner part of the sherds were crushed and grounded to a powder using a pestle and mortar.

Polar and nonpolar residues were extracted using H_2O/MeOH (4:1) v/v and chloroform, respectively (Guash-Jane et al., 2004). In particular, varying amounts of the pulverized residues from the inner and outer parts of potsherds (100–500 mg) as well as from the soil crusts deposited on the inside surface of the vessels (80 mg–1.5 g) were extracted with 5 mL H_2O/MeOH (4:1) v/v or/and chloroform to collect hydro- and lipo-philic residues, respectively. Then, a bath sonicator was utilized for 20 min to improve the extraction efficiency of solvent (Namiesnik et al., 2015). Finally, the samples were centrifuged for 15 min at 6000 rpm to facilitate the removal of solid particles.

Table 10. Archaeological samples collected from ancient Minoan potsherds.

Pottery object	Sample	Brief description	Extract
Ceramic amphora	MP1I	500 mg from the inside surface	Hydrophilic
		100 mg from the inside surface	Lipophilic
	MP1O	500 mg from the outside surface	Hydrophilic
	MP1S	1.5 g soil from the inside	Hydrophilic
			Lipophilic
Ceramic cylinder vessel	MP2S	80 mg encrustation from the inside	Hydrophilic
Ceramic cylinder vessel	MP3S	1.5 g soil from the inside	Lipophilic

In the current study, the residues from three Minoan pottery vessels (named MP samples) were analysed. Specifically, samples MP1I and MP1O were obtained by abrading 500 mg of inner and outer surface of ceramic amphora (named object 1), respectively, whereas sample MP1S was obtained by collecting 1.5 g of soil deposited on the inside surface of object 1. Samples MP2S and MP3S were obtained by collecting 80 mg and 1.5 g of encrusted soil deposited on the inside surface of two ceramic cylinder vessels (object 2 and 3, respectively). A short description of the samples, objects, and extracting solvents is included in Table 10.

CHAPTER 4: Comparison of Residues from Archaeological Potsherds with Phenolic Standard Solution

4.1 Storage of Goods, Types of Containers, and Processing of Foodstuffs in Minoan Civilization

Current archaeological evidence shows that viticulture originated from Zagros mountains, in the region that nowadays belongs to Iran, 6000 years ago and that storage of wine was feasible due to invention of ceramic fabric (ca. 18000 BCE). Phoenician traders probably imparted wine-making knowledge to Greeks during fourth millennium BCE (Reynolds, 2017). In Minoan Crete, wine production started in the first-palace period (ca. 3000 BCE) and climaxed during the second-palace period (ca. 1900 BCE), whereas olive oil production began in the second-palace period and peaked during the post-palatial period (ca. 1450 BCE; Hamilakis, 1996).

Pottery vessels were used in varying ways in ancient communities and served three main purposes concerning food: transfer, process (such as cooking), and storage. In general, the process of cooking may cause degradation of organic residues and thus reduce their potential survival over long timescales. The archaeological organic residues may accumulate in different parts within the interior of a vessel, that is base, body, neck, or rim. Charters et al. (1993) has performed GC-MS to establish the accumulation of absorbed lipids in different parts of pots, i.e. jars and bowls. The study enabled the classification of vessel use between different vessel types by comparing the regions of lipid accumulation. The same study also reported that preservation of lipids was higher in the rim and body of pottery vessels used for cooking rather than the base. An explanation to this may be that thermal degradation of lipids was induced by fire in the lower parts of the vessels.

The identification of ketones in archaeological pottery may indicate the use of vessels as cooking pots. Studies have revealed the formation of monosaturated ketones (C_{29}—C_{35}) during pyrolysis of free fatty acids and triacylglycerols within a clay matrix. The formation of long-chain ketones is attributed to the heating-induced ketonic decarboxylation, that is a type of condensation reaction (Evershed et al., 1995; Raven et al., 1997). Archaeological analysis also links the shape with the function of an archaeological vessel. For example, analysis of organic food remains showed that high-mouthed vessels were probably used to store or transfer liquids, whereas bowl-shaped pots were often utilized to produce dairy products or to cook solid food (Roffet-Salque et al., 2017).

Artefacts related to olive oil processing show that olive cultivation and olive oil production in Minoan Crete originated in the second millennium BCE (Riley, 2004). Olive oil was extracted by the domesticated olive trees O*lea Europaea* in Crete during the Bronze Age (Runnels and Hansen, 1986). Ancient objects that help us reconstruct the Aegean methods of olive oil production encompass excavated stone pressers, clay containers for storage, and organic materials like carbonized olive wood (Riley, 2002). Minoans were chiefly using the oil for culinary purposes and the olive wood for cooking or heating. Olive oil production technology in Aegean Bronze Age comprised of three main steps: olive crushing, olive pressing, and separation of oil from water. The crushing apparatus usually included a stone rotary mill consisted of a bowl and mortar. The crushed olives were then placed within cloths and pressed on a press bed made of stone. The resulting product was transferred inside a container and then the floated oil was skimmed (Foxhall, 2007).

In Minoan Crete, narrow basins with spouts were likely utilized for olive crushing. While, clay or stone basins with handles and a spout at the base were probably used for wine making, especially if collecting vessels are found in the proximity. Evidence shows that cups were used for wine drinking. Apart from consumption of olive oil, oil lamps have been found in religious sites and interpreted as ritual objects (Hadzisavvas, 2012). Most artefacts related to wine and oil processing have been discovered around Minoan Palaces (Mallia, Zakros) and elite houses in large towns (Palaikastro, Kommos). One possible explanation is that wine and oil were precious ancient commodities and were likely related to ritual ceremonies and feasts (Hamilakis, 1996).

To date, several archaeological studies have focused on the agricultural development in Crete during Bronze Age (around 2000 BCE). Archaeological findings show that vine was cultivated and wine was consumed in Minoan Crete (Hamilakis, 1996). The macroscopic evidence of viticulture from Bronze Age Crete comes from three main sources: artefacts used for the processing and storage of grapes, manuscripts, and plant macrofossils. All these macroscopic evidence categories lead to ambiguous results when considering wine making. First, ancient wine production mostly required pressing equipment for the grapes and storage vessels (e.g. pithoi, amphorae). Nevertheless, both equipment and storage vessels were used for several purposes apart from wine-associated processes. Second, Minoan texts (especially those written in Linear B) pose interpretation problems, making it difficult to deduce information about viticulture based exclusively on them. Third, the plant macrofossils domain comprises of preserved seeds thanks to carbonisation or fossilisation processes. However, none of the grape processing stages involves fire and thus preservation of grape seeds due to carbonisation is highly unlikely to occur. Also, even if fossilised grape seeds are found, one is still uncertain whether they lead to dried grape consumption or to wine making.

The direct archaeological evidence presented above proves to be an inadequate source of information and should thus couple with molecular approaches such as organic residue analysis. The analysis of archaeological organic remains originating from pottery applies to the comprehension of the ancient technologies, in terms of vessels production, decoration, use, specialization, and repair. For example, a study based on GC-MS revealed that several pithoi

originating from Aphrodite's Kefali on the Isthmus of Ierapetra (constructed between 3200 and 2700 BCE) probably contained wine (biomarkers: syringic acid, tartaric acid) while others stored olive oil (biomarker: oleic acid; Koh and Betancourt, 2010).

Archaeological samples studied for the purpose of the current thesis were collected from the Minoan Palace in the Tourkogeitonia district of Archanes, which is located 15 Km south of Minoan Palace of Knossos (Crete, Greece). The Palace complex is a three-storey building risen in the 1900 BCE. The whole settlement was excavated during 1999–2001 under the direction of Effie and Ioannis Sakellarakis; excavation unearthed a total of 234 pithoi. Two storage rooms inside the Palace housed pottery vessels probable used to store food and drinks.

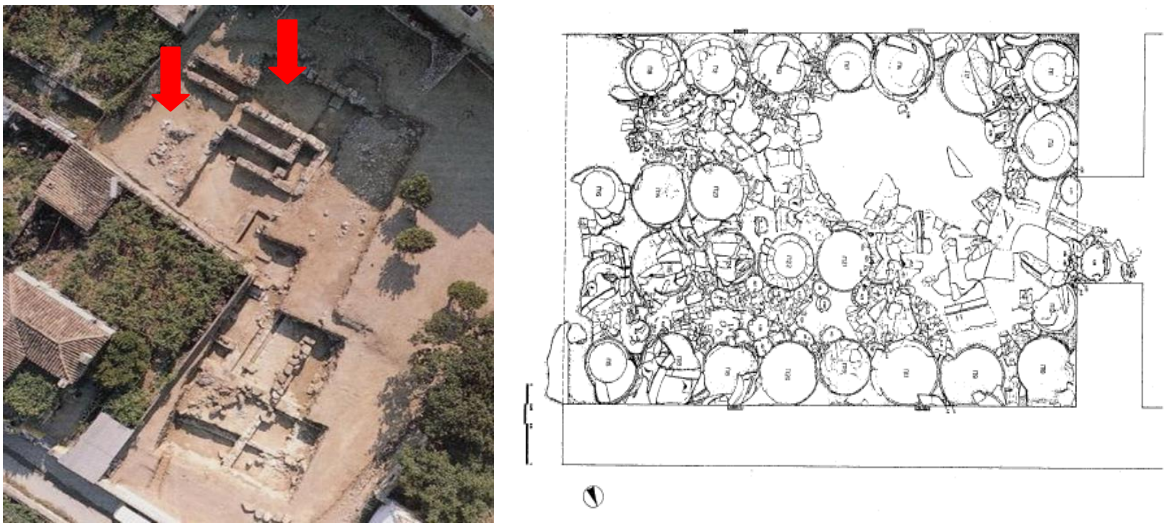

a **b**

Scheme 13. (a) Ground plan of the excavated Royal Minoan Palace at Archanes, Heraklion, Crete. The red arrows indicate the storage rooms of pithoi and vessels. (b) Unearthed vessels layout at one of the storage rooms.

4.2 Organic Residues in Wine: Fluorophores Preservation over Time

Alcoholic drinks consist chiefly of water and water-soluble compounds such as sugars and alcohols. These compounds are unlikely to persist over archaeological time since they are susceptible to leaching, and are thus highly improbable to serve as wine biomarkers. Wine also contains a wide range of minor constituents, some of which are fluorescent. Polyphenols (flavonoids, anthocyanins –in red wines–, tannins), phenolic acids, vitamins, stilbenes, and amino acids number among natural occurring fluorophores in wines (Arnaoutakis, 2016).

Tartaric acid exists in many vegetables and fruits, albeit in high concentration in grapes (5–7.5 g/L) (Soyer et al., 2003). Tartaric acid is the major organic acid in grapes and dissociates into tartarate salts in wines. The polar nature of tartarate salts makes them prone to solubility in water and thus hinders their survival over archaeological timescales. However, the polarity of tartarate salts enables them also to bind to the ceramic fabric, supporting their preservation (Steele, 2013). Tartaric acid has been identified in amphorae from a Bronze Age shipwreck at

Uluburun, Turkey and has been also successfully recovered from modern ceramics soaked in wine (Stern et al., 2008). Consequently, tartaric acid may act as a biomarker for wine provided that cautious extraction and detection methods are applied.

Despite suitable techniques for the extraction and detection of tartaric acid, interpretive challenges arise from a number of contamination sources that lead to false-positive of wine identification. First, tartaric acid can leach out of associated soil into buried vessels or in reverse due to acid's solubility in water. For that reason, the adjacent soil should be examined alongside the artefacts of interest (Mc Govern et al., 2017). Second, plastic bags used for the storage of sherds represent a modern source of contamination. Phthalates originated from plastics may be responsible for tartaric acid contamination in the post-excavation stage. In order to avoid false-positive conclusions, a minimum detection limit of 1 μg of tartaric acid per 1 g of ceramic is proposed to verify its unequivocal presence in fruits (Drieu et al., 2020).

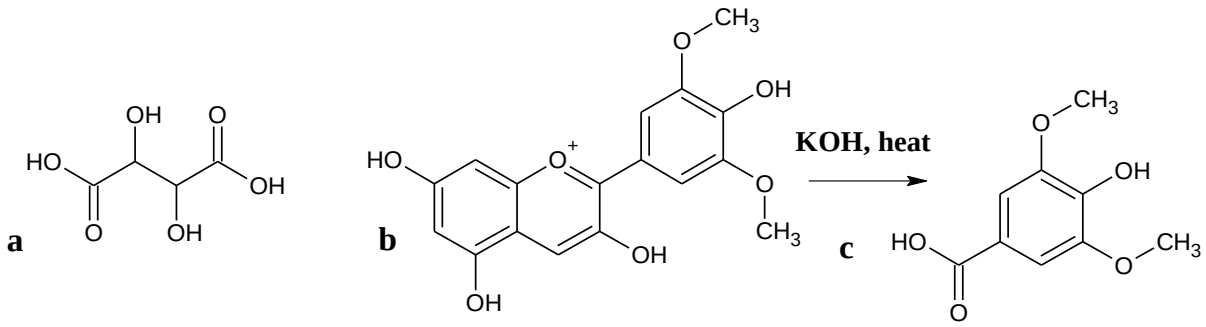

Scheme 14. Structures of potential biomarkers of wine: (a) tartaric acid, (b) malvidin, and (c) syringic acid.

The polymerisation process occurs in a plethora of phenolic derivatives in wine and promotes the preservation of organic residues over long timescales (Guasch-Jané et al., 2004). Malvidin is the major anthocyanin in red wines. During aging, malvidin polymerises and releases syringic acid after alkaline treatment as seen in Scheme 14 (Ribéreau-Gayon et al., 2006). Syringic acid is an ambiguous red wine biomarker, given its broad presence in natural products (e.g. in honey) (Pyrzynska and Biesaga, 2009) and its emission due to lignin degradation during biomass combustion (Simoneit et al., 1993). The syringic acid can be only associated with red wine, if it can be established to originate from malvidin precursors.

Grapes and wines also contain phenolic acids with prominent fluorescence properties (Ribéreau-Gayon et al., 2006). Two broad categories of phenolic acid derivatives are present in concentrations of 10–200 mg/L in wines: cinnamic acids (such as *p*-coumaric, ferulic, and caffeic acid) and benzoic acids (such as. gallic, syringic, and gentistic acid). Romanus et al. (2009) has identified preserved polyphenols including phenolic acids in Roman amphorae fragments (around 500 CE) excavated in Sagalassos, Turkey using GC-MS. The same study proved that wine polyphenols can intrude the ceramic matrix even when the vessel is pitched, i.e. coating the interior of a vessel with a resin to reduce its permeability. Therefore, it is interesting to examine further the preservation of phenolic acids deposited in archaeological potsherds.

4.3 ^{1}H NMR Study

All archaeological samples from the Archanes site were analysed by ^{1}H NMR spectroscopy (Tsana, 2018) prior to analyses on the basis of UV-vis absorption and fluorescence spectroscopy (Table 11). Two samples (polar MP1I and MP1O extracts) from a Minoan ceramic amphora (object 1) produced distinct organic NMR profiles typical of 2,3-butanediol; in hydrophilic extract MP1I, acetoin was also detected (Scheme 15). Such profiles were not observed in the polar MP1S extract and nonpolar MP1I and MP1S extracts. Nevertheless, identification of both acetoin and 2,3-butanediol in interior and exterior surface deposits provides evidence that wine was stored in object 1.

Table 11. Biomarkers from ancient Minoan potsherds detected by NMR spectroscopy.

Pottery object	Sample	Extract	Biomarker
Ceramic amphora	MP1I	Hydrophilic	Acetoin / 2,3-butanediol
		Lipophilic	No biomarkers detected
	MP1O	Hydrophilic	2,3-butanediol
	MP1S	Hydrophilic	No biomarkers detected
		Lipophilic	No biomarkers detected
Ceramic cylinder vessel	MP2S	Hydrophilic	Oleic acid / Linoleic acid
Ceramic cylinder vessel	MP3S	Lipophilic	Oleic acid / Linoleic acid

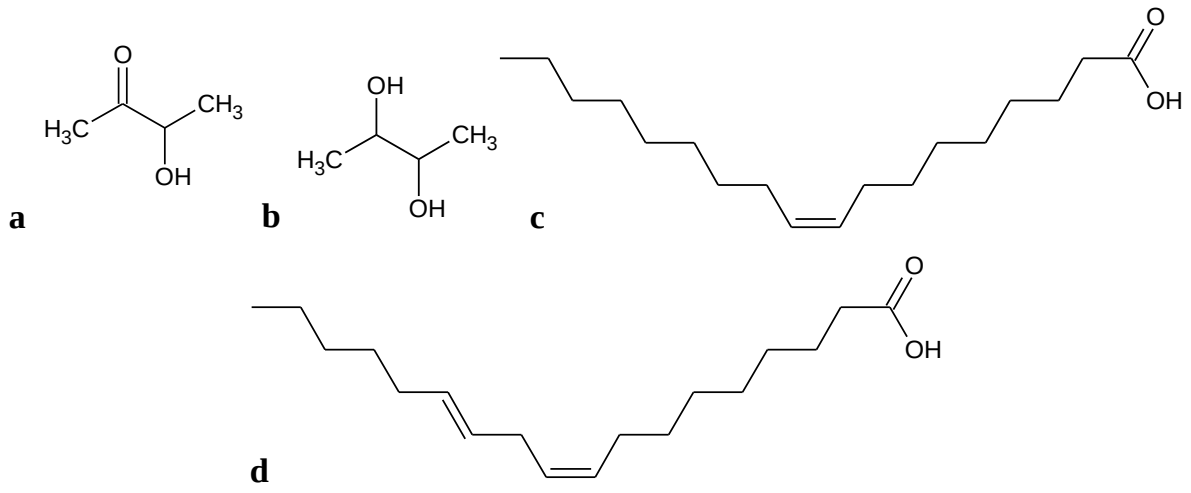

Scheme 15. Structures of wine biomarkers (a) acetoin, (b) 2,3-butanediol and oil biomarkers (c) oleic acid, (d) linoleic acid detected by NMR spectroscopy.

Yeasts produce acetoin from reduction of diacetyl in the first steps of alcoholic fermentation and then yield 2,3-butanediol following reduction of acetoin (Peinado and Mauricio, 2009). Wine contains < 150 mg of acetoin and 2,3-butanediol per litre (Romano and Suzzi, 1996).

NMR analyses in two interior soil deposits (samples MP2S and MP3S) originating from two ceramic cylinder vessels (objects 2 and 3) revealed the presence of unsaturated fatty acids dominated by oleic ($C_{18:1}$) and linoleic ($C_{18:2}$) acids. The occurrence of unsaturated fatty acids within well-preserved pottery vessels is considered as arising from ancient oil storage (Matlova et al., 2017).

4.4 Results

The absorption and fluorescence profiles (from 1D-excitation and emission spectra as well as 2D-fluorescence maps) collated herein are generated from seven archaeological samples derived from three ancient objects (see Section 3.6) unearthed at the site of Minoan Palace in Archanes, Greece. The absorption and fluorescence features of phenolic standards are also reported and compared to those of archaeological samples. The selection of phenolic acids is based upon the fact that they exhibit fluorescence and occur in wines and oils (Dufour et al., 2006) extensively produced and stored in Minoan communities. In particular, aqueous solutions of benzaldehyde- (vanillin), cinnamic- (ferulic acid, caffeic acid), and benzoic-like (gallic acid, syringic acid) acids were analysed, as well as a standard phenolic mixture comprising of above-mentioned phenolic acids. Ultimately, the concentration of fluorophores in polar sample MP1I were determined using quinine sulfate dihydrate, anthracene, and ferulic acid as reference standards.

4.4.1 Absorption and Fluorescence Study of Biomarkers found in Archaeological Potsherds from Minoan Palace in Archanes

The absorption and fluorescence properties of archaeological residues recovered using a polar solvent were first investigated in samples from a Minoan ceramic amphora (object 1; samples MP1I, MP1O, MP1S). In Figure 11 the absorption, emission, and excitation spectra as well as the 2D-fluorescence map are presented for sample MP1I. Figure 11a shows that sample MP1I absorbs in the UV spectral region with a maximum at 195 nm. In addition, sample MP1I presents excitation maximum at 300–340 nm (Fig. 11c) and emission maximum at 410–430 nm (Fig. 11b). 2D-fluorescence landscape illustrates that fluorescence emission shifts to higher wavelengths (red-shift) as excitation wavelength increases (Fig. 11d). In all excitation-emission maps (contour plots) displayed herein, the color scale represents the exhibiting intensity with blue and red corresponding to the weakest and strongest fluorescence intensities, respectively.

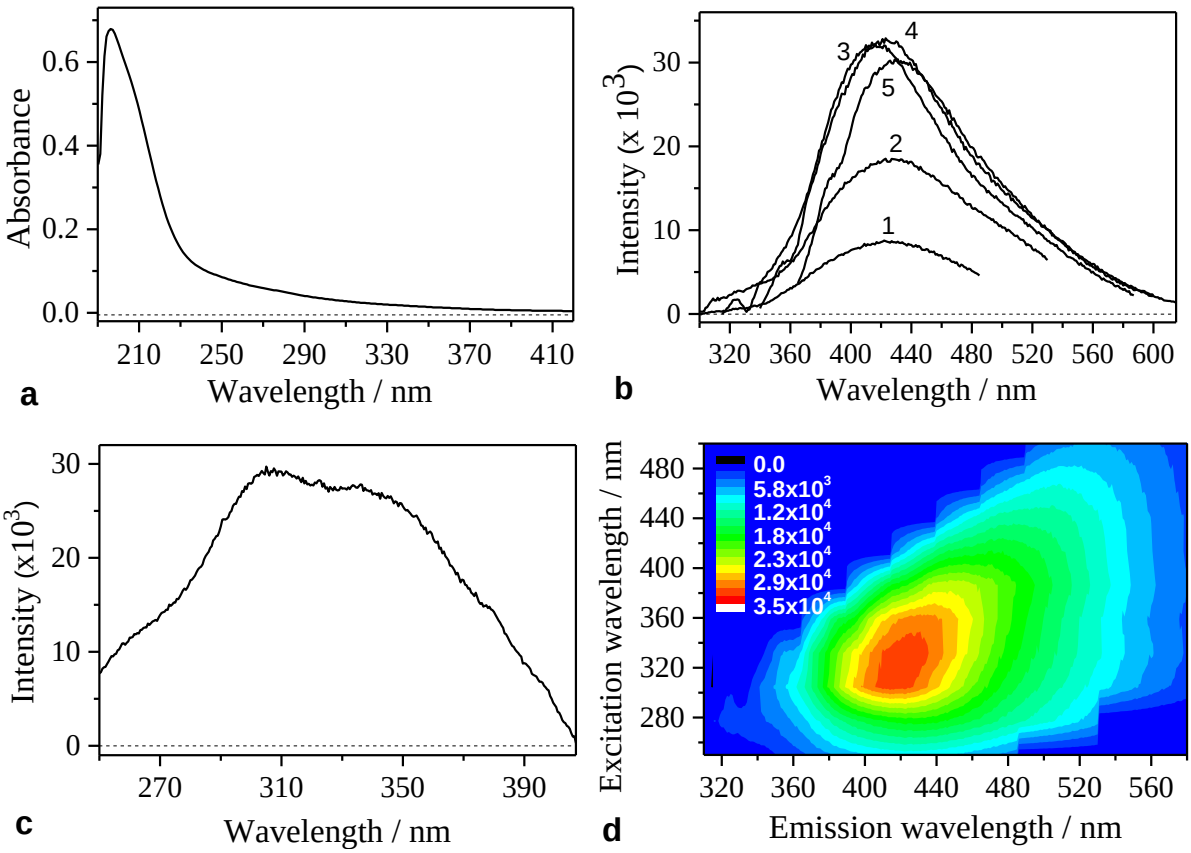

Figure 11. Spectra of sample MP1I in water/methanol (4:1) v/v: (a) absorption spectrum; (b) fluorescence emission spectra at excitation wavelength 250 nm (1), 275 nm (2), 300 nm (3), 325 nm (4), 350 nm (5); (c) fluorescence excitation spectrum at emission wavelength 420 nm; (d) 2D fluorescence emission-excitation spectral map.

The spectroscopic properties of sample MP1O (Fig. 12) appear similarities to those of sample MP1I (Fig. 11). Specifically, the maximum absorption of sample MP1O is at 200 nm (Fig. 12a) and maximum areas of excitation and emission appear at 300–340 nm (Fig. 12c) and at 420–430 nm (Fig. 12b), respectively. 2D-fluorescence map indicates a slight red-shift of emission wavelengths as excitation wavelength increases (Fig. 12d). Notwithstanding their spectral similarities, samples MP1I and MP1O are different concerning band intensities. More precisely, the absorption and fluorescence spectra of sample MP1O present lower band intensities (roughly 2.5-fold) compared with sample MP1I.

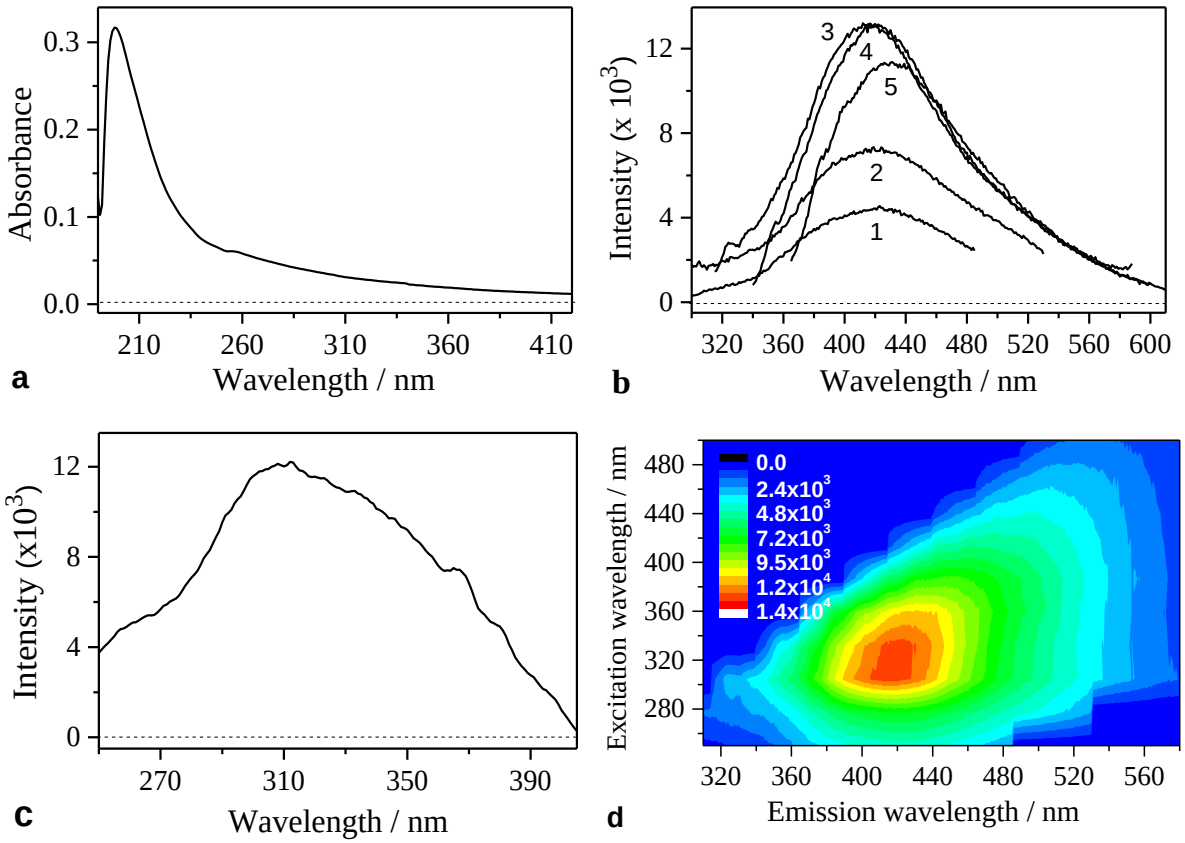

Figure 12. Spectra of sample MP1O in water/methanol (4:1) v/v: (a) absorption spectrum; (b) fluorescence emission spectra at excitation wavelength 250 nm (1), 275 nm (2), 300 nm (3), 325 nm (4), 350 nm (5); (c) fluorescence excitation spectrum at emission wavelength 420 nm; (d) 2D fluorescence emission-excitation spectral map.

Apparent similarities can be found between absorption and fluorescence profiles, including band intensities, of samples MP1S (Fig. 13) and MP1I (Fig. 11). In particular, absorption, excitation, and emission for sample MP1S maximise at 195 nm (Fig. 13a), at 300–330 nm (Fig. 13c), and at 400–430 nm (Fig. 13b), respectively. Figure 13d illustrates that the area of fluorescence contour of sample MP1S is narrower compared with that of sample MP1I (Fig. 11d).

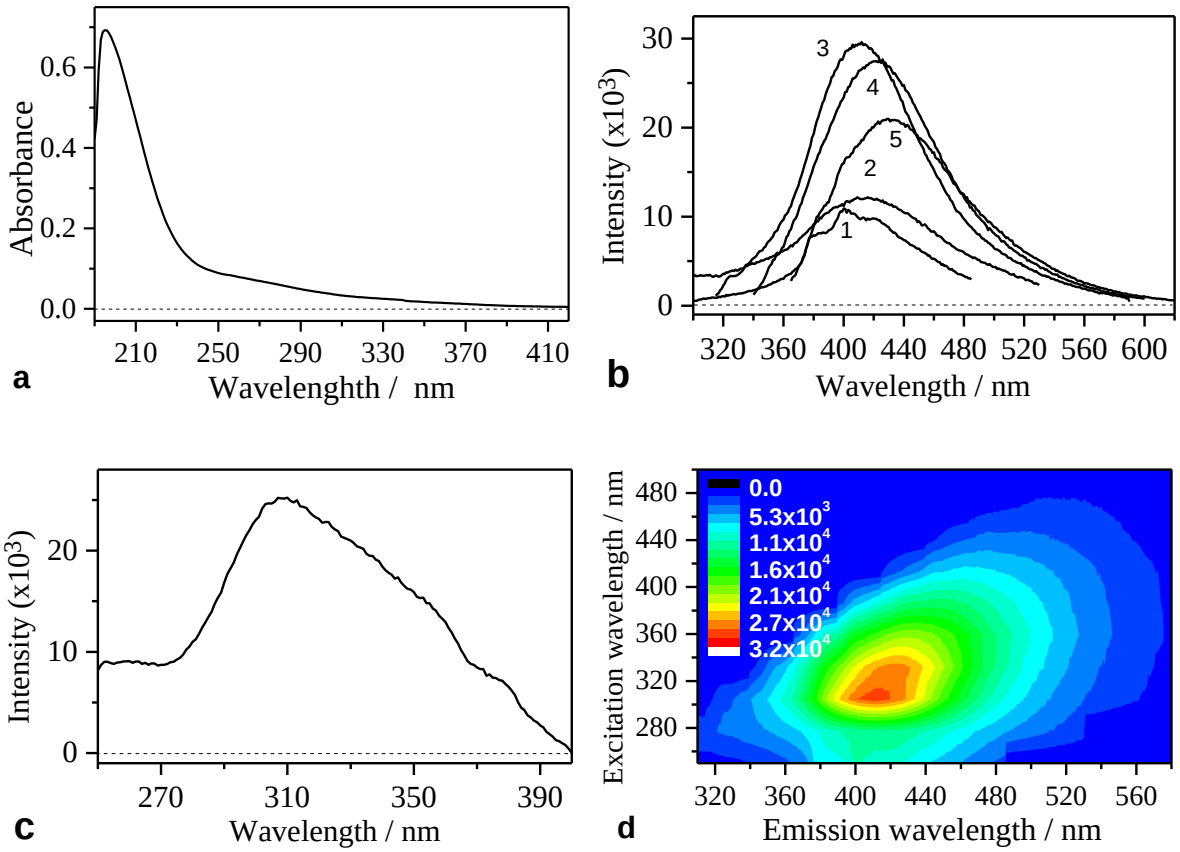

Figure 13. Spectra of sample MP1S in water/methanol (4:1) v/v: (a) absorption spectrum; (b) fluorescence emission spectra at excitation wavelength 250 nm (1), 275 nm (2), 300 nm (3), 325 nm (4), 350 nm (5); (c) fluorescence excitation spectrum at emission wavelength 420 nm; (d) 2D fluorescence emission-excitation spectral map.

The absorption and fluorescence properties of nonpolar ancient residues (recovered using chloroform) were also studied in samples from Minoan artefact 1 (samples MP1I, MP1S) in order to enrich the insight of preserved organic residues. In sample MP1I, two absorption bands appear with maxima at 260 nm and 295 nm (Fig. 14a). Furthermore, the 1D-fluorescence emission spectra present two maxima (Fig. 14b): One at 360 nm that is generated from excitation at maximum 300 nm and a shoulder at 260 nm, and a second at 435 nm upon excitation at maximum 360 nm and a hump at 260 nm (Fig. 14c). As a result, the 2D-fluorescence map shows two distinct fluorescent regions: the first one has excitation maximum at 280–310 nm and emission maximum at 330–390 nm, whereas the second one has excitation maximum at 280–400 nm and emission maximum at 420–460 nm.

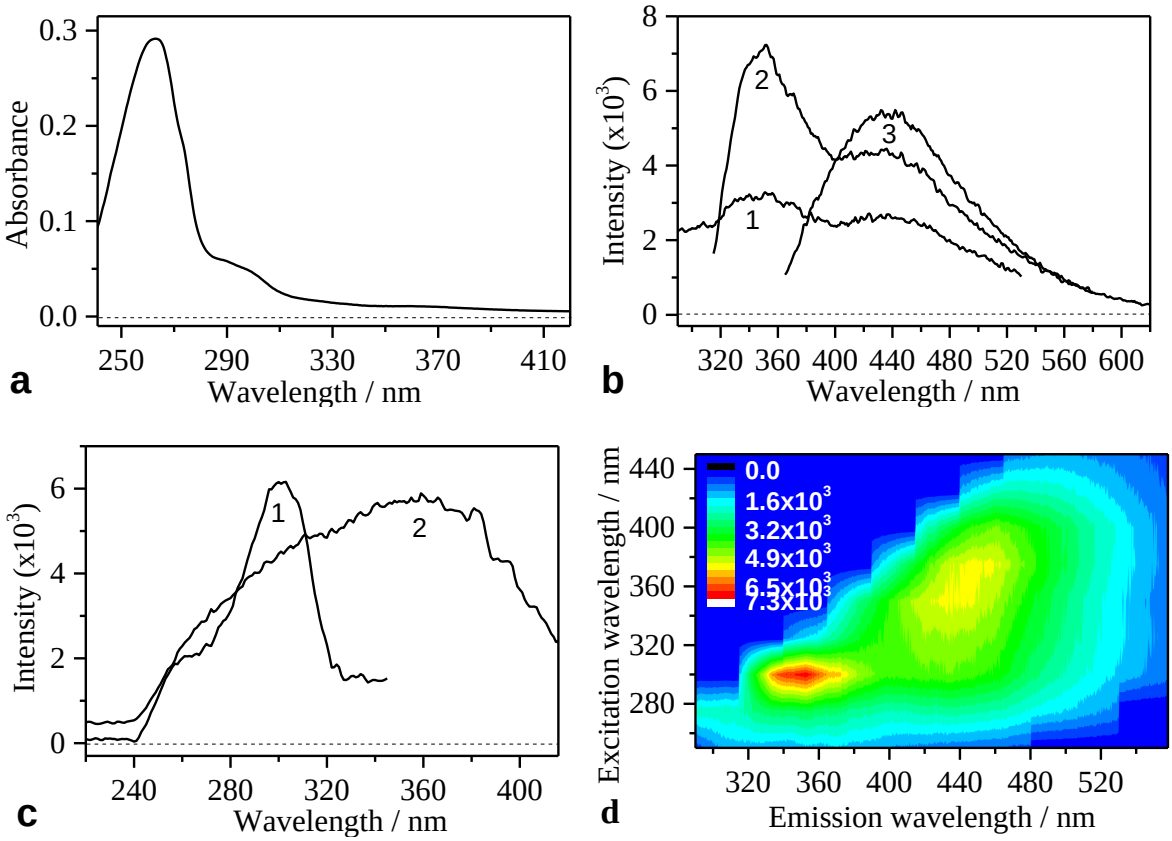

Figure 14. Spectra of sample MP1I in chloroform: (a) absorption spectrum; (b) fluorescence emission spectra at excitation wavelength 275 nm (1), 300 nm (2), 350 nm (3); (c) fluorescence excitation spectrum at emission wavelength 360 nm (1) and 435 nm (2); (d) 2D fluorescence emission-excitation spectral map.

The spectral features of nonpolar fluorophores present in archaeological sample MP1S can be seen in Figure 15. The principal absorption band at 260 nm with a shoulder at 290 nm (Fig. 15a) matches with that of sample MP1I (Fig. 14a), although maximum absorption of sample MP1S is approximately eight times weaker compared with that of sample MP1I. Emission profiles of sample MP1S are dominated by a maximum at 380–440 nm (Fig. 15b) and are significantly different compared with those of sample MP1I (Fig. 14b). Figure 15c shows that the excitation spectrum of sample MP1S presents a maximum at 340 nm and a hump at 300 nm that reminds one of the excitation spectra for sample MP1I (Fig. 14c). In addition, the 2D-fluorescence landscape for sample MP1S reveals a contour with excitation/emission at maxima 300–360 nm/380–440 nm (Fig. 15d).

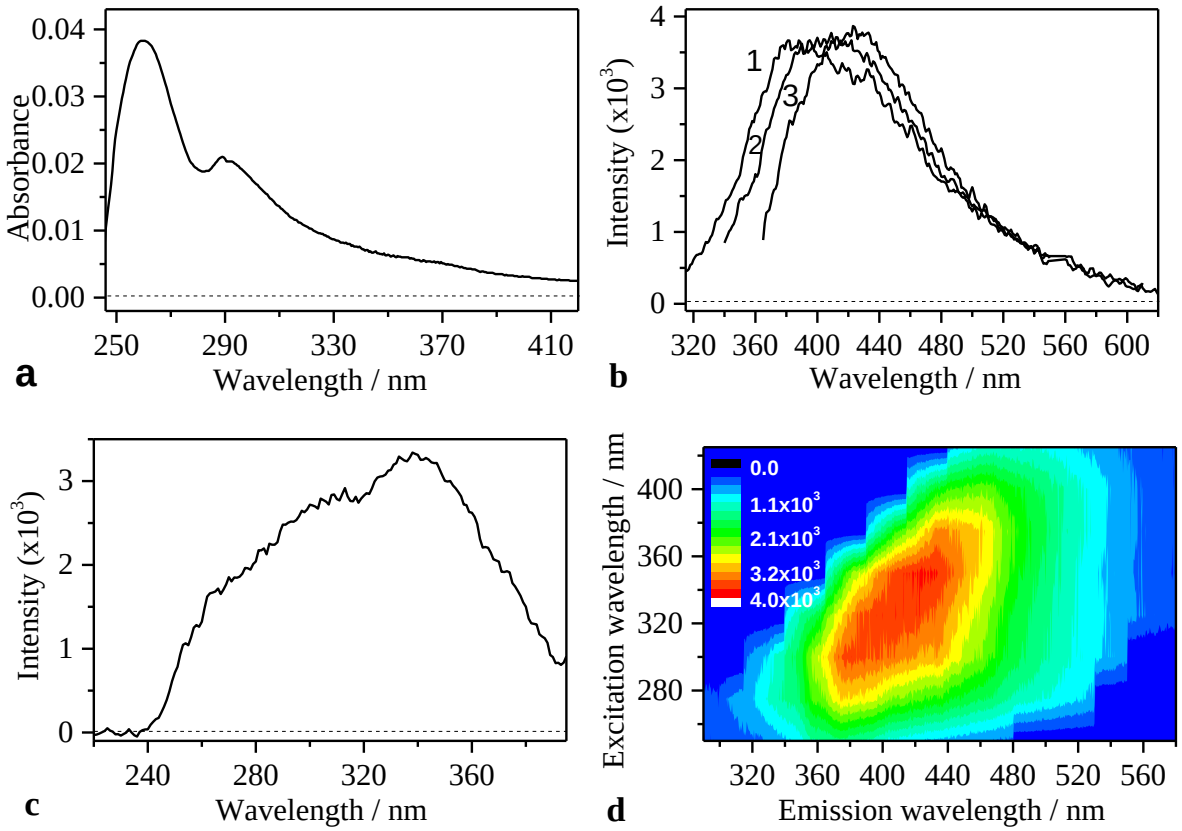

Figure 15. Spectra of sample MP1S in chloroform: (a) absorption spectrum; (b) fluorescence emission spectra at excitation wavelength 300 nm (1), 325 nm (2), 350 nm (3); (c) fluorescence excitation spectrum at emission wavelength 410 nm; (d) 2D fluorescence emission-excitation spectral map.

Figure 16 shows the absorption and fluorescence spectra corresponding to polar extract of encrustation adhered to the inside of a ceramic cylinder vessel (object 2; sample MP2S). In particular, the absorption profile presents a tail-like shape in the UV spectral region with a shoulder at 260 nm (Fig. 16a). The maximum area of emission is at 425–445 nm (Fig. 16b), whereas the excitation is at maximum 350 nm with a small hump at 265 nm (Fig. 16c); it should be noted that the position of shoulder in excitation spectrum matches with that of absorption spectrum. Moreover, the 2D-fluorescence map shows a contour with maximum areas of excitation at 320–360 nm and emission at 420–470 nm.

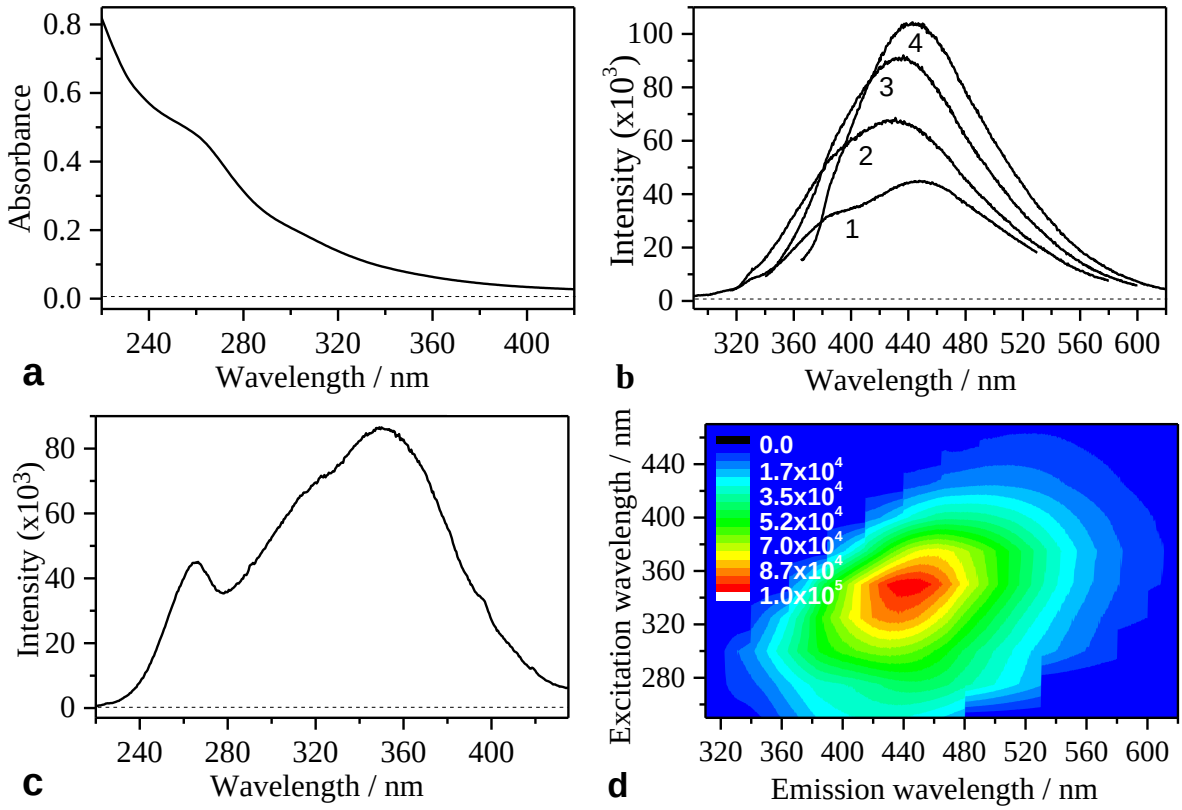

Figure 16. Spectra of sample MP2S in water/methanol (4:1) v/v: (a) absorption spectrum; (b) fluorescence emission spectra at excitation wavelength 275 nm (1), 300 nm (2), 325 nm (3), 350 nm (4); (c) fluorescence excitation spectrum at emission wavelength 450 nm; (d) 2D fluorescence emission-excitation spectral map.

Figure 17 illustrates the absorption and fluorescence features of nonpolar fluorophores extracted from soil deposited on the inside of a Minoan cylinder vessel (object 3; sample MP3S). As can be seen from Figure 17a, a tail-like profile dominates the absorption spectrum. Following spectrofluorimetric analyses, sample MP3S presents excitation maximum at 380 nm and a shoulder at 280 nm (Fig. 17c) and a strong emission band centred at 450 nm (Fig. b). Finally, the 2D-fluorescence landscape reveals a contour with maximum excitation/ emission areas at 350–400 nm/420–480 nm.

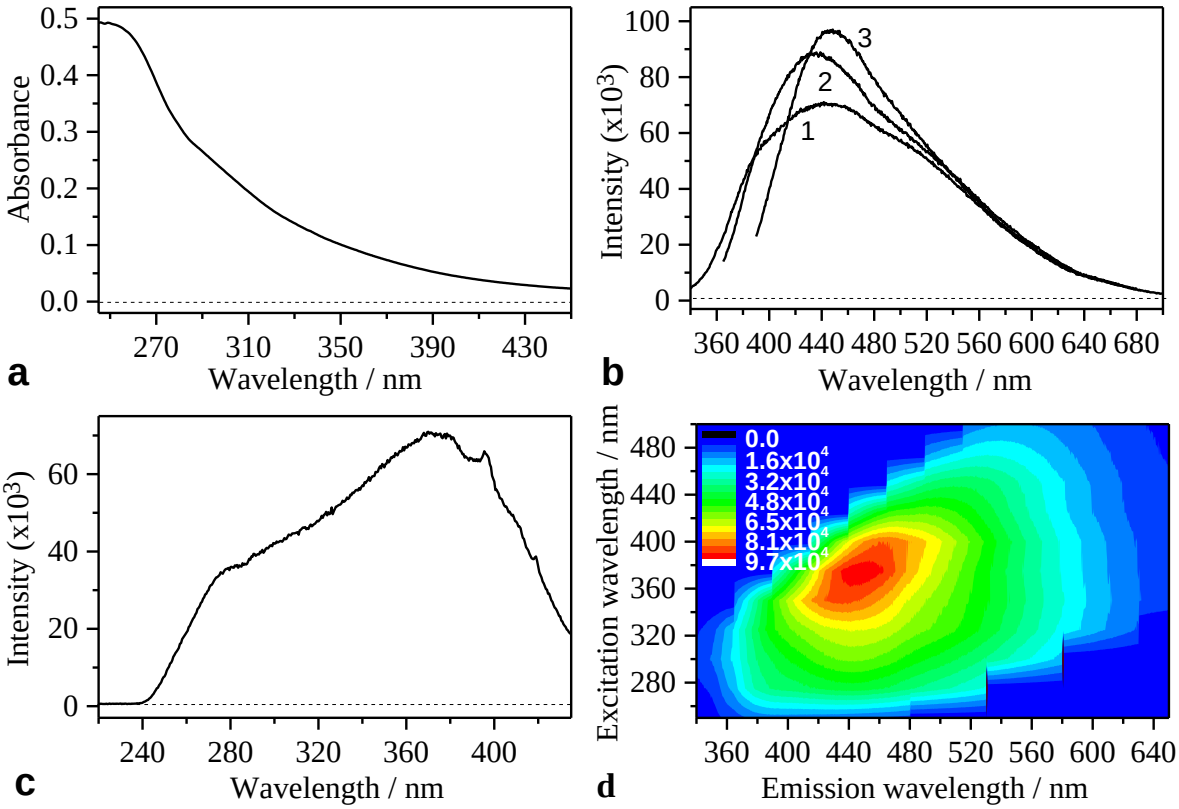

Figure 17. Spectra of sample MP3S in chloroform: (a) absorption spectrum; (b) fluorescence emission spectra at excitation wavelength 325 nm (1), 350 nm (2), 375 nm (3); (c) fluorescence excitation spectrum at emission wavelength 450 nm; (d) 2D fluorescence emission-excitation spectral map.

4.4.2 Absorption and Fluorescence Study of Phenolic Standard Solution

Following detection of absorption and fluorescence properties from archaeological samples, several additional analyses were performed to identify the preserved fluorophores in ancient artefacts. For this purpose, standard phenolic derivatives were studied by absorption and fluorescence spectroscopy since they are fluorescent compounds included in oils and wines – widespread commodities in Minoan communities– and are known to preserve within clay matrices over archaeological timescales. In particular, a set of phenolic acids including caffeic acid, ferulic acid (cinnamic-like derivatives), gallic acid, syringic acid (benzoic-like derivatives), and vanillin (benzaldehyde-like derivative) were meticulously analysed.

Figure 18 shows the absorption spectra of phenolic acids and standard phenolic mixture consisting of the five pure phenolic acid derivatives. In general, compounds of similar structure are expected to exhibit similar profiles in absorption spectra. Indeed, there is a clear resemblance between absorption spectra of cinnamic-like derivatives presenting four absorption maxima: at 215, 230, 285, and 310 nm. Similarly, benzoic-like compounds show absorption maxima at 210 and 260 nm while vanillin shows absorption bands centred at 205, 230, 280, and 310 nm. Phenolic standard solution holds a mixture of phenolic compounds, all of which contribute to the overall absorption fingerprint. Unsurprisingly, the phenolic standard solution shows absorption maxima at 210, 230, 285, and 310 nm (Fig. 18b) as a result of the

spectral properties of all phenolic derivatives.

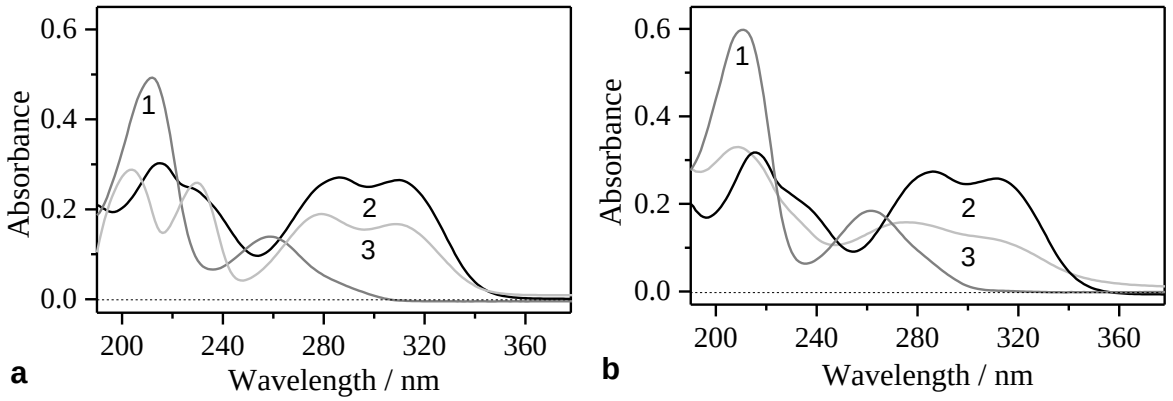

Figure 18. Absorption spectra of phenolic standard solutions in water: (a) gallic acid (1), ferulic acid (2), vanillin (3); (b) syringic acid (1), caffeic acid (2), phenolic standard solution (3). The concentrations of pure phenolic acid solutions are $2x10^{-5}$ M; in mixture each fluorophore is $4x10^{-6}$ M.

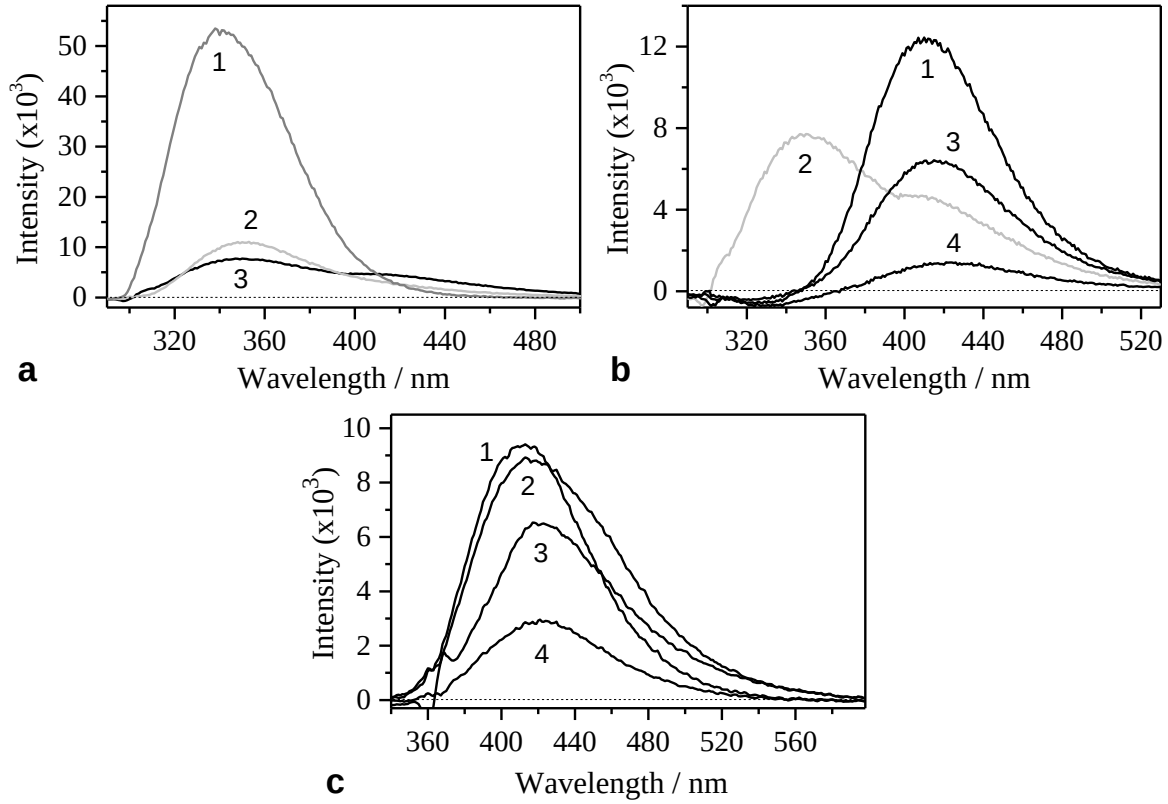

Figure 19. Fluorescence emission spectra of phenolic standard solutions in water: (a) excitation wavelength 275 nm syringic acid (1), gallic acid (2), phenolic standard solution (3); (b) excitation wavelength 275 nm ferulic acid (1), phenolic standard solution (2), caffeic acid (3), vanillin (4); (c) excitation wavelength 325 nm ferulic acid (1), caffeic acid (2), phenolic standard solution (3), vanillin (4).

Among the wide absorption range of phenolic solutions, a set of two excitation wavelengths

was selected in order to proceed with spectrofluorimetric analyses: 275 nm in which all phenolic solutions are excited and 325 nm in which solely cinnamic- and benzaldehyde-like compounds are excited. Upon excitation at 275 nm, gallic acid and syringic acid fluoresce utmost at 340–350 nm (Fig. 19a). When exciting ferulic acid, caffeic acid, and vanillin at 275 nm (Fig. 19b) and at 325 nm (Fig. 19c), an emission band at maximum 410–420 nm is recorded. Upon excitation at 275 nm, the phenolic standard solution exhibits two emission maxima as a combination of the fluorescence properties of phenolic constituents: at 350 and at 420 nm. In case of excitation at 325 nm, the phenolic standard solution generates an emission band with a maximum at 420 nm due to the presence of cinnamic- and benzaldehyde-like derivatives.

Fluorescence emission maxima indicate the right wavelength to set in emission monochromator, in order to record an optimum excitation spectrum. As can be seen from Figure 20a, the excitation spectra of gallic acid, syringic acid, and phenolic standard solution are dominated by a band centred at 265–275 nm when emission wavelength is set at 350–360 nm. Figure 20b shows that excitation spectra of ferulic acid, caffeic acid, vanillin, and phenolic standard solution present an excitation maximum at 320 nm with a shoulder at 285 nm. Fluorescence excitation profiles are expected to agree with the corresponding absorption profiles. However, the excitation and absorption spectra of ferulic acid, caffeic acid, vanillin, and phenolic standard solution demonstrate differences in band's shape. This is probably owing to weak emission profile of Xe-lamp (irradiating source in spectrofluorimeter) in wavelength range between 220 and 300 nm.

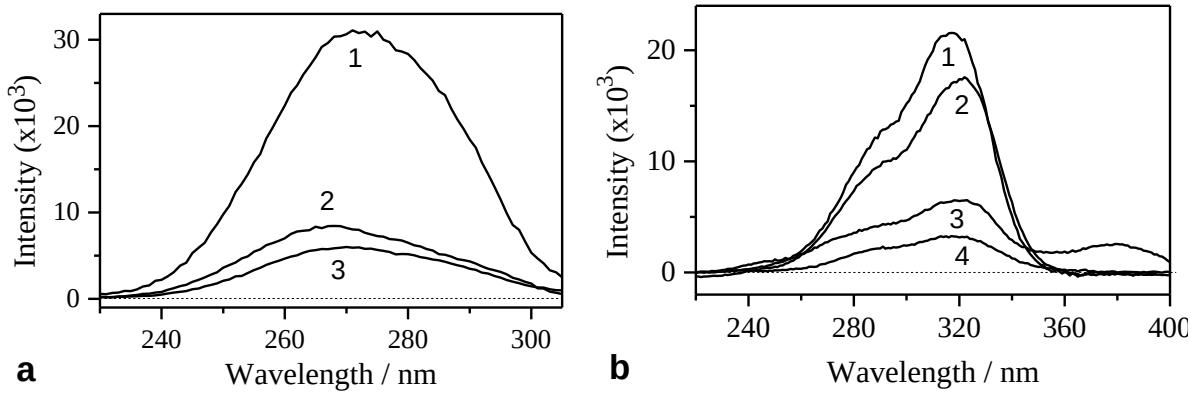

Figure 20. Fluorescence excitation spectra of phenolic standard solutions in water: (a) syringic acid Em 360 nm (1), gallic acid Em 350 nm (2), phenolic standard solution Em 350 nm (3); (b) ferulic acid Em 410 nm (1), caffeic acid Em 420 nm (2), phenolic standard solution Em 415 nm (3), vanillin Em 420 nm (4).

Figure 21 shows the 2D-fluorescence map of phenolic standard solution. The 2D-fluorescence emission-excitation spectral map demonstrates three distinct fluorescent regions at maximum excitation/emission of 275/350 nm, 325/420 nm, and 375/460 nm. The first contour profile (at lower wavelengths) is attributed to benzoic-like compounds (gallic acid, syringic acid), the second one to cinnamic-like compounds (ferulic acid, caffeic acid) and benzaldehyde-like compound (vanillin), and the third one to deprotonated form of caffeic acid (Smith and Haskell, 2000).

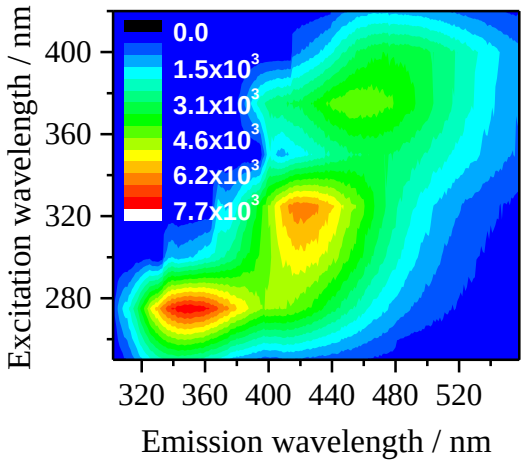

Figure 21. 2D fluorescence emission-excitation spectral map of phenolic standard solution in water.

4.4.3 Archaeological Biomarkers Quantification using Reference Standards

An understanding of how many organic residues were recovered is necessary to elucidate the adequacy of the extracting protocol. To this end, absorption and fluorescence spectroscopy were used to gain considerable insight into the concentration of recovered fluorescent molecules from polar sample MP1I. In order to quantify archaeological fluorophores, solutions of anthracene, quinine sulfate, and ferulic acid were used as reference standards and calculations were based on two assumptions concerning fluorescence quantum yields: they remain constant over a wide spectral range (Table 12) and they are equal among reference standards and archaeo-residues. Although such an approach provides a circuitous way to estimate the quantity of organic residues and entails rough approximations, it is still perceived as a fast method to evaluate ancient residue extraction and detection.

Table 12. Fluorescence quantum yields of quinine sulfate, anthracene, and ferulic acid.

Compound	Solvent	Emission range (nm)	Fluorescence quantum yield, φ_F
Quinine sulfate[a]	1 N H_2SO_4	380−600	0.55
Anthracene[a]	Cyclohexane	360−480	0.36
Ferulic acid[b]	Phosphate buffer	360−560	0.002

Data from: (a) Taniguchi and Lindsey, 2018, (b) Wünsch et al., 2015.

The first step for evaluating fluorescent organic residues is to match the absorbances, i.e. have the same value, of reference standard and sample MP1I at a wavelength that absorbance has a value less than 0.05 in order to avoid the interference of primary and secondary absorption. Hence, the absorbance values were considered for 325 nm, including the reference standards and archaeological sample (Fig. 22a). The next step is to perform fluorescence emission analyses on the basis of previously selected wavelength, that is 325 nm, and record the

maximum area of exhibiting fluorescence (Fig. 22b).

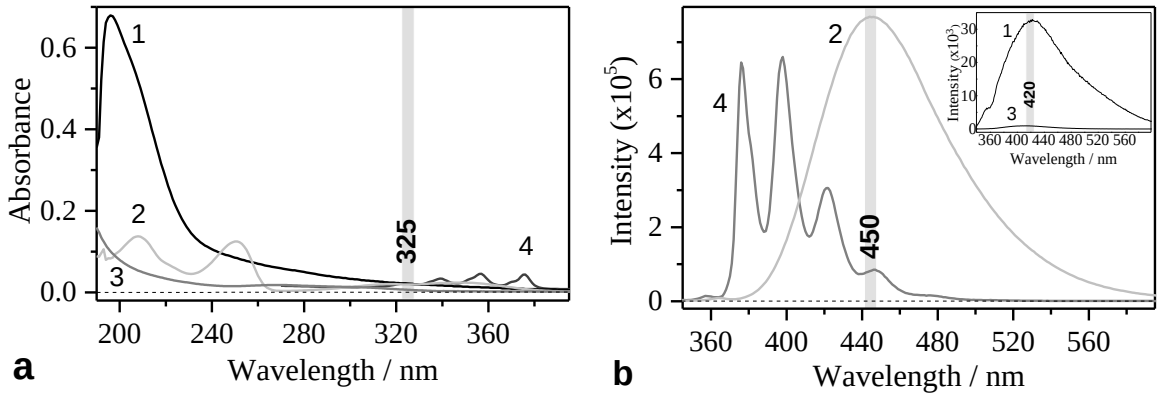

Figure 22. Spectra of sample MP1I in water/methanol (4:1) v/v (1); quinine sulfate dihydrate in 0.5 M sulfuric acid, $2.5x10^{-7}$ M (2); ferulic acid in water, $2x10^{-6}$ M (3); anthracene in ethanol, $6x10^{-6}$ M (4): (a) absorption spectra, (b) fluorescence emission spectra at excitation wavelength 325 nm.

Once emission spectra have been generated, maximum emission intensities should be corrected on the basis of equal absorbances (0.018) at 325 nm (Table 13). This method should be employed since absorbances of reference standards and archaeological sample MP1I differ at 325 nm.

Table 13. Absorbance at 325 nm and fluorescence emission intensity of sample MP1I in H_2O/MeOH (4:1) v/v and reference standards quinine sulfate dihydrate in 0.5 M H_2SO_4, anthracene in ethanol, and ferulic acid in water.

	Absorbance at 325 nm	Fluorescence emission intensity, Exc 325 nm
MP1I in H_2O/MeOH (4:1) v/v	0.018	33000 (Em 423 nm)
Quinine sulfate dihydrate in 0.5 M H_2SO_4, $2.5x10^{-7}$ M	0.018	767000 (Em 450 nm)
Anthracene in CH_3CH_2OH, $6x10^{-6}$ M	0.014	85000 (Em 447 nm) 109000 (Em 447 nm)*
Ferulic acid in H_2O, $2x10^{-6}$ M	0.006	900 (Em 410 nm) 2700 (Em 410 nm)*

* corrected emission intensity if absorbance was 0.018

To evaluate recovered fluorescent residues from polar extract MP1I, emission maximum intensities for both reference standard and archaeological extract as well as concentration of reference standard should be applied in equation 4.1.

$$X=\frac{I_{fluo}\ (\text{reference fluorophore})}{I_{fluo}\ (\text{sample MP1I})} \qquad X=\frac{C\ (\text{reference fluorophore})}{C\ (\text{sample MP1I})} \qquad (4.1)$$

Concentrations of archaeological fluorophores were variable depending on reference standards used for calculation. More specifically, the calculating approach yielded relative concentrations of fluorescent biomarkers ranging approximately from 10^{-8} M to 10^{-5} M (Table 14). Despite this variability, the resulting concentrations are within the detection limit of fluorescence spectroscopy (roughly 10^{-10} M) and provide a general evaluation of the effectiveness of the utilised extraction protocol. The concentration of recovered fluorophores calculated on the basis of ferulic acid corresponds to 400 μg/g of potsherd.

Table 14. Concentration of fluorophores in sample MP1I in H_2O/MeOH (4:1) v/v using quinine sulfate, anthracene, and ferulic acid as reference fluorophores.

Reference fluorophore	X	Inner part extract concentration	
		(M)	(ppb)
Quinine sulfate	23.24	$1.08x10^{-8}$	3.51
Anthracene	3.30	$1.82x10^{-6}$	325.70
Ferulic acid	0.08	$2.50x10^{-5}$	4850

Overall, the evaluation of biomarkers based solely on the above-described approach involves discrepancies owing to selected reference standards, however it proves to be a simple method to gain preliminary understanding of how many ancient fluorophores have been recovered by using a proposed extracting protocol. Undoubtedly, deviations from true values can be limited if the choice of reference standards is governed by an awareness of the biomarkers' nature seeking to quantify.

4.5 Discussion

Broadly speaking, identification of organic residues within archaeological contexts relies on the detection of unique chemical fingerprints arising from complex mixture components. These mixtures originate from intricate degradation pathways of intact biomarkers and pose dual interpretation challenges regarding lack of thorough understanding of microbial digestion during vessels interment and effect of burial conditions such as pH, soil composition, water presence, and oxygen levels. The broadening of contour profiles in all studied archaeological samples provides compelling evidence that extracts contained complex mixtures of degradation products.

Three archaeological samples were extracted from soil adhered to the interior of vessels (MP1S, MP2S, MP3S) and were considered as to include biomarkers indicative of the original content of pre-existing pottery. As a proof of concept, the absorption and fluorescent profiles of inner surface deposits resemble those of encrusted soil in the interior (Fig. 11, Fig. 13) obtained from the same archaeological object (MP1I, MP1S). NMR spectroscopy has been

previously employed to study Minoan samples and led to detection of wine biomarkers (acetoin, 2,3-butanediol) in polar samples MP1I, MP1O, MP1S and oil biomarkers (unsaturated fatty acids) in nonpolar samples MP2S, MP3S (Tsana, 2018). Absence of biomarkers was confirmed in nonpolar samples MP1I, MP1S.

Three archaeological samples (MP1I, MP1O, MP1S) coming from different parts of the same Minoan vessel produced similar absorption and fluorescent profiles (Fig. 11, Fig. 12, Fig. 13) suggesting the presence of similar-structured fluorescent biomarkers. In particular, all of the samples absorbed in the UV spectral region with a maximum at 195 nm and exhibited a major emission peak at 420 nm (upon excitation at 325 nm) that was red-shifted as excitation wavelength was increased. The red-shift is ascribed to the presence of similar-structured degradation products. These findings agree with fluorescent profiles of intact standard phenolic acids and specifically with those associated with cinnamic- (ferulic acid, caffeic acid) and benzaldehyde-like (vanillin) derivatives (Fig. 19, Fig. 20, Fig. 21). Therefore, it is recommended that recovered phenolics from object 1 were not subjected to degradation processes during burial.

In addition, considering the polar extracts MP1I, MP1O, and MP1S, relative intensities of both absorption and fluorescence spectra denote higher quantities of recovered fluorophores in interior deposits compared with adhered soil crust and higher quantities of the latter compared with exterior deposits (sampling and extraction protocol were the same for the samples in question). The presence of biomarkers in exterior surface is probably attributed to intrusion of phenolic acids into pottery matrix during storage of wine. Indeed, polyphenols originating from wine are known to permeate into both pitched and non-pitched ceramic fabric (Romanus et al., 2009).

The fact that biomarkers were detected neither in nonpolar sample MP1I nor in MP1S on the basis of NMR spectroscopy is possibly attributed to three different scenarios: (i) biomarkers have not preserved within ceramic matrix, (ii) biomarkers conserved within pottery but have not been recovered using the specific extracting protocol, or alternatively (iii) biomarkers were effectually extracted but are under the NMR detection limit. Regardless of cause, the successful detection of biomarkers using fluorescence spectroscopy (albeit in low intensities) highlights the complementary relationships among fluorescence and NMR results and that it is rather unexpected for fluorescence and NMR findings to coincide. More specifically, sample MP1I in chloroform yielded two contours at maximum excitation/emission 300 nm/350 nm and 360 nm/440 nm, respectively (Fig. 14) recommending thus the concomitant presence of residues associated with two different chemical classes. Interestingly, the former contour appears to emerge from slightly-degraded biomarkers as their fluorescence profile is exceptionally localised and does not expand as excitation wavelength increases. The latter contour is possibly ascribed to the presence of conjugated di- and tri-enes containing carbonyl functional groups (known as secondary oxidation products) that are considered as biomarkers of olive oil resources (Sikorska et al., 2012).

Regarding sample MP1S in chloroform, a principal contour is recorded at maximum excitation/emission 340 nm/420 nm (Fig. 15) proposing the existence of one certain class of bio-organic material. It is rather surprising to note that the fluorescence features of nonpolar

sample MP1S disagree with those of nonpolar sample MP1I but resemble those of polar samples MP1I, MP1O, and MP1S suggesting the extraction of similar-structured fluorophores (phenolic acids) utilising both chloroform and water/methanol (4:1) as extracting solvents. As a result of fluorescence findings for both polar and nonpolar extracts, it is proposed that Minoan amphora (object 1) was used to store wine and olive oil since both wine and oil biomarkers were detected.

Soil samples MP2S and MP3S originating from objects 2 and 3 appear a similar area of maximum fluorescence at 340–380 nm and 420–460 nm for excitation and emission, respectively. These fluorescence features associate with secondary oxidation products of unsaturated lipids. Alongside fluorescence results, NMR analyses performed on both MP2S and MP3S samples have securely identified a series of unsaturated fatty acids (e.g. oleic acid, linoleic acid) as preserved organic residues, providing evidence for olive oil storage. In conjunction with fluorescence and NMR studies, it is suggested that cylinder Minoan vessels (objects 2 and 3) served as olive oil containers.

As a final comment, one should bear in mind that every single sherd excavated from an archaeological site is a potential source of concurrent biomarkers coming from multiple natural products processed and stored throughout vessel's use. For instance, a vessel originally filled with wine could afterwards be used to store oil, whereas the reverse seems improbable to occur as oil is hard to utterly remove from ceramic fabric in the absence of appropriate detergents. Consequently, it is a quite challenging effort to detect and characterise the whole range of preserved organic materials and reconstruct unambiguously the patterns of diet across ancient communities.

CHAPTER 5: Organic Residue Extraction from Modern and Artificially Aged Potsherds

5.1 Analytical Protocol for Olive Oil Extraction from Potsherds

The detection and identification of bio-organic residues from potsherds depend on the extracting methodologies utilised to recover residues from ceramic fabric. The selection of extracting solvents should be made with great caution, ideally taking into account the nature of organic remnants (e.g. polarity, solubility) seeking to detect (Cnuts and Rots, 2018). Here, it is described a stepwise procedure developed to effectively extract organic residues from clay matrices on the basis of two solvents of different polarity: water (polar) and isooctane (nonpolar).

Fresh extra virgin olive oil was used as model sample to establish the extraction method from modern potsherds (Table. 15). First, a cleaning protocol was designed to remove contaminants and thus purify clay matrices. For this purpose, eight ceramic fragments (7−12 g) were rinsed with 5 mL and then soaked into 20 mL nanopure water within a beaker for 72 h using a clean glass petri dish to prevent airborne contamination. Afterwards, potsherds were removed from water by metal forceps and soaked once again into 5 mL fresh nanopure water for 2 h. The water extract was analysed on the basis of absorption and fluorescence spectroscopy revealing that ceramic fragments were cleaned from polar fluorescent contaminants. The same cleaning procedure was repeated via the use of isooctane as a cleaning agent of nonpolar contaminants present within body sherds. Following absorption and fluorescence study, the final isooctane extract showed the absence of nonpolar fluorescent contaminants rendering the eight ceramic fragments suitable for absorbing oil residues.

In order to be spiked with different oil residue types, the cleaned potsherds were dried and soaked into 20 mL fresh extra virgin olive oil for 48 h. In addition, spiked potsherds were placed on a perforated piece of aluminum foil, underneath of which was laid a piece of paper towel to absorb the excess of oil.

The extraction methodology was performed crushing and grounding spiked potsherds to a powder using a pestle and mortar. Amounts of 500 mg of the ceramic powders originating from each spiked potsherd were transferred in two vials containing 5 mL isooctane and 5 mL nanopure water each. An ultrasonic bath was used for 30 min to improve solubility of organic compounds in extracting solvent by weakening intermolecular interactions and bonds formed between oil markers and clay particles. After 72 h, ceramic powders were removed from the extracting solvents by simple filtration. Solutions were then centrifuged (6000 rpm) for 20 min

to remove suspended particulate matter and the supernatants containing oil residues were once again filtered.

Table 15. Analytical protocol for cleaning, spiking and recover organic residues from ceramic fragments.

Protocol	Experimental procedure
Potsherd cleaning	1. Rinse potsherds with 5 mL nanopure water. 2. Soak potsherds into 20 mL nanopure water for 72 h and then discard the extract. 3. Soak potsherds into 5 mL nanopure water for 2 h. 4. Study the latter extract by absorption and fluorescence spectroscopy. i. In case of hydrophilic contaminants detection, repeat steps 1−3. ii. In case of absence of hydrophilic contaminants, proceed to step 5. 5. Repeat steps 1−4 using isooctane to remove lipophilic contaminants.
Liquid foodstuff spiking	1. Soak potsherds into 20 mL liquid foodstuff for 48 h. 2. Dry spiked potsherds on a perforated aluminum foil placing a dish cover to preclude airborne contamination.
Organic residue extraction	1. Crush and ground spiked potsherds using a pestle and mortar. 2. Transfer 500 mg of ceramic powder to 5 mL isooctane to extract nonpolar residues. 3. Transfer 500 mg of ceramic powder to 5 mL nanopure water to extract polar residues. 4. Enhance extraction in steps 2−3 utilising an ultrasonic bath for 30 min. 5. After 72 h, separate extracting solvents from ceramic powders by simple filtration. 6. Centrifuge the extracts (6000 rpm) for 20 min. 7. Filter the supernatants to remove any ceramic particles.

5.2 Evaluating the Success Rate of Extraction Protocol

The extraction methodology described in the previous section was developed for spectroscopic analysis of organic food residues within potsherds. Quantitative knowledge concerning the success of employed recovery protocol provides a comprehensive insight into how many organic residues have been removed from ceramic matrix and raises awareness of experimental circumstances that need to be modified in order to attain higher extraction efficiency (Barker et al., 2012). Extra virgin olive oil standard solutions diluted in isooctane were prepared to evaluate the effectiveness of suggested extraction method monitoring chlorophyll *a* emission band, viz at 670 nm. Chlorophyll-derivatives are the most appropriate reference residues relevant to the intrinsic fluorophores present in oils (Zandomeneghi et al., 2005).

Extra virgin olive oil was obtained from the local market and was diluted in isooctane yielding six samples with varying oil-content concentrations: 1:100, 1:300, 1:500, 1:700, 1:850, 1:1000 v/v. Considering that density of extra virgin olive oil is 0.917 mg/mL (Peri, 2014), concentrations of six standard oil samples equal to: 0.92, 1.10, 1.37, 1.83, 3.03, and 9.17 μg/mL. This dataset was selected because it complies with Beer-Lambert's law (Fig. 23a). Chlorophyll *a* has a principal emission band at 670 nm upon excitation at 400 nm (Fig. 23 b−c). To assess the success of proposed extraction protocol, a calibration curve was generated by plotting emission intensities of chlorophyll *a* against concentrations of standard oil solutions (Fig. 23d).

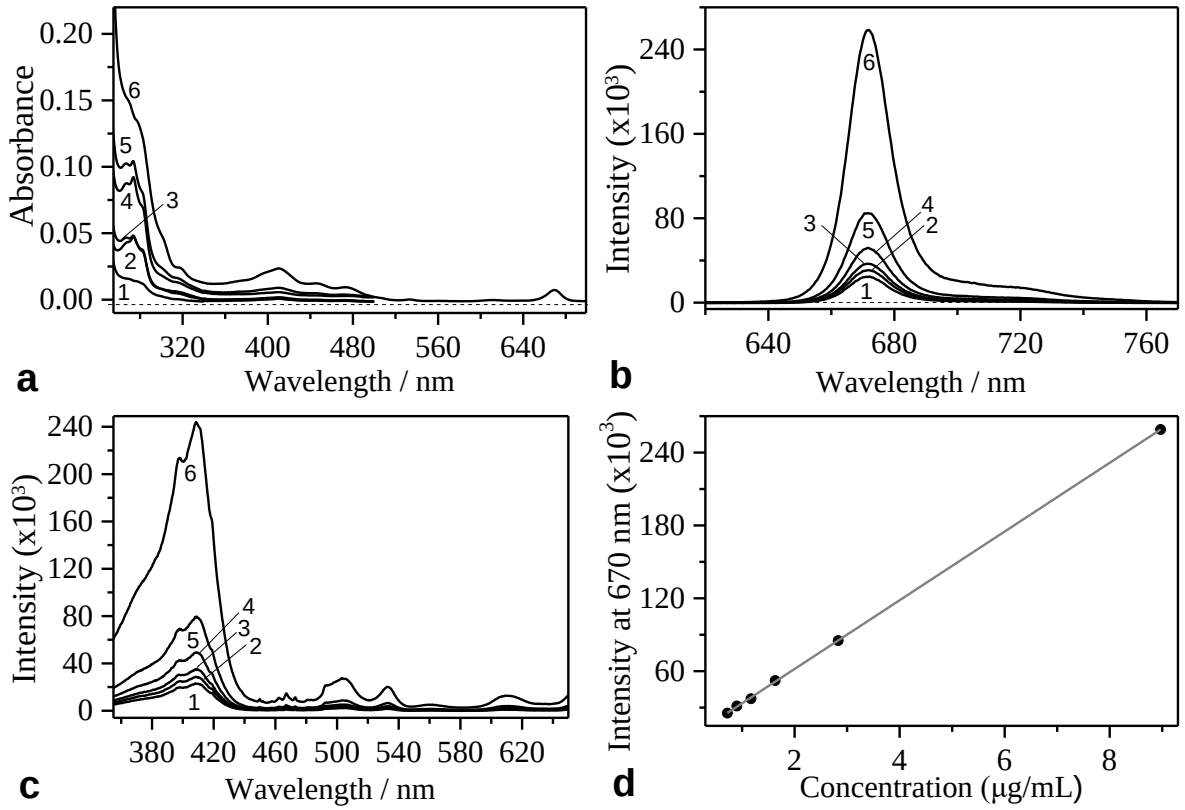

Figure 23. Spectra of extra virgin olive oil in isooctane with concentration 0.92 (1), 1.10 (2), 1.37 (3), 1.83 (4), 3.03 (5), 9.17 (6) μg/mL: (a) absorption spectra; (b) fluorescence emission spectra at excitation wavelength 400 nm; (c) fluorescence excitation spectra at emission wavelength 670 nm; (d) calibration curve showing the effect of concentration of extra virgin olive oil in isooctane on the emission intensity of chlorophyll *a* at 670 nm.

Extraction of bound chlorophyll *a* using isooctane was assessed on the basis of spectrofluorimetric analysis. In particular, 7 g of blank ceramic was spiked with 1.5 g neat extra virgin olive oil (total mass 8.5 g). Then, the oil-spiked potsherd was crushed and grounded to a fine powder. The extraction method was performed on 500 mg of spiked-ceramic powder containing 90 mg of neat olive oil. Quantitative assessment of chlorophyll *a* recovery provides a reliable method for evaluating the degree of success of extraction protocol. Figure 24 shows that extracted chlorophyll *a* exhibits fluorescence of intensity about 5500 arbitrary units. Therefore, the recovered olive oil content was determined to be 0.5 μg on the basis of

calibration curve (Fig. 23d) and taking into account that extraction was performed by using 5 mL isooctane.

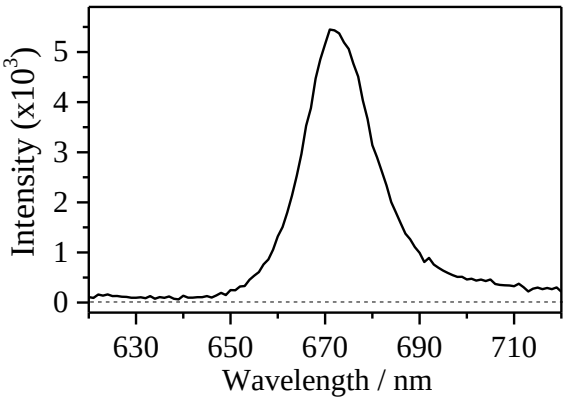

Figure 24. Fluorescence emission spectrum of chlorophyll *a* extracted from 500 mg ceramic using isooctane at excitation wavelength 400 nm.

The extraction procedure proposed herein yielded recovery efficiency less than 0.1% (Eqn 5.1). Although the preliminary results show very low olive oil extraction (0.1 μg/mL), they yet prove that sensitivity of fluorescence spectroscopy is eligible for evaluation of extraction methodology. To improve the recovery of chlorophyll pigments from olive oil it is suggested to use alternative solvent treatments. For instance, diethyl ether and dimethylformamide (DMF) have been successfully used to extract chlorophylls *a* and *b* (Cichelli and Pertesana, 2004).

$$\% \text{ Extraction Efficiency} = \frac{\text{mass of recovered olive oil}}{\text{mass of spiked olive oil}} \text{ x } 100\% \qquad (5.1)$$

5.3 UV Artificial Aging Process

The project presented in this section was designed to simulate the aging processes of olive oil and phenolic standard solution in a UV-irradiating environment. Although this approach does not represent natural aging of organic residues during interment of artefacts since they are not exposed to light, it yet provides a method to accelerate natural aging. Analytical procedures are divided into five phases of experimentation (Scheme 16). In the first phase, sherds from a modern ceramic plate were meticulously cleaned with water. After washing, the potsherds were assessed by means of fluorescence spectroscopy to ascertain whether undesirable fluorophores were removed from the clay matrices. The second phase was designed to spike cleaned potsherds with foodstuff residues. In the third phase, spiked potsherds were artificially aged in a custom-built UV-aging chamber. Protracted exposure to UV illumination is considered to cause photodegradation of organic residues. In the fourth, phase, an efficient extraction protocol was performed to recover aged residues from the ceramic matrices. In the fifth and final phase, the aged extracts were studied in UV-vis absorption and fluorescence spectroscopy.

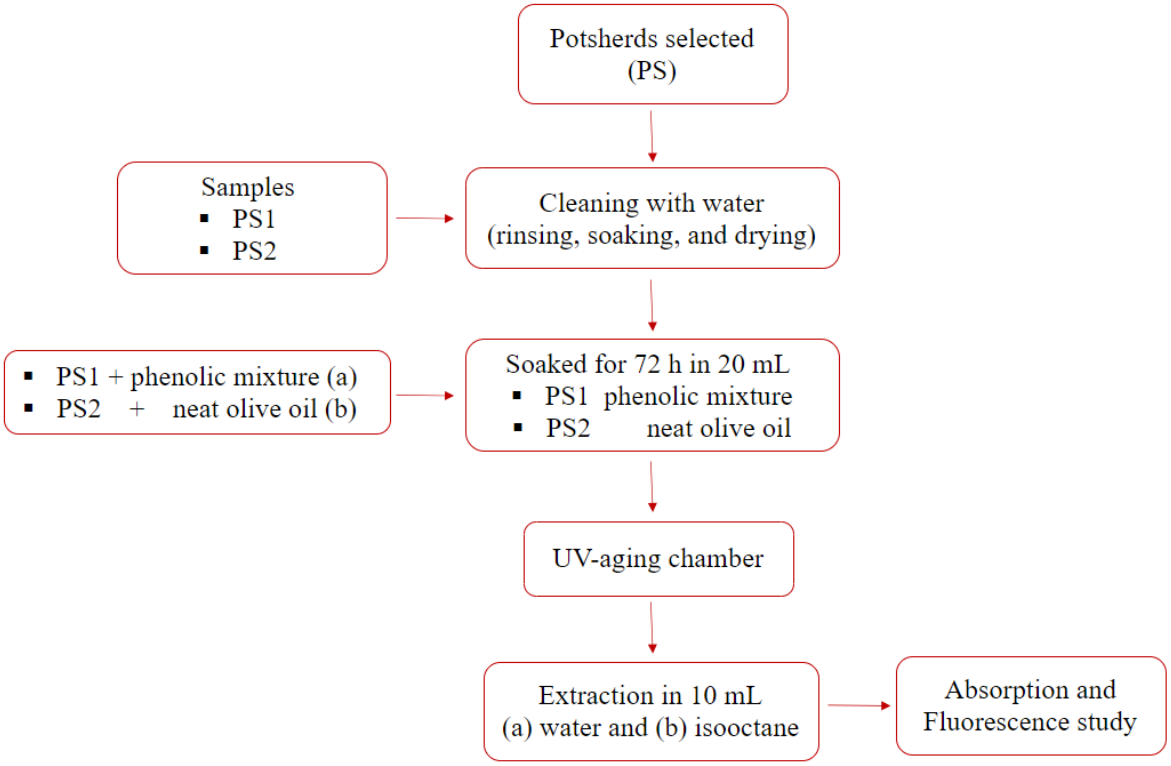

Scheme 16. The sampling and extraction protocol established for this project.

Ceramic fragments were cleaned and spiked by applying strategies described in Table 15. Neat olive oil and phenolic standard solution were absorbed in two potsherds (Scheme 17) and then placed in the aging chamber. The artificial aging was carried out in a custom-built aging chamber using mercury discharge lamps (Philips, Master TL−D super 80) that emit a broad spectral illumination in near-UV (maximum at 360 nm) and visible regions.

Scheme 17. Potsherds spiked with neat olive oil and phenolic standard solution and transferred in a custom-built UV-aging chamber.

Illumination intensity was measured via a commercial digital light meter (Tecpel DLM532). Neat olive oil- and phenolic standard solution-containing potsherds were illuminated for 1800 h and 5400 h, corresponding to 4.7×10^7 lx h and 1.4×10^8 lx h, respectively. Aged foodstuff residues were recovered from potsherds employing extraction methodology described in Table

15. In particular, oil and phenolic residues were recovered using isooctane and water, respectively, as extracting solvents.

5.4 Results

This section reports the spectral features of photodecomposition products formed by prolonged exposure of olive oil and standard phenolic solution to UV-illuminated conditions. Phenolics were selected as they constitute part of minor fluorescent constituents in vegetable oils known to degrade into fluorescent derivatives upon oxidative reactions. Intact samples were loaded on potsherds, placed in a custom-built artificially aging chamber, and recovered employing the extraction protocol described in Section 5.1. Experimentation demonstrated that foodstuff residues degraded during the UV-aging process, were successfully recovered from the potsherds by using viable extraction methodologies, and were identified using UV-vis absorption and fluorescence spectroscopy.

5.4.1 Absorption and Fluorescence Study of Artificially Aged Samples

Figure 25 depicts the absorption and fluorescence spectra of artificially photodegraded phenolic standard solution in water containing ferulic acid, caffeic acid, vanillin, syringic acid, and gallic acid. The aged sample absorbs in the UV spectral region exhibiting a featureless tail-like profile (Fig. 25a). Degradation products of intact phenolics contribute to the fluorescence features of artificially aged sample. As seen in Figure 25b−c, a strong fluorescence emission at 360 nm is generated by excitation at 300 nm. The 2D-fluorescence map shows a contour with excitation at maximum 290−310 nm and maximum emission at 350−380 nm (Fig. 25d). Note that emission shifts to higher wavelengths as excitation wavelength increases being in accordance with 1-D emission spectra.

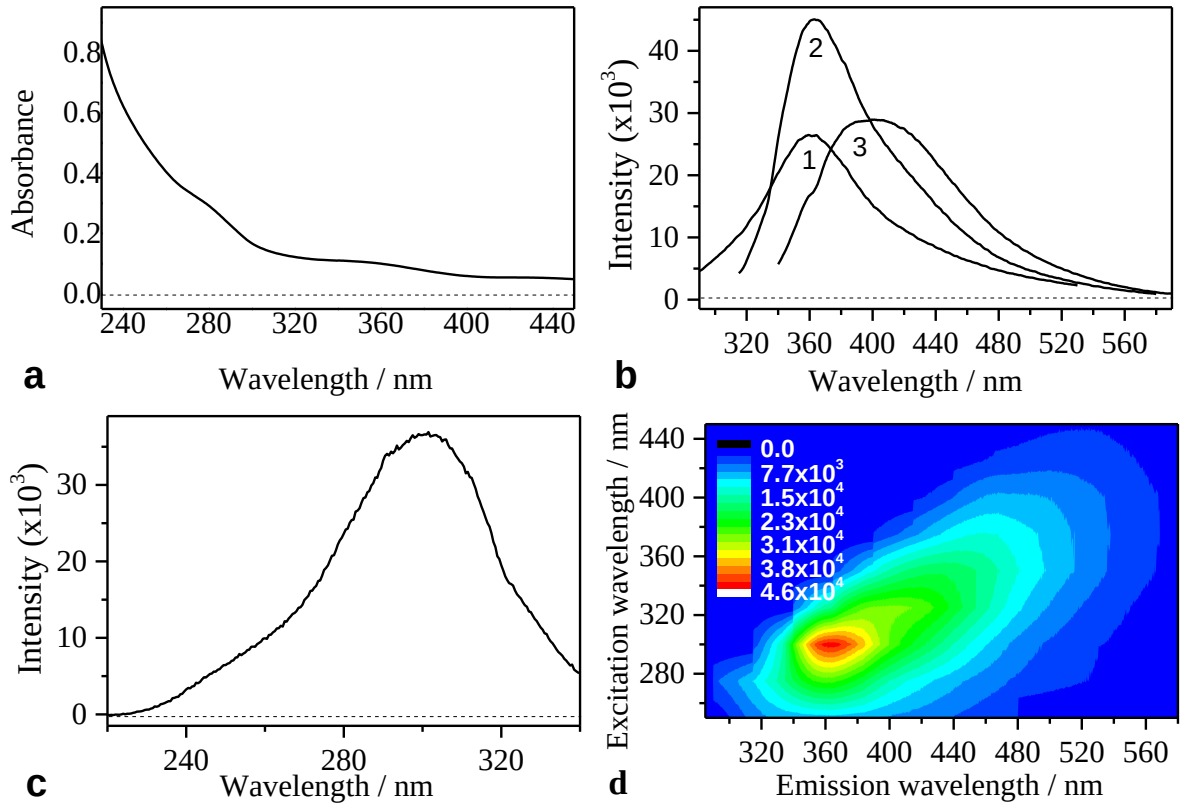

Figure 25. Spectra of artificially aged phenolic standard solution in water: (a) absorption spectrum; (b) fluorescence emission spectra at excitation wavelength 275 nm (1), 300 nm (2), 325 nm (3); (c) fluorescence excitation spectrum at emission wavelength 360 nm; (d) 2D fluorescence emission-excitation spectral map.

Figure 26 shows the spectral features of an artificially aged oil sample exposed to a custom-built irradiating-environment. The photodegraded oil sample absorbs UV-radiation (especially below 320 nm) demonstrating two humps at 280 and 325 nm (Fig. 26a). The 1D-fluorescence spectra illustrate three emission bands of similar intensities centred at 325, 360, and 450 nm (Fig. 26b) by exciting at wavelengths 275, 300, and 400 nm, respectively. Excitation spectra demonstrate the existence of more than one fluorophore as excitation at 350 and 420 nm generates emission at maxima 290 and 370 nm, respectively (Fig. 26c). The 2D-fluorescence landscape reveals the concomitant presence of three different regions of fluorescence: one demonstrating excitation maximum at 270−280 nm and emission maximum at 310−340 nm, a second with maximum areas of excitation and emission at 290−305 nm and 350−370 nm, respectively, and a third presenting excitation maximum at 395−405 nm and emission maximum at 440−465 nm (Fig. 26d).

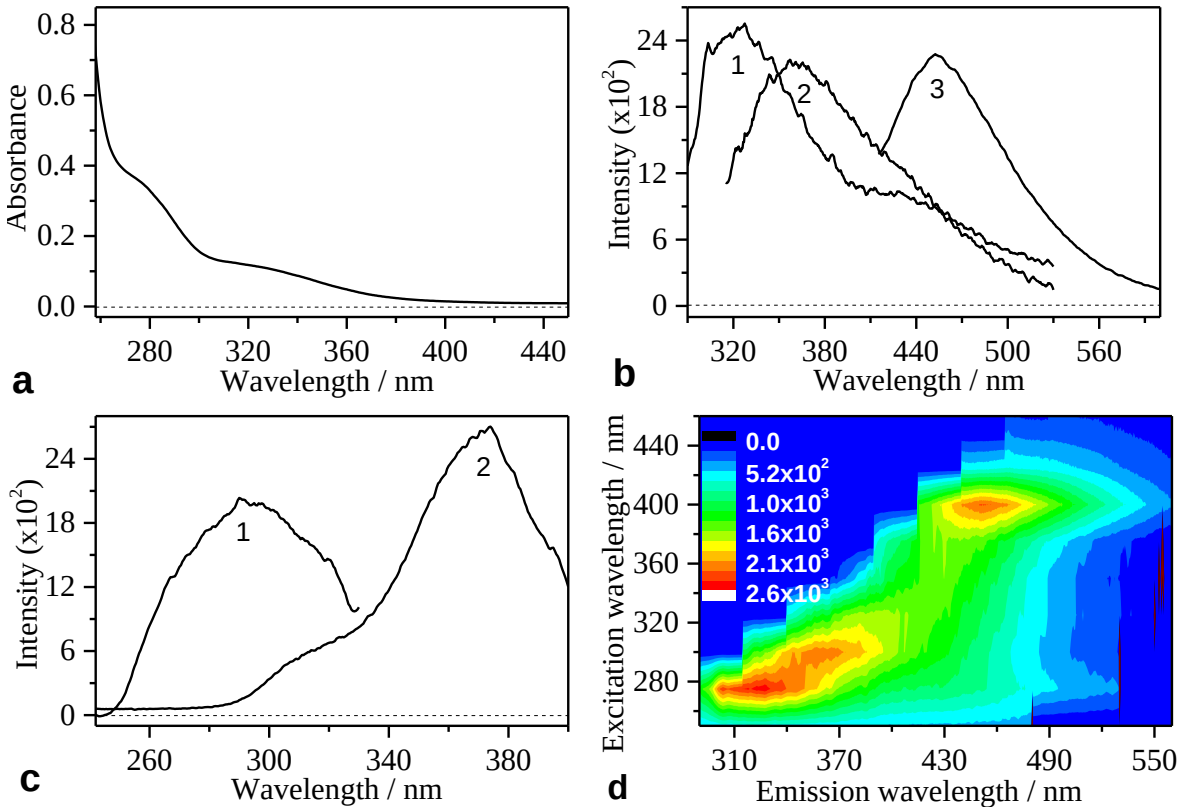

Figure 26. Spectra of artificially aged extra virgin olive oil in isooctane: (a) absorption spectrum; (b) fluorescence emission spectra at excitation wavelength 275 nm (1), 300 nm (2), 400 nm (3); (c) fluorescence excitation spectra at emission wavelength 350 nm (1), 420 nm (2); (d) 2D fluorescence emission-excitation spectral map.

5.5 Discussion

Prolonged exposure of vegetable oils to UV-light provokes deterioration of oil constituents via oxidative reactions. These UV-induced oxidation processes are considered to simulate reasonably the natural aging of olive oils and are therefore utilised to explore the formation of new fluorescent products. Intact olive oil contains 75−85% fatty acids dominated by the presence of oleic acid ($C_{18:1}$) which is a monosaturated fatty acid (Irmak and Tokusoglu, 2017). Fresh olive oil also holds a variety of fluorescent compounds albeit in low content such as phenolic compounds, tocopherols and pigments, chiefly carotenoids and chlorophylls (Lang et al., 1991). These minor components generate autofluorescence of olive oils, while polyphenols and tocopherols also determine their antioxidant potential (Giuliani et al., 2011). Oleuropein is the major polyphenol in olive fruits (Damak et al., 2008) and decomposes into phenolic oligomers during olive oil extraction process with tyrosol, hydroxytyrosol, and vanillic acid (Scheme 18) being the principal degradation products (Uylaser, 2014). Both fatty acids and fluorescent compounds present in olive oils are susceptible to temperature and light exposure leading to thermal- and photo-oxidation processes.

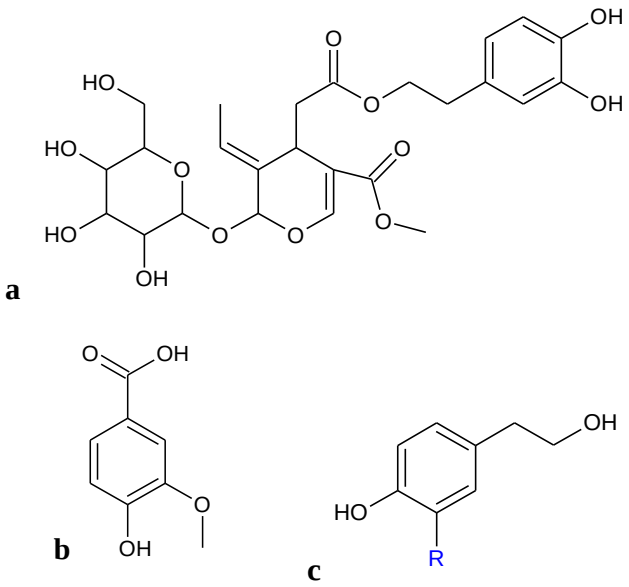

Scheme 18. Structures of major phenolic compounds present in olive oil: (a) oleuropein; (b) vanillic acid; (c) tyrosol (R=H), hydroxytyrosol (R=OH).

Degradation products formed by complex photo-induced oxidation mechanisms affect the exhibiting fluorescence of aged oil samples. In particular, the chlorophyll content reduces progressively and vanishes completely under 4-month UV-illuminated conditions (Hernandez-Sanchez et al., 2017). Likewise, carotenoids display low photo-stability and drastically decrease in concentration following exposure to light (Criado et al., 2007). Tocopherols also diminish upon exposure to UV-light hampering oxidative reactions of fatty acids until they are completely decomposed (Rabiej and Szydlowska-Czerniak, 2020). The detection of chlorophyll-, carotenoid-, and tocopherol-related compounds by means of fluorescence spectroscopy is thus excluded in aged oil samples as a consequence of their rapid decomposition into nonfluorescent derivatives through light-induced pathways.

Limited research efforts have been performed concerning the degradation processes of phenolic compounds during photo-induced artificial aging. What is known is that phenolic compounds are quite resistant upon UV treatment, with gallic acid and vanillic acid being the most stable (Volf et al., 2013). The present work provides strong evidence that points to formation of new fluorescent compounds from intact phenolic oligomers exposed to protracted UV radiation. As depicted in Figure 25, degradation products absorb UV light and specifically emit fluorescence in the region 350−380 nm upon excitation at 290−310 nm. Interestingly, these fluorescence properties coincide with benzoic- and benzaldehyde-like acids (Fig. 19−20). A possible hypothesis is the conversion of cinnamic-derivatives (e.g. ferulic acid, caffeic acid) to vanillic- and benzoic-derivatives (e.g. gallic acid, syringic acid) via cleavage of carbon-carbon bond in the acrylic acid group. There is ample evidence that the proposed mechanism governs the decomposition of phenolics upon thermal treatment (Ali et al., 2020) but it requires further research to clarify whether light-induced degradation evolves through the same pathway.

Heat, light, and molecular oxygen exposure promote the oxidation of unsaturated fatty acids, ultimately yielding to the formation of fluorescent compounds (Scheme 19). Major lipid oxidation mechanisms involve the autooxidation process that evolves via free radical chain reactions and the photooxidation procedure that requires reactive singlet oxygen formed by chlorophyll during photosynthesis (Dominguez et al., 2019). Auto- and photo-oxidative reactions yield the same degradation products following different oxidation steps. In the case of photooxidation, unsaturated fatty acids initially react with singlet oxygen and form hydroxyperoxides, known as primary oxidation products (Rahmani and Csallany, 1998). Since these compounds are labile, they rapidly decompose into secondary oxidation products that include conjugated di- and tri-enes carrying hydroxyl or carbonyl functional groups (alcohols, aldehydes, ketones) (Mishra et al., 2018). Both primary and secondary oxidation products absorb light in the UV spectral region maximising at 230 and 270 nm, respectively (Grigoriadou and Tsimidou, 2006). Secondary oxidation products have been extensively reported in literature and are known to fluoresce in the region 450−480 nm upon excitation between 350 and 370 nm (Manzano et al., 2019; Rotich et al., 2020).

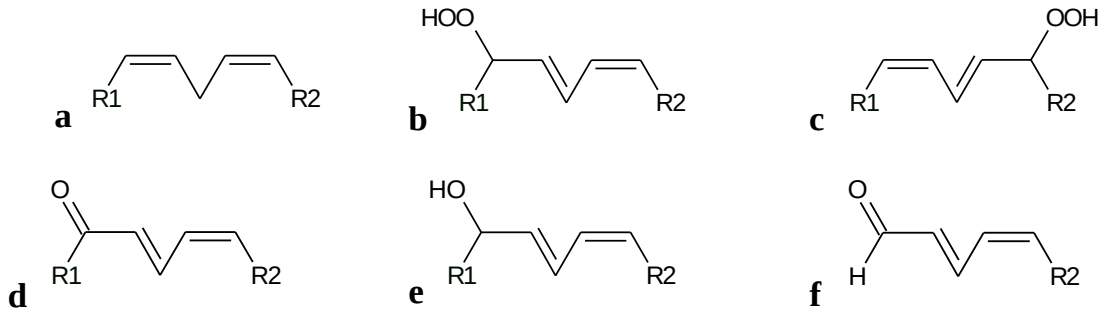

Scheme 19. Structures of: (a) an unsaturated lipid; (b) and (c) conjugated dienes of a lipid hydroxyperoxide (primary oxidation products); conjugated diene of a lipid (d) ketone, (e) alcohol and (f) aldehyde (secondary oxidation products).

As seen in Figure 26, the artificially aged oil sample studied for the purpose of this work demonstrated absorption and fluorescence features that correlate well with those of constituents formed by photooxidation of unsaturated lipids (Sikorska et al., 2007). In particular, the hump at 280 nm observed in absorption spectrum as well as the fluorescence band at excitation/emission 400/450 nm is probably associated with secondary oxidation products (conjugated di- and tri-enes). Furthermore, the fluorescence properties of oil minor constituents were also detected in aged oil sample. Fluorescence emission at 325 nm upon excitation at 275 nm is suggested to arise from tyrosol and hydroxytyrosol (Llorent-Martinez et al., 2013) while emission at 360 nm generated by excitation at 300 nm is possibly ascribed to vanillic acid (Cabrera-Banegil et al., 2017). It is interesting to note that the latter fluorescence region is similar to the one generated from artificially aged phenolic compounds (Fig. 25d).

Conclusion

Spectrochemical tools hold potential to enrich archaeological research by expediting the selection of "good candidates" for analysis at the molecular level. In light of this expectation, absorption combined with fluorescence spectroscopy was applied to differentiate between fluorescent organic residues originating from archaeological potsherds with the prime objective to establish a link of biomarkers to natural sources. To this end, a total of seven polar and nonpolar extracts from different parts of three Minoan ceramic vessels were studied by means of absorption and fluorescence spectroscopy. The spectral features of standard phenolic derivatives (ferulic acid, caffeic acid, vanillin, syringic acid, gallic acid) were also investigated to aid the identification of extracted organic residues from archaeological samples. Following conclusions can be drawn from the analysis of results:

(i) Phenolics and secondary oxidation products of lipids are considered as wine and oil markers, respectively.

(ii) Minoan amphora (object 1) probably served two purposes: it was used as olive oil and wine container as both oil and wine molecular indicators were detected. It is suggested that the initial mode of use was the storage of wine and then the storage of oil.

(iii) Phenolics from object 1 possibly were not subjected to degradation processes due to diagenesis as their fluorescence profiles coincided with those of intact standard phenolic compounds.

(iv) Minoan cylinder vessels (objects 2 and 3) were probably utilised as olive oil containers since it was verified the presence of secondary degradation products of lipids.

Furthermore, archaeological biomarkers from polar extract of the inner part of object 1 (sample MP1I) were quantified on the basis of three reference standards (ferulic acid, anthracene, quinine sulfate). Ferulic acid provides a more realistic choice because it represents the archaeo-residues seeking to quantify, i.e. phenolics. The evaluation approach based on ferulic acid yielded concentration of extracted biomarkers of approximately 400 μg/g of potsherd.

Methodologies for purifying clay matrices, spiking potsherds with food residues, and extracting organic remnants from ceramics were designed using olive oil as model sample. The effectiveness of extraction protocol was measured via fluorescence detection of chlorophyll *a* emission band from standard olive oil samples and was determined to be less than 0.1%.

Finally, absorption and fluorescence spectroscopies were deployed to monitor changes in phenolics and olive oil caused by protracted exposure to UV-radiation. The study showed that non-conjugated double and triple bonds in lipids present in oils convert into conjugated bonds in di- and tri-enes following oxidation processes, while cinnamic-like derivatives degrade to benzoic-like compounds via carbon-carbon cleavage in the acrylic acid functional group.

From the society stand point, the present master's thesis integrates science and humanities as well as it raises social awareness regarding the holistic understanding and protection of humans' cultural heritage. It is my hope that the research effort described herein is going to

introduce the systematic use of spectrochemical tools and thus contribute to the growth of the cross-disciplinary research field of organic residue analysis. The whole of this process is expected to create a stronger link between analytical scientists and archaeologists strengthening scientific knowledge in heritage science by bridging the gap between empirical macroscopic assessment and use of high-end analytical tools.

Future Perspectives

It is not possible to bring to fruition each idea emerging during a master's project. The following future developments are recommended for improving the depth of archaeo-residues investigation based on the tackle of rising questions throughout the experimental procedure already discussed. The principal objectives are the maximization of recovery efficiency of the proposed extraction protocol and the accurate quantification of recovered archaeo-residues. To this end, a set of alternative polar and nonpolar solvents could be used to effectively extract fluorescent constituents from model samples as well as convenient reference standards could be used to precisely calculate the amount of extracted archaeological bio-organic residues. The second objective is the synchronous application of state-of-the-art spectroscopic and chromatographic methods in order to detect and characterise ancient organic remnants. To accomplish this expectation, a large body of ancient samples from different archaeological sites could be at first examined on the basis of modern spectroscopic techniques (fluorescence, NMR, Raman) in order to explore the presence of biomarkers and then apply chromatographic methods (gas chromatography, liquid chromatography) coupled with mass spectrometry to separate components in complex mixtures and chemically characterise the organic materials. The third objective is to unveil the pathways that contribute to degradation of organic residues and affect bio-materials preservation within archaeological timescales. In light of this ambition, standard compounds (proteins, waxes, resins, lipids) could be placed in a custom-built UV-aging chamber and degradation products could be monitored regularly using chromatography-based methods. The final objective is to enable the detection of non-fluorescent compounds – lipids, polysaccharides, etc.– and the amplification of emission signal generated from poorly fluorescent materials, so that they can be investigated using fluorescence spectroscopy. In order to achieve this, extrinsic fluorescent probes (e.g., Congo Red, Picro Sirius Red) could be used to label the molecules of interest.

References

Ahmadi, S., Absalan, G., Craig, D., Goltz, D. Photochemical properties of purpurin and its implications for capillary electrophoresis with laser induced fluorescence detection. *Dyes Pigm., 105*, **2014**, 57–62.

Ali, H., Iqbal, M., Atta, B., Ullah, R., Khan, M. Phenolic profile and thermal stability of monovarietal extra virgin olive oils based on synchronous fluorescence spectroscopy. *J. Fluoresc.*, *30*, **2020**, 939−947.

Ames, J. The Maillard reaction. In: Hudson, B. (Ed.) *Biochemistry of food proteins.* Springer, Boston, **1992**, 99–153.

Arnaoutakis, G. Fluorescence spectroscopy of wine. *Edinburgh Instruments, AN_P17, 15*(3) **2016.**

Asara, J., Schweitzer M., Freimark, L., Phillips, M., Cantley, L. Protein sequences from mastodon and *Tyrannosaurus rex* revealed by mass spectrometry. *Science, 316*, **2007**, 280–285.

Auer, B. M., Skinner, J. L. IR and Raman spectra of liquid water: Theory and interpretation. *J. Chem. Phys., 128*, **2008**, 224511.

Bada, J. Amino acid cosmogeochemistry. *Phil. Trans. R. Soc. Lond. B, 333*, **1991**, 349–358.

Bailey, A., Paul R., Knott, L. Mechanisms of maturation and ageing of collagen. *Mech. Ageing. Dev., 106*, **1998**, 1–56.

Barker, A., Venables, B., Stevens, S., Seeley, K., Wang, P., Wolverton, S. An optimized approach for protein residue extraction and identification from ceramics after cooking. *J. Arcaheol. Method Theory, 19*, **2012**, 407–439.

Barnard, H., Shoemaker, L., Craig, O., Rider, M., Parr, R., Sutton, M., Yohe, R. Introduction to the analysis of protein residues in archaeological ceramics. In: Barnard, H., Eerkens, J. (Eds.) *Theory and practice of archaeological residue analysis*. Archaeopress, Oxford, **2007**, 216–235.

Barnett, N. W., Francis, P. S. Luminescence: overview. In Worsfold, P. J., Townshend, A., Poole, C. F. (Eds.), *Encyclopedia of Analytical Science*. 2nd edition, vol. 3, Elsevier, Oxford, **2005**, 305–315.

Becker, M., Christensen, J., Frederiksen, C., Haugaard, V. Front-face fluorescence spectroscopy and chemometrics in analysis of yogurt: Rapid analysis of riboflavin. *J. Dairy Sci., 86*, **2003**, 2508–2515.

Bengoechea, L., Hernandez, T., Quesada, C., Bartolome, B., Estrella, I., Gomez-Cordoves, C. Structure of hydroxycinnamic acid derivatives established by high-performance liquid chromatography with photodiode-array detection. *Chromatographia*, *41*, **1995**, 94–98.

Boatman, E., Goodwin, M., Holman, H., Fakra, S., Zheng, W., Gronsky, R., Schweitzer, M. Mechanisms of soft tissue and protein preservation in *Tyrannosaurus rex. Sci. Rep.*, *9*, **2019**, 15678.

Bonaduce, I., Colombini, M. Gas chromatography/mass spectrometry for the characterization of organic materials in frescoes of the Monumental Cemetery of Pisa (Italy). *Rapid Commun. Mass Spectrom.*, *17*, **2003**, 2523–2527.

Bruni, S., Guglielmi, V. Identification of archaeological triterpenic resins by the non-separative techniques FTIR and ^{13}C NMR: The case of *Pistacia* resin (mastic) in comparison with frankincense. *Spectrochim. Acta A Mol. Biomol. Spectrosc.*, *121*, **2014**, 613–622.

Cabrera-Banegil, M., Hurtado-Sanchez, M., Galeano-Diaz, T., Duran-Meras, I. Front-face fluorescence spectroscopy combined with second-order multivariate algorithms for the quantification of polyphenols in red wine samples. *Food Chem.*, *220*, **2017**, 168−176.

Cappellini, E., Prohaska, A., Racimo, F., Welker, F., Pedersen, M., Allentoft, M., Damgaard, P., Gutenbrunner, P., Dunne, J., Hammann, S., Roffet-Salque, M., Ilardo, M., Moreno-Mayar, J., Wang, Y., Sikora, M., Vinner, L., Cox, J., Evershed, R., Willerslev, E. Ancient biomolecules and evolutionary interference. *Annu. Rev. Biochem.*, *87*, **2018**, 1029–1060.

Charters, S., Evershed, R., Goad, L., Leyden, A., Blinkhorn, P., Denham, V. Quantification and distribution of lipid in archaeological ceramics: Implications for sampling potsherds for organic residue analysis and the classification of vessel use. *Archaeometry*, *35*(2), **1993**, 211–223.

Christensen, J., Norgaard, L., Bro, R., Engelsen, S. Multivariate autofluorescence of intact food systems. *Chem. Rev.*, *106*(6), **2005**, 1979–1994.

Cichelli, A., Pertesana, G. High-performance liquid chromatographic analysis of chlorophylls, pheophytins and carotenoids in virgin olive oils: Chemometric approach to variety classification. *J. Chromatogr. A.*, *1046*, **2004**, 141−146.

Cnuts, D., Rots, V. Extracting residues from stone tools for optical analysis: Towards an experiment-based protocol. *Archaeol. Anthropol. Sci.*, *10*, **2018**, 1717−1736.

Colombini, M., Giachi, G., Modugno, F., Ribechini, E. Characterisation of organic residues in pottery vessels of the Roman age from Antinoe (Egypt). *Microchem. J.*, *79*, **2005**, 83–90.

Connan, J. Use and trade of bitumen in antiquity and prehistory: Molecular archaeology reveals secrets of past civilizations. *Phil. Trans. R. Soc. Lond. B.*, *354*, **1999**, 33–50.

Craig, O., Saul, H., Lucquin, A., Nishida, Y., Tache, K., Clarke, L., Thompson, A., Altoft, D., Uchiyama, J., Ajimoto, M., Gibbs, K., Isaksson, S., Heron, C., Jordan, P. Earliest evidence for the use of pottery. *Nature*, *496*, **2013**, 351–354.

Craig, O., Mulville, J., Pearson, M., Sokol, R., Gelsthorpes, K., Stacey, R., Collins, M. Detecting milk proteins in ancient pots. *Nature*, *408*, **2000**, 312.

Criado, M., Motilva, M., Goni, M., Romero, M. Comparative study of the effect of the maturation process of the olive fruit on the chlorophyll and carotenoid fractions of drupes and virgin oils from *Arbequina* and *Farga* cultivars. *Food Chem.*, *100*, **2007**, 748−755.

Dallongeville, S., Garnier, N., Rolando, C., Tokarski, C. Proteins in art, archaeology, and paleontology. *Chem. Rev., 116*(1), **2016**, 2–79.

Damak, N., Bouaziz, M., Ayadi, M., Sayadi, S., Damak, M. Effect of the maturation process on the phenolic fractions, fatty acids, and antioxidant activity of the Chetoui olive fruit cultivar. *J. Agric. Food Chem.*, *56*, **2008**, 1560−1566.

Degano, M., Modugno, F., Bonaduce, I., Ribechini, E., Colombini, M. Recent advances in analytical pyrolysis to investigate organic materials in heritage science. *Angew. Chem. Int. Ed., 57,* **2018**, 2–13.

Demtroeder, W. Laser spectroscopy: Vol.1 Basic principles. Fourth edition, Springer, Germany, **2008**.

Diaz-Garcia, M. E., Badia-Laino, R. Fluorescence: overview. In: Worsfold, P. J., Townshend, A., Poole, C. F. (Eds.), *Encyclopedia of Analytical Science*. 2nd edition, vol. 3, Elsevier, Oxford, **2005**, 97–106.

Dixon, J. M., Taniguchi, M., Lindsey, J. S. PhotochemCAD 2: A refined program with accompanying spectral databases for photochemical calculations. *Photochem. Photobiol.* 81, **2005**, 212–213.

Dominguez, R., Pateiro, M., Gagaoua, M., Barba, F., Zhang, W., Lorenzo, J. A comprehensive review on lipid oxidation in meat and meat products. *Antioxidants (Basel), 8*, **2019**, 429−460.

Drieu, L., Rageot, M., Wales, N., Stern, B., Lundy, J., Zerrer, M., Gaffeny, I., Bondetti, M., Spiteri, C., Thomas-Oates, J., Craig, O. Is it possible to identify ancient wine production using biomolecular approaches? *Sci. Technol. Archaeol. Res. J., 6*, **2020**, 1–14.

Dufour, E., Letort, A., Laguet, A., Lebecque, A., Serra, J. Investigation of variety, typicality and vintage of French and German wines using front-face fluorescence spectroscopy. *Anal. Chim. Acta, 563*, **2006**, 292–299.

Dufour, E., Riaublanc, A. Potentiality of spectroscopic methods for the characterization of daity products: Front-face fluorescence study of raw, heated, and homogenised milks. *Lait, 77*(6), **1997**, 657–670.

Evershed, R., Copley, M., Dickson, L., Hansel, F. Experimental evidence for the processing of marine animal products and other commodities containing polyunsaturated fatty acids in pottery vessels. *Archaeometry, 50*(1), **2008**, 101–113.

Evershed, R., Tuross, N. Proteinaceous material from potsherds and associated soils. *J. Archaeol. Sci.*, 23, **1996**, 429–436.

Evershed, R., Stott, A., Raven, A., Dudd, S., Charters, S., Leyden, A. Formation of long-chain ketones in ancient pottery vessels by pyrolysis of acyl lipids. *Tettrahedron Lett., 36*(48), **1995**, 8875–8878.

Evershed, R. Biomolecular archaeology and lipids. *World Archaeol., 25*(1), **1993**, 74–93.

Foxhall, L. (Ed.) Processing olives. In: *Olive cultivation in Ancient Greece: Seeking the Ancient economy*. 1st edition, Oxford University Press, New York, **2007**, 131–218.

Fratzl, P., Weinkamer, R. Nature's hierarchical materials. *Prog. Mater. Sci., 52*(8), **2007**, 1263–1334.

Gill, A. Examination of the contents of a Mycenean vase found in Egypt. *Am. J. Archaeol.. 10*, **1906**, 300–301.

Giuliani, A., Cerretani, L., Cichelli, A. Chlorophylls in olive and in olive oil: Chemistry and occurrences. *Crit. Rev. Food Sci. Nutr.*, *51*, **2011**, 678−690.

Grigoriadou, D., Tsimidou, M. Quality control and storage studies of virgin olive oil: Exploiting UV spectrometry potential. *Eur. J. Lipid Sci. Technol.*, *108*, **2006**, 61−69.

Guash-Jane, M. R., Ibern-Gomez, M., Andres-Lacueva, C., Jauregui, O., Lamuela-Raventos, R. M. Liquid chromatography with mass spectrometry in tandem mode applied for the identification of wine markers in residues from ancient Egyptian vessels. *Anal. Chem., 76*, **2004**, 1672−1677.

Guimet, F., Ferre, J., Boque, R., Rius, X. Application of unfold principal component analysis and parallel factor analysis to the exploratory analysis of olive oils by means of excitation-emission matrix fluorescence spectroscopy. *Anal. Chim. Acta, 515*(1), **2004**, 75–85.

Hadzisavvas, S. Wine and olive in Crete and Cyprus: Socio-economic aspects. In: Cadogan, G., Iacovou M., Kopaka, K., Whitley, J. (Eds.) *Parallel lives: Ancient island societies in Crete and Cyprus*. British School at Athens, London, **2012**, 157–173.

Hamilakis, Y. Wine, oil and the dialectics of power in Bronze Age Crete: A review of the evidence. *Oxf. J. Archaeol., 15*(1), **1996**, 1–32.

Hansel, F., Copley, M., Madureira, L., Evershed, R. Thermally produced ω-(*o*-alkylphenyl)alkanoic acids provide evidence for the processing of marine products in archaeological pottery vessels. *Tetrahedron Lett., 45*(14), **2004**, 2999–3002.

Hendy, J., Welker, F., Demarchi, B., Speller, C., Warinner, C., Collins, M. A guide to ancient protein studies. *Nat. Ecol. Evol., 2*, **2018**, 791–799.

Hernandez-Sanchez, N., Lleo, L., Ammari, F., Cuadrado, T., Roger, J. Fast fluorescence spectroscopy methodology to monitor the evolution of extra virgin olive oils under illumination. *Food Bioprocess Technol.*, *10*, **2017**, 949−961.

Heron, C., Stacey, R. Archaeology: Uses of chromatography. In: Wilson, D. (Ed.) *Encyclopedia of separation science.* Academic Press, London, **2000**, 2083–2089.

Heron, C., Evershed, R., Goad, L. Effects of migration of soil lipids on organic residues associated with buried potsherds. *J. Archaeol. Sci., 18,* **1991**, 641–659.

Historic England. Organic residue analysis and archaeology: Guidance for good practice. *Historic England, Swindon*, **2017a**, 1–49.

Historic England. Organic residue analysis and archaeology: Supporting information. *Historic England, Swindon*, **2017b**, 1–32.

Horiba group (Ed.), *FluoroMax-3 and FluoroMax-P: Operation manual.* Jobin Yvon Inc., New Jersey, **2001**.

Irmak, S., Tokusoglu, O. Saturated and unsaturated fatty acids composition of olive oils obtained from less salty black table olives preserved with vacuum, MAP and gamma irradiation technologies. *J. Nutr. Food Sci.*, *7*, **2017**, 1−15.

Iwaki, L., Dlott, D. Ultrafast vibrational energy redistribution within C-H and O-H stretching modes of liquid methanol. *Chem. Phys. Lett., 321*, **2000**, 419–425.

Kirby, D., Buckley, M., Promise, E., Trauger, S., Holdcraft, R. Identification of collagen-based materials in cultural heritage. *Analyst, 138*, **2013**, 4849–4858.

Koh, A., Betancourt, P. Wine and olive oil from an early Minoan I hilltop fort. *Mediterr. Archaeol. Archaeom., 10*(2), **2010**, 15–23.

Lakowicz, J. R. (Ed.) Principles of fluorescence spectroscopy. 3rd edition, Springer, Boston, **2006**.

Lamb, J., Loy, T. Seeing red: the use of Congo Red dye to identify cooked and damaged starch grains in archaeological residues. *J. Archaeol. Sci., 32,* **2005**, 1433–1440.

Lang, M., Stober, F., Lichtenthaler, H. Fluorescence emission spectra of plant leaves and plant constituents. *Radiat. Environ. Biophys.*, *30*, **1991**, 333−347.

Leo, G., Bonaduce, I., Andreotti, A., Marino, G., Pucci, P., Colombini, M., Birolo, L. Deamidation at asparagine and glutamine as a major modification upon deterioration/aging of proteinaceous binders in mural paintings. *Anal. Chem., 83,* **2011**, 2056–2064.

Levi, V., Flecha, L. Labeling of proteins with fluorescent probes. *Biochem. Mol. Biol. Educ., 31*(5), **2003**, 333–336.

Llorent-Martinez, E., Jiminez-Lopez, J., Cordova, M., Barrales, P., Ruiz-Medina, A. Quantitation of hydroxytyrosol in food products using sequential injection analysis fluorescence optosensor. *J. Food Compost. Anal.*, *32*, **2013**, 99−104.

Manzano, J., Pena, A., Meras, I. Front-face fluorescence combined with second-order multiway classification, based on polyphenol and chlorophyll compounds for virgin olive oil monitoring under different photo- and thermal-oxidation procedures. *Food Anal. Methods*, *12*, **2019**, 1399−1411.

Matlova, V., Roffet-Salque, M., Pavlu, I., Kyselka, J., Sedlarova, I., Filip, V., Evershed, R. Defining pottery use and animal management at the Neolithic site of Bylany (Czech Republic). *J. Archaeol. Sci Rep., 14*, **2017**, 262–274.

Mayer, L. M. Relationships between mineral surfaces and carbon concentrations in soils and sediments. *Chem. Geol., 114*(3–4), **1994**, 347–363.

Mc Govern, P., Jalabadze, M., Batiuk, S., Callahan, M., Smith, K. et al. Early Neolithic wine of Georgia in the south Caucasus. *Proc. Natl. Acad. Sci. U.S.A., 114*, **2017**, E10309–E10318.

Miksik, I., Sedlakova, P., Pataridis, S., Bortolotti, F., Gottardo, R. Proteins and their modifications in a medieval mummy. *Protein Sci., 25*, **2016**, 2037–2044.

Mishra, P., Lleo, L., Cuadrado, T., Ruiz-Altisent, M., Hernandez-Sanchez, N. Monitoring oxidation changes in commercial extra virgin olive oil with fluorescence spectroscopy-based phototype. *Eur. Food Res. Technol.*, *244*, **2018**, 565−575.

Monnier, G., Ladwig, J., Porter, S. Swept under the rug: the problem of unacknowledged ambiguity in lithic residue identification. *J. Archaeol. Sci., 39, **2012**,* 3284–3300.

Namiesnik, J., Spietelun, A., Marcinkowski, L. Green sample preparation techniques for chromatographic determination of small organic compounds. *Int. J. Chem. Eng. Appl., 6*(3), **2015**, 215−219.

Nerlich, A., Parsche, F., Kirsch, T., Wiest, I., Vonderman, K. Immunohistochemical detection of interstitial collagen in bone and cartilage tissue remnants in an infant Peruvian mummy. *Am. J. Phys. Anthrop., 91*(3), **1993**, 279–285.

Nevin, A., Cather, S., Burnstock, A., Anglos, D. Analysis of protein-based media commonly found in paintings using synchronous fluorescence spectroscopy combined with multivariate statistical analysis. *Appl. Spec., 62*, **2008a**, 481–489.

Nevin, A., Anglos, D., Cather, S., Burnstock, A. The influence of visible light and inorganic pigments on fluorescence excitation emission spectra of egg-, casein- and collagen-based painting media. *Appl. Phys. A, 92*, **2008b**, 69–76.

Nevin, A., Cather, S., Anglos, D., Fotakis, C. Analysis of protein-based binding media found in paintings using laser induced fluorescence spectroscopy. *Anal. Chim. Acta, 573-574*, **2006**, 341–346.

Peinado, R., Mauricio, J. Biologically aged wines. In: Moreno-Arribas, M., Polo, M. (Eds.) *Wine chemistry and biochemistry*. Springer, New York, **2009**, 82–101.

Peri, C. (Ed.) The extra-virgin olive oil handbook. Wiley Blackwell, England, West Sussex, **2014**.

Philippidis, A., Papliaka, Z., Anglos, D. Surface enhanced Raman and 2D-fluorescence spectroscopy for the investigation of amino acids and egg proteins. *Microchem. J., 126*, **2016**, 230–236.

Pyrzynska, K., Biesaga, M. Analysis of phenolic acids and flavonoids in honey. *Trends Anal. Chem., 28*(7), **2009**, 893–902.

Rabiej, D., Szydlowska-Czerniak, A. Fluorescence and UV-vis spectroscopy to determine the quality changes of rapeseed oil fortified with new antioxidant after storage under various conditions. *Food Anal. Methods*, *13*, **2020**, 1973−1982.

Rahmani, M., Csallany, A. Role of minor constituents in the photooxidation of virgin olive oil. *J. Amer. Oil Chem. Soc.*, *75*, **1998**, 837−843.

Raven, A., van Bergen, P., Stott, A., Dudd, S., Evershed, R. Formation of long-chain ketones in archaeological pottery vessels by pyrolysis of acyl lipids. *J. Anal. Appl. Pyrol., 40–41*, **1997**, 267–285.

Regert, M., Bland, H., Dudd, S., van Bergen, P., Evershed, R. Free and bound fatty acid oxidation products in archaeological ceramic vessels. *Proc. R. Soc. Lond. B., 265*, **1998**, 2027–2032.

Rene de la Rie, E. Fluorescence of paint and varnish layers (Part II). *Stud. Conserv., 27*, **1982**, 1–7.

Reynolds, A. The grapevine, viticulture, and winemaking: A brief introduction. In: Meng, B, Martelli, G., Golino, D., Fuchs, M. (Eds.) *Grapevine viruses: Molecular Biology, diagnostics, and management.* Springer, Cham, **2017**, 3–29.

Ribéreau-Gayon, P., Glories, Y., Maujean, A., Dubourdieu, D. Handbook of Enology: The chemistry of wine stabilization and treatment. 2nd edition, vol. 2, Chechester: John Wiley, England, **2006**.

Riley, F. The olive industry of Bronze Age Crete: Evidence for volcanic damage to olive grooves and property in central and Eastern Crete. *Akroterion, 49,* **2004**, 1–6.

Riley, F. Olive oil production on Bronze Age Crete: Nutritional properties, processing methods and storage life of Minoan olive oil. *Oxf. J. Archaeol., 21*(1), **2002**, 63–75.

Rodrıguez-Delgado, M. A., Malovana, S., Perez, J. P., Borges, T., Garcıa Montelongo, F. J. Separation of phenolic compounds by high-performance liquid chromatography with absorbance and fluorimetric detection. *J. Chromatogr. A, 912*(2), **2001**, 249–257.

Roffet–Salque, M., Dunne, J., Altoft, D., Casanova, E., Cramp, L., Smyth, J., Whelton, H., Evershed, R. From the inside out: Upscaling organic residue analyses of archaeological ceramics. *J. Archaeol. Sci., 16*, **2017**, 627–640.

Roffet-Salque, M., Regert, M., Evershed, R., Outram, A., Cramp, L., Decavallas, O., Dunne, J., Gerbault, P., Mileto, S., Mirabaud, S. Widespread exploitation of the honeybee by early Neolithic farmers. *Nature, 527*, **2015**, 226–231.

Romano, P., Suzzi, G. Origin and production of acetoin during wine yeast fermentation. *Appl. Environ. Microbiol.*, 62*(2)*, **1996**, 309–315.

Romanus, K., Baeten, J., Poblome, J., Accardo, S., Degryse, P., Jacobs, P., De Vos, D., Waelkens, M. Wine and olive oil permeation in pitched and non-pitched ceramics: relation with results from archaeological amphorae from Sagalassos, Turkey. *J. Archaeol. Sci., 36*, **2009**, 900−909.

Rosiak, A., Kaluzna-Czaplinska, J., Gatarek, P. Analytical interpretation of organic residues from ceramics as a source of knowledge about our ancestors. *Crit. Rev. Anal. Chem., 50*(3), **2020**, 189–195.

Rotich, V., Al Riza, D., Giametta, F., Suzuki, T., Ogawa, Y., Kondo, N. Thermal oxidation assessment of Italian extra virgin olive oil using UltraViolet (UV) induced fluorescence imaging system. *Spectrochim. Acta A Mol. Biomol. Spectrosc., 237*, **2020**, 118373.

Runnels, C., Hansen, J. The olive oil in the Prehistoric Aegean: The evidence for domestication in the early Bronze Age. *Oxf, J. Archaeol., 5*(3), **1986**, 299–308.

Sadecka, J., Tothova, J. Fluorescence spectroscopy and chemometrics in the food classification: A review. *Czech. J. Food Sci., 25*(4), **2007**, 159–173.

Sandu, I., Roque, A., Matteini, P., Schafer, S., Agati, G., Correia, C., Viana, J. Fluorescence recognition of proteinaceous binders in works of art by a novel integrated system of investigation. *Microsc. Res. Tech*., *75*(3), **2012a**, 316–324.

Sandu, I., Schafer, S., Magrini, D., Bracci, S., Roque, C. Cross-section and staining-based techniques for investigating organic materials in painted and polychrome works of art: A review. *Microsc. Microanal. 18,* **2012b**, 860–875.

Shimadzu group (Ed.), *UV-1900: Instruction manual, operation guide.* Shimadzu Corp., Japan, **2018**.

Sikorska, E., Khmelinskii, I., Sikorski, M. Analysis of olive oils by fluorescence spectroscopy: Methods and applications. In: Boskou, D. (Ed.) *Olive oil: Constituents, quality, health properties, and bioconversions.* IntechOpen, England, **2012**, 63–88.

Sikorska, E., Khmelinskii, I., Sikorski, M., Caponio, F., Bilancia, M., Pasqualone, A., Gomes, T. Fluorescence spectroscopy in monitoring of extra virgin olive oil during storage. *Int. J. Food Sci. Technol.*, *43*, **2007**, 52−61.

Simoneit, B., Rogge, W., Mazurek, M., Standley, L., Hildemann, L., Cass, G. Lignin pyrolysis products, lignans, and resin acids as specific tracers of plant classes in emissions from biomass combustion. *Environ. Sci. Technol., 27,* **1993**, 2533–2541.

Smith, G., Haskell, T. The fluorescent oxidation products of dihydroxyphenylalanine and its esters. *J. Photochem. Photobiol. B: Biol.*, *55*, **2000**, 103–108.

Soyer, Y., Koca, N., Karadeniz, F. Organic acid profile of Turkish white grapes and grape juices. *J. Food Compos. Anal*., *16*, **2003**, 629–636.

Stacey, R. Organic residues: Origins, analysis, and scope: An overview for the archaeological ceramist. *The Old Potter's Almanack,14*(1), **2009**, 1–8.

Steele, V. Organic residues in archaeology-the highs and lows of recent research, *ACS Symp. Ser., 1147*, **2013**, 1–28.

Stephenson, B. A modified Picro-Sirius Red (PSR) staining procedure with polarization microscopy for identifying collagen in archaeological residues. *J. Archaeol. Sci., 61*, **2015**, 235–243.

Stern, B., Heron, C., Tellefsen, T., Serpico, M. New investigations into the Uluburun resin cargo. *J. Archaeol. Sci., 35*, **2008**, 2188–2203.

Taniguchi, M., Lindsey, J. Database of absorption and fluorescence spectra of >300 common compounds for use in PhotochemCAD. *Photochem. Photobiol., 94*, **2018**, 290–327.

Traore, M., Kaal, J., Cortizas, A. Potential of pyrolysis-GC-MS molecular fingerprint as a proxy of Modern Age Iberian shipwreck wood preservation. *J. Anal. Appl. Pyrol., 126*, **2017**, 1–13.

Tsana, I. Analysis of organic residues in archaeological pottery by NMR spectroscopy. MSc Thesis, University of Crete, Heraklion, **2018**.

Uylaser, V. Changes in phenolic compounds during ripening in Gemlik variety olive fruits obtained from different locations. *J. Food*, *13*, **2014**, 167−173.

Vandenabeele, P., Edwards, H., Moens, L. A decade of Raman spectroscopy in art and archaeology. *Chem. Rev., 107*(3), **2006**, 675–686.

Van de Velde, T., Deschepper, E., Mestdagh, B., Clercq, W., Vandenabeele, P., Lynen, F. Lipids, funerals, gifts and feasts: Organic residue analysis on Merovingian ceramics from the Elversele burial field (Belgium). *J. Archaeol. Sci. Rep., 24*, **2019**, 30–38.

Volf, I., Ignat, I., Neamtu, M., Popa, V. Thermal stability, antioxidant activity, and photooxidation of natural polyphenols. *Chemical Papers*, *68*, **2013**, 121−129.

Wu, X., Zhang, C., Goldberg, P., Cohen, D., Pan, Y., Arpin, T., Bar-Yosef, O. Early pottery at 20000 years ago in Xianrendong Cave, China. *Science, 336*, **2012**, 1696–1700.

Wünsch, U. J., Murphy, K. R., Stedmon, C. A. Fluorescence quantum yields of natural organic matter and organic compounds: Implications for the fluorescence-based interpretation of organic matter composition. *Front. Mar. Sci., 98*(2), **2015**, 1−15.

Yakupova, E., Bobyleva, L., Vikhlyantsev, I., Bobylev, A. Congo Red and amyloids: history and relationship. *Biosci. Rep., 39*(1), **2019**, 1–22.

Zandomeneghi, M., Carbonaro, L., Caffarata, C. Fluorescence of vegetable oils: Olive oils. *J. Agric. Food Chem., 53*, **2005**, 759−766.